


Chapter 6



<https://doi.org/10.32685/pub.esp.37.2019.06>
Published online 29 May 2020

Structural Styles of the Eastern Cordillera of Colombia

Andreas KAMMER^{1*}, Alejandro PIRAQUIVE² , Cristhian GÓMEZ³,
Andrés MORA⁴, and Antonio VELÁSQUEZ⁵

Abstract The Eastern Cordillera of Colombia is bracketed between the moderately west-dipping flank of the Central Cordillera on its western side and the little disturbed to gently bent Guiana Shield on its eastern side. Unlike other Andean foreland-oriented belts, it is completely disconnected from the main Andean trunk system. Transverse shortening of 4 mm/y records a considerable displacement transfer to the upper plate; this is twice the long-term rate of 2.2 mm/y, which is the average for a shortening of 65 km over a period of 30 Ma and suggests an increased recent shortening phase. We differentiate three structural domains. The southern domain records significant shortening by penetrative strain at lower structural levels and folding at higher structural levels, which supports the idea of partitioning into pure-shear deformation within the pre-Cretaceous basement and into buckling in the Upper Cretaceous to Paleogene units. Similar constellations of a relatively weak crustal welt enclosed between domains with backstop characteristics have been examined in analogue and numerical experiments (“vise model”). A northern intermediate domain is characterized by large-scale, basement-cored antiforms, whose formation may be ascribed to the partial reactivation of Late Triassic normal faults. The northernmost domain comprises the Cocuy Syntaxis, which constitutes an antiformal lobe with significant topographic relief. It is affected by secondary folds with a down-slope vergence. These changes in structural style record increased support by the subducting slab, according to the spatial coincidence of the outer slab hinge and the highest topographic relief within this northern Andean flat slab segment.

To examine a possible cause for a rheological break between deformable cordilleran crust sandwiched between relatively rigid and strong surrounding basement blocks, we review the Cretaceous back-arc setting. Tectonic subsidence and sedimentation patterns suggest its division into a forebulge and flanking basins that may be ascribed to the framework of an impinging mantle plume. Temporal constraints further suggest that forebulge evolution may have been triggered by an initial foundering of the slab at the onset of a Cretaceous subduction cycle. In such a small-scale convection system, downwelling mantle flow between the back-arc region and the stable shield may maintain a relatively well-defined rheological limit over long periods. This situation complies with the model of an edge-driven convective flow.

Rheological contrasts between the back-arc basin and the shield persisted into the Cenozoic and contributed to a protracted evolution of the Andean cordilleran mountain fronts. The eastern mountain front accumulated structural relief of more than

- 1 akammer@unal.edu.co
Universidad Nacional de Colombia
Departamento de Geociencias
Carrera 30 n.º 45-03
Bogotá, Colombia
 - 2 apiraquive@sgc.gov.co
Servicio Geológico Colombiano
Dirección de Asuntos Nucleares
Carrera 50 n.º 26-20
Bogotá, Colombia
 - 3 cngomezp@unal.edu.co
Universidad Nacional de Colombia
Departamento de Geociencias
Carrera 30 n.º 45-03
Bogotá, Colombia
 - 4 andres.mora@ecopetrol.com.co
Ecopetrol S.A
Vicepresidencia de Exploración
Bogotá, Colombia
 - 5 antonio.velasquez@ecopetrol.com.co
Ecopetrol S.A
Vicepresidencia de Exploración
Bogotá, Colombia
- * Corresponding author

Citation: Kammer, A., Piraquive, A., Gómez, C., Mora, A., & Velásquez, A. 2020. Structural styles of the Eastern Cordillera of Colombia. In: Gómez, J. & Mateus-Zabala, D. (editors), *The Geology of Colombia, Volume 3 Paleogene – Neogene*. Servicio Geológico Colombiano, *Publicaciones Geológicas Especiales 37*, p. 143–183. Bogotá. <https://doi.org/10.32685/pub.esp.37.2019.06>

10 000 m during an initial Oligocene to late Miocene shortening phase. Fold growth incited by the buttressing of the strong foreland block of the shield can be tested by the tri-shear model, in which propagation of faulting is halted, and displacement is consumed by fold amplification. During a Pliocene stress reorganization, this Miocene mountain front was breached by a shallowly dipping thrust, which gave rise to a more foreland-oriented deformation front. During this outward-stepped faulting, proximal foreland sequences became involved in a wedge-top position and were exhumed at the thrust tip along emergent ramps. These second-cycle erosion products were widely dispersed into the Llanos Basin and were incorporated into modern fluvial terraces.

Keywords: *back-arc basin, fault reactivation, gravitational collapse, Eastern Cordillera of Colombia.*

Resumen La cordillera Oriental de Colombia está encajada entre el flanco inclinado ligeramente al oeste de la cordillera Central, al costado occidental, y el Escudo de Guayana levemente flexionado, al costado oriental. A diferencia de otros cinturones andinos de antepaís, esta cadena montañosa está completamente desconectada del sistema principal andino. El acortamiento transversal de 4 mm/año registra una transferencia considerable de desplazamiento a la placa superior; este es el doble de una tasa de 2,2 mm/año, que es el promedio para un acortamiento de 65 km durante un intervalo de tiempo de 30 Ma y sugiere una acelerada fase de acortamiento reciente. En este trabajo diferenciamos tres dominios estructurales. El dominio meridional registra un acortamiento significativo por deformación penetrativa a niveles estructurales inferiores y plegamiento a niveles estructurales superiores, lo que respalda la idea de diferenciar entre deformación por cizalla pura en el basamento precretácico y entre un plegamiento por acortamiento horizontal en las unidades del Cretácico Superior al Paleógeno. Constelaciones similares de un entorno cortical relativamente débil contenido entre dominios con características de contrafuerte han sido examinadas en experimentos análogos y numéricos (*visé model*). Un dominio intermedio más septentrional se caracteriza por antiformentes a gran escala, que involucran el basamento en su núcleo y cuya formación está predispuesta por la reactivación parcial de fallas normales del Triásico Tardío. El dominio más septentrional comprende la Sintaxis de Cocuy, un lóbulo antiformal de un mayor relieve topográfico. Esta se ve afectada por pliegues secundarios con una vergencia en dirección de la pendiente. Estos cambios en estilo estructural registran un aumento en el soporte de la losa subducida, como puede concluirse a partir de la coincidencia espacial entre bisagra externa de la losa en subducción y el relieve topográfico descomunal en este segmento de losa plana del norte andino.

Con el fin de examinar una posible causa para la existencia de un cinturón altamente deformable y encajado entre bloques circundantes de basamento relativamente rígidos y fuertes, examinamos la configuración de la cuenca de retroarco del Cretácico. Los patrones de subsidencia tectónica y sedimentación sugieren la existencia de una región axial dominada por un abombamiento amplio o *forebulge*, que se delimita por cuencas marginales y cuyo origen se atribuye al impacto de una pluma mantélica. Las limitaciones temporales sugieren, además, que la evolución del abombamiento puede haber sido desencadenada por un hundimiento inicial de la losa al inicio de un ciclo de subducción cretácico. En un sistema de convección a tan pequeña escala, el flujo del manto descendente entre la región de retroarco y el escudo estable puede mantener un límite reológico relativamente bien definido durante largos períodos de tiempo. Esta situación cumple con el modelo de un flujo convectivo de tipo *edge-driven*.

Contrastes reológicos entre la cuenca de retroarco y el escudo perduraron hasta el Cenozoico y contribuyeron a una evolución prolongada de los frentes cordilleranos andinos. Un antiforme del frente montañoso oriental acumuló un relieve estructural de más de 10 000 m durante una fase de acortamiento inicial entre el Oligoceno y el Mioceno tardío. El crecimiento de este pliegue fue inducido por el efecto de contrafuerte del bloque de antepaís del escudo. Este proceso puede ser probado por el modelo *tri-shear*, en el cual se detiene la propagación de falla y se consume el desplazamiento por la amplificación de este frente montañoso. Durante una reorganización del campo de esfuerzos en el Plioceno, este frente montañoso fue afectado por una falla fuera de secuencia con un buzamiento moderado, que dio lugar a un frente de deformación orientado más hacia el antepaís. En este fallamiento, las secuencias proximales de antepaís se involucraron en una posición de tipo supracuña o *wedge-top* y se exhumaron a lo largo de una falla emergente, que forma la base de un manto corrido. Estos productos de erosión de segundo ciclo se dispersaron ampliamente en la Cuenca de los Llanos, incorporándose a las terrazas fluviales modernas.

Palabras clave: *cuenca de retroarco, reactivación de falla, colapso gravitacional, cordillera Oriental de Colombia.*

1. Introduction

Within the North Andean Terrane, the Eastern Cordillera of Colombia (EC) is completely detached from the main Andean trunk system and forms a distinct morphotectonic feature, before the Andean system reassembles into the morphologically little differentiated mountain belts at the southern Caribbean Plate margin (Figure 1). Its width of >200 km in its central part is comparable to the combined transverse dimensions of the Central and Western Cordilleras further to the west (Figure 1). These three mountain belts are separated from each other by the interandean Cauca and Magdalena Valleys, of which the latter has subdued topography (<500 m) and contains several tectonic elements that are highlighted by an array of intra-basinal basement highs, which were first outlined by Morales (1958, Figure 1). As it approaches the Maracaibo Block, the Eastern Cordillera connects with the northwest-trending leg of the Santander Massif (Figure 1), which is composed of a narrow basement high and is bordered at its western margin by the left-lateral strike-slip Bucaramanga Fault. At their junction, the Bucaramanga Fault splays into an array of curved secondary faults, which are considered to form a horsetail structure at the southern termination of the Bucaramanga Fault (Acosta et al., 2007; Velandia & Bermúdez, 2018). At this same cordilleran relay, the Mérida Andes take off from the EC and constitute an independent chain in its northeasterly continuation, but separated by a sinistral step. Near this relay, the EC reaches its highest elevation at the syntaxial bend of the Cocuy Massif (Figure 1). Together with the peaks of the Sierra Nevada de Santa Marta, this massif contains the only North Andean non-volcanic summits that exceed the present snow line at 5000 m.

This intricate morphotectonic pattern suggests the control of Andean folding by inherited crustal or lithospheric features, as evidenced by Late Triassic – Early Jurassic precursor faults and associated graben structures that straddle the Bucaramanga Fault (Kammer & Sánchez, 2006). Moreover, a back-arc setting involves a long-standing Cretaceous Basin evolution (Guerro, 2002 and references therein) and the inversion of this basin likely attests to a weakened crust that preferentially consumed shortening during Neogene folding, as observed in other back-arc settings (e.g., the Canadian Cordillera; Hyndman & Currie, 2011). A further regional consideration is related to the bend between the Andean and the Caribbean active margin and a consequent relaxation in lateral constraints between the converging mantle flows. This situation promoted lateral mantle flow in the upper plate and the margin-parallel translation of crustal blocks (Beck et al., 1993; Gephart, 1994; Russo & Silver, 1994), as presently occurs with the northward escape of the North Andean Terrane (Egbue & Kellogg, 2010).

In this contribution, we disentangle some of the relationships between the inherited crustal structures of the North Andean basement and the Neogene folding. We restrict ourselves to the middle segment of the EC, which contains the High Plain of Bogotá to the south, extends to the structural bend laid out by the NNW-striking Bucaramanga Fault, and is outlined further by the syntaxial bend of the Cocuy Massif (Figure 1). Since the pioneering works of Campbell & Bürgl (1965), Bürgl (1967), and Julivert (1970), the EC has been considered to have emerged from a Cretaceous rift structure, and its origin by the inversion of a back-arc basin has been further acclaimed in recent studies (Mora et al., 2006, 2009, 2013; Teixell et al., 2015; Tesón et al., 2013). In this account, we re-examine the link between the Cretaceous back-arc tectonics and Andean folding

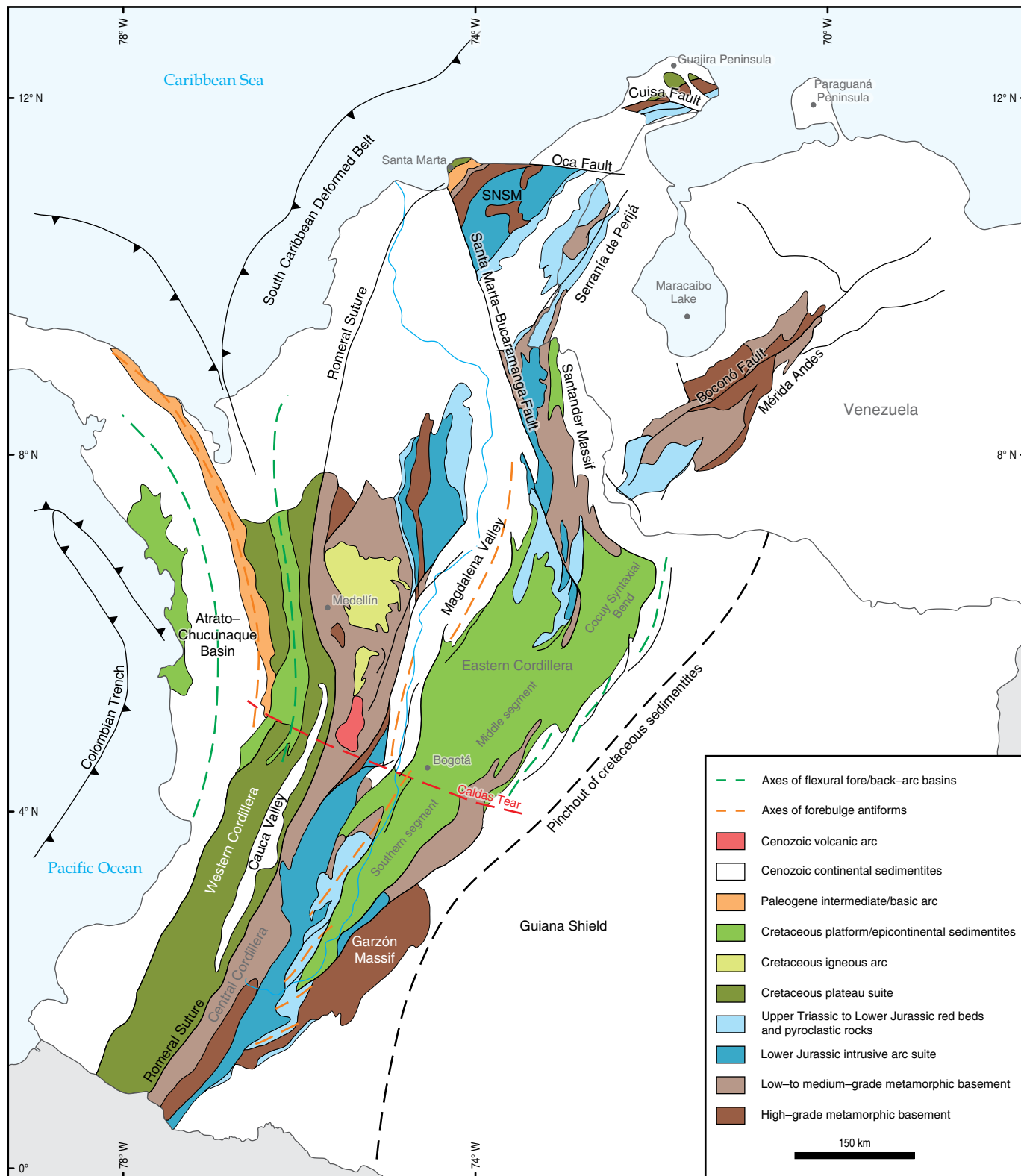


Figure 1. Sketch map of the three Andean mountain chains and the northwestern Maracaibo Block, which form the North Andean Terrane. The map depicts the pre-Cenozoic cordilleran basement units. It highlights the successive branching of the eastern mountain belts from the main Andean trunk system, as documented by the appearance of the interandean Magdalena Valley and the splaying of the EC into the Santander Massif and the Mérida Andes.

and attempt to gain an understanding of its geodynamic implications. We address three questions related to the Cretaceous rift event: (1) how is Cretaceous fault activity linked to the evolution of the marginal basins?, (2) are the Cretaceous border faults of this back-arc domain comparable to breakaway faults in extensional provinces?, and (3) are the extensional processes of the back-arc region related to the subduction dynamics of the Cretaceous active margin?

Much of the discussion of Cenozoic fault reactivation and cordilleran folding has focused on the relative importance of and temporal relationship between basement-involved and thin-skinned deformational styles (see the reviews in Cortés et al., 2006; Tesón et al., 2013). In our approach, we address the following questions: (1) did the overall shortening form a crustal root or result in crustal-scale buckling, which was eventually supported by the oceanic slab?, (2) considering the bivergent structure of the EC, were the deformation phases equally distributed across this orogenic pop-up, or do they record progressively east- (or west-) advancing deformation fronts?, and (3) is the small-scale folding of the High Plain of Bogotá a superficial expression of homogeneous basement shortening, or is it related to detachment folds conditioned by the existence of a basal Cretaceous evaporitic horizon, as contended by Cortés et al. (2006) and Teixell et al. (2015)?

2. Regional Framework

With respect to the modern plate tectonic framework, the EC and its northern extension, the Santander Massif, trend obliquely with respect to the present E-W oriented convergence between the Nazca Plate and South America (Trenkamp et al., 2002). Based on an average convergence rate of 60 mm/y (Trenkamp et al., 2002) and a shortening rate of 4 mm/y across the EC, as derived from GPS measurements (Mora-Páez et al., 2016), approximately 7% of the convergence is presently transferred to the eastern limit of the North Andean Terrane and converted into deformation. More important than this strike-perpendicular shortening is, however, a strike-parallel, apparently widely distributed slip component of 8 mm/y (Mora-Páez et al., 2016). Within the Mérida Andes (northwestern continuation of the EC), much of this slip is converted into dextral displacement along the Boconó Fault (Figure 1), which trends parallel to the axial zone of this mountain chain and has accommodated 7–10 mm/y of dextral displacement for the past 15 000 y (Audemard et al., 2008). This finding points to a recent kinematic plate reorganization, in which the convergence changed from margin-perpendicular to the present margin-oblique E-W direction.

The topographic aspects of the present-day plate interactions between the Nazca, Caribbean, and South American Plates are shown in Figure 2, which combines regional tectonomorphic features of the present-day plate setting with the projections of the hypocentral solutions of >30 000 earthquakes that were

extracted from the catalog of the Colombian National Seismological Network (Chiarabba et al., 2015; Vargas & Mann, 2013). These events are projected onto 8 transverse sections with topographically highly exaggerated elevations, to provide a reference for the different mountain belts. The earthquakes are strongly clustered and highlight the slab contours. This map shows the now well-known relay of a southern, moderately east-dipping slab segment and a northern, flat-dipping slab segment (Chiarabba et al., 2015; Pennington, 1981; Taboada et al., 2000; Vargas & Mann, 2013), which correlates with the onset of a volcanic gap north of 5° N. The seismic response to these slab segments is well-defined and has been referred to as the Caldas Tear (Vargas & Mann, 2013; Figures 1, 2). Surface structures image these different slab configurations in detail and document a doubling of the width of the EC within the flat slab realm, largely brought about by the inception of the frontal thrust sheets on either side of the EC (Figures 1, 3a).

Transverse sections 4 and 5 (Figure 2) document the surface response of the EC above the flat slab segment by its broadening and increased topographic relief. Within the basal Cretaceous sedimentites, paleothermometric index values based on vitrine reflectance, that were obtained from Lower Cretaceous sequences, are anomalously high near the tear zone ($Ro > 6$) with respect to regional background values ($3 < Ro < 4.5$; Parra et al., 2009a, 2009b; Mora et al., 2013) and point to the probable existence of a thermal window, which is further suggested by an elevated geothermal gradient of 44°/km for pre-Campanian sedimentites (Mora et al., 2008). Affirming the existence of a long-standing thermal anomaly, a pronounced ductile deformation style is expected to have persisted close to the relay zone, as may be deduced independently from the fold style at the eastern deformation front, which includes tight fault-related folds (Mora et al., 2006; Kammer et al., 2007). To inquire more about changes in structural style related to this slab-related framework, we investigate the three transverse sections of Figure 4, the locations of which are shown in Figure 3a.

3. Cordilleran Cross-Sections

The southern transverse section (see composite sections 1, 2, 3 in Figure 4) exposes the structural framework just north of the relay between the southern normally dipping and the northern shallowly dipping slab segments (indicated in Figure 2 by the shift of the outer slab bends between transverse sections 7 and 5). Here, the High Plain of Bogotá occupies a depressed axial zone in which the pre-Cretaceous basement is slightly more elevated than the basement of the foreland areas. Its condensed syn- to post-kinematic Neogene sequences mark a starved basin since at least the Pliocene (Torres et al., 2005; van der Hammen et al., 1973). Upper Cretaceous to Paleogene sedimentites are involved in open folds of relatively short and uniform wavelengths, ranging from 5 to 10 km in width.

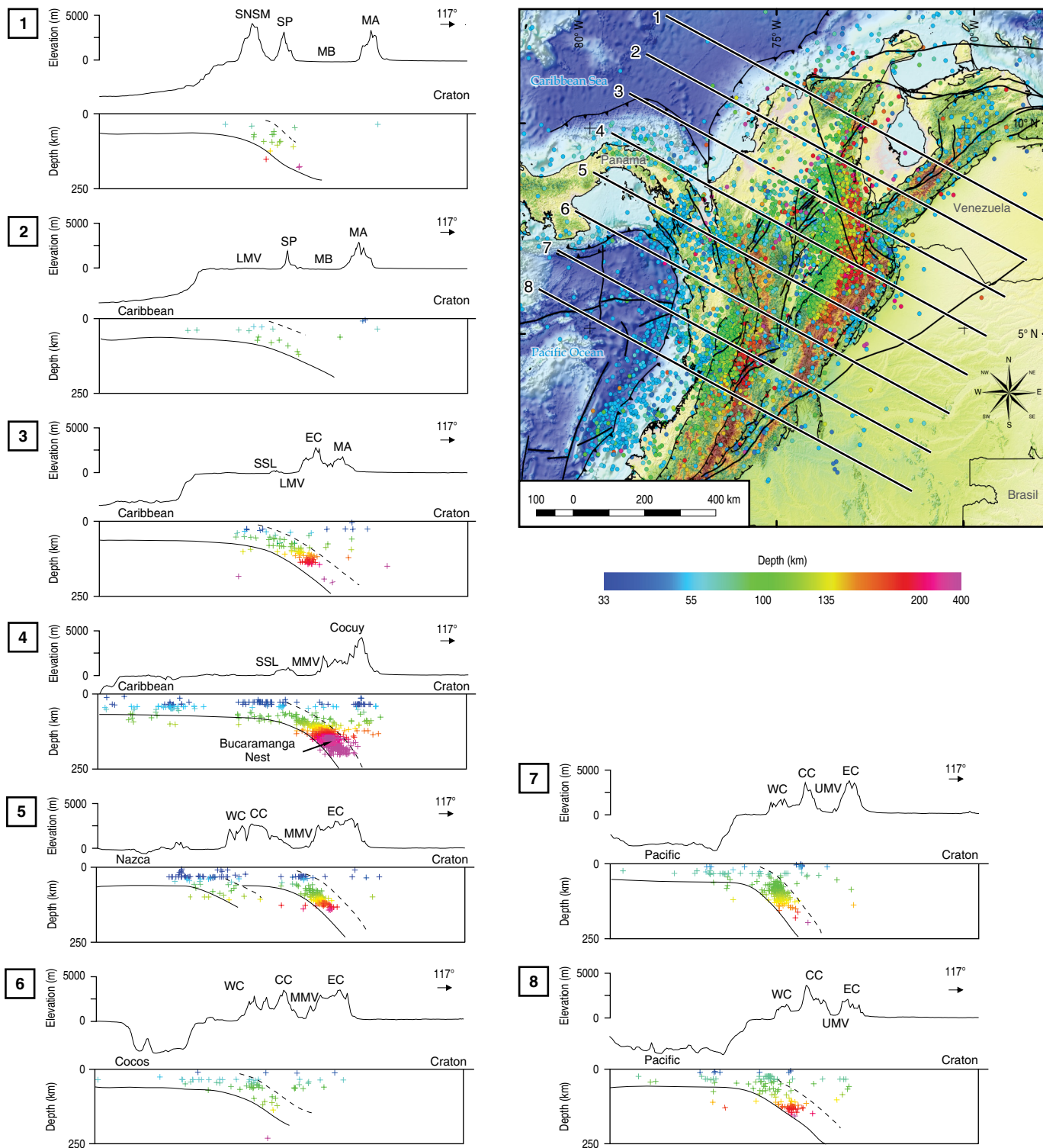


Figure 2. Tectono-morphologic map of northwestern South America with the distribution of the hypocentral solutions of >30 000 earthquakes extracted from the catalog of the Colombian National Seismological Network. The earthquake hypocenters are projected into 8 transverse sections to show the slab geometries. The highly exaggerated topography demarcates the Andean chains. Data compiled by Vargas & Mann (2013) and Chiarabba et al. (2015). (SNSM) Sierra Nevada de Santa Marta; (SP) Serranía de Perijá; (MB) Maracaibo Basin; (MA) Mérida Andes; (LMV) Lower Magdalena Valley; (MMV) Middle Magdalena Valley; (UMV) Upper Magdalena Valley; (SSL) Serranía de San Lucas; (EC) Eastern Cordillera; (CC) Central Cordillera; (WC) Western Cordillera.

The bounding marginal highs (the Villeta Anticlinorium to the west and the Montecristo Anticline to the east; Figure 4) expose Lower Cretaceous to upper Paleozoic sequences. Active modern (Pliocene or younger) deformation fronts are represented by the thrusts of the Guaicáramo and Cambao Faults (Figure 4), whose thrust sheets form minor frontal ranges at their leading edge.

The time frame for the formation of the eastern marginal high is given by a thick Oligocene to Pliocene clastic foreland sequence of a relict foreland trough, which is now folded and carried piggyback toward the foreland (see sections 2, 3 in Figure 4). Its clastic input records the exhumation of the Montecristo Anticline in detail, spanning an erosion window from Lower to Upper Cretaceous sedimentites. The final unroofing and deposition of Paleozoic marker clasts, however, was delayed until the deposition of the modern terraces in front of the Guaicáramo Thrust (Figure 4). They highlight a distinct foreland evolution without the formation of a depositional foredeep. This two-stage evolution involved the long-lasting build-up (Oligocene to late Miocene) of a mountain front with a structural relief of >10 km and its collapse as the frontal thrust stepped forward. The final exhumation of the Montecristo Anticline and the inception of the frontal Guaicáramo Thrust are thus closely linked, which is documented by the Pliocene/Pleistocene unroofing of the Paleozoic basement and an accelerated exhumation rate of >1 to 2 mm/y during the past 3 Ma for the Quetame Massif (location in Figure 3b; Mora et al., 2008, 2010a). The sequential processes of crustal thickening and foreland-directed expansion support the scenario of orogenic collapse (Rey et al., 2001).

A similar evolutionary sequence of a relatively stagnant mountain front and the Pliocene/Pleistocene breakdown by the activation of low-angle faults is thought to also apply to the western mountain front (Cortés et al., 2006). In section 1 (Figure 4), Oligocene to Miocene foredeep sedimentites are overthrust by the western flank of the Guaduas Syncline along the Cambao Fault. This thrusting entailed a westward shift of the Pliocene/Pleistocene accumulation space of the volcanoclastic Mesa Formation (Gómez et al., 2003).

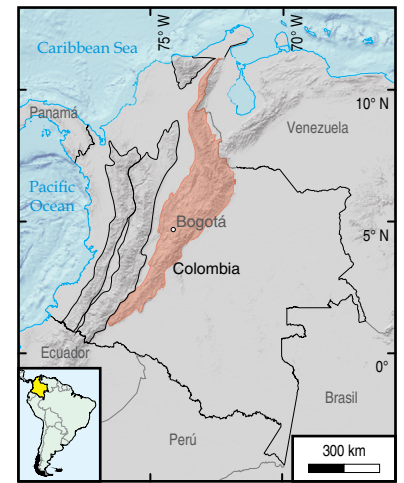
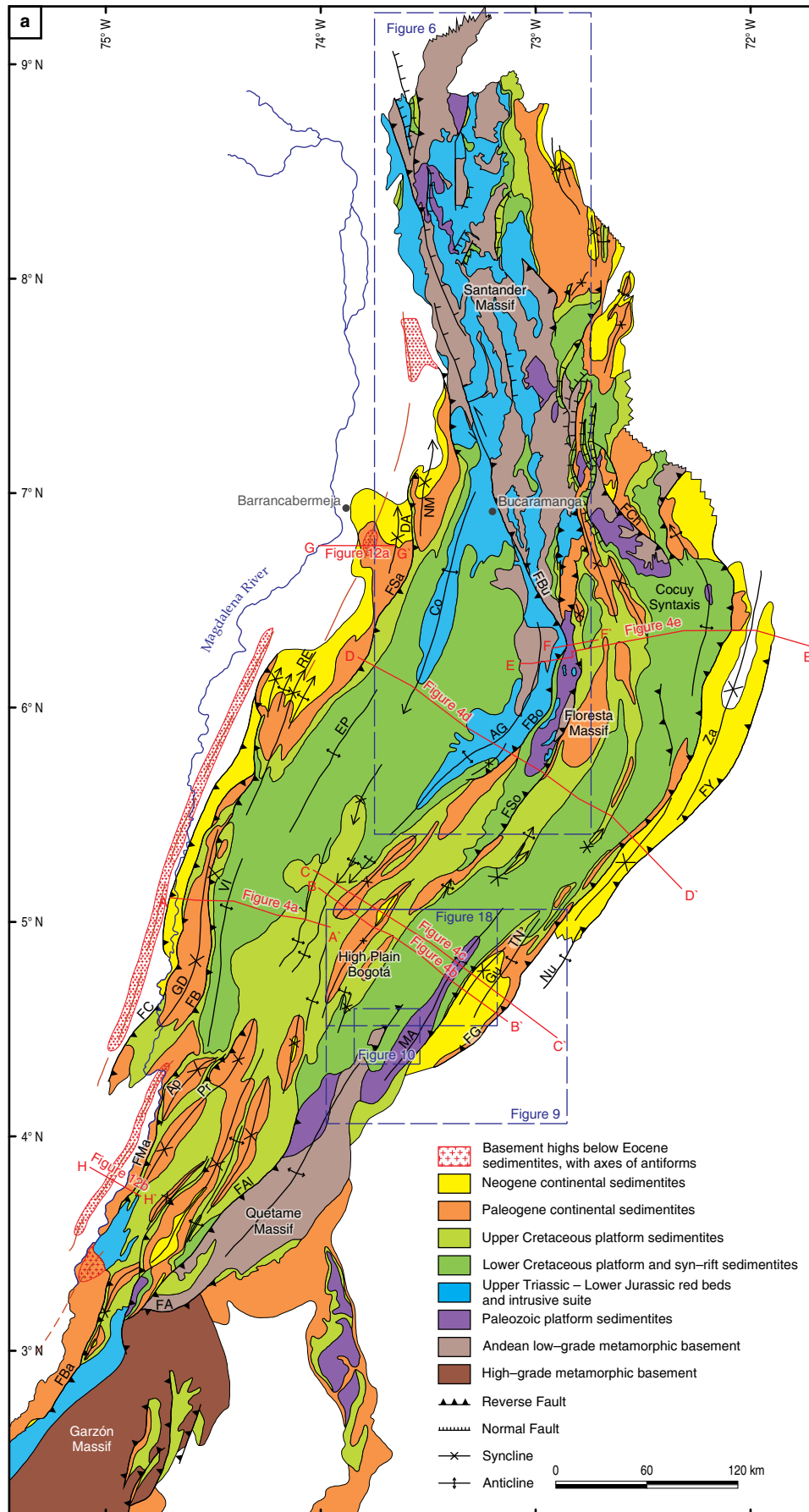
The Cretaceous to Paleogene sequences of the High Plain of Bogotá are affected by upright folds of relatively short wavelengths that, upon reaching the gently inclined flanks of this axial depression, assume a vergence toward the marginal highs (see sections 2, 3 in Figure 4). Within these flanks, deformation partitioning by buckling at higher structural levels and homogeneous shortening by cleavage formation at lower structural levels is observed (Kammer & Mora, 1999). These relations are documented in Figure 3b by the compilation of bed-parallel 2D-strain markers, such as deformed ammonites and brachiopods. Whereas the folded beds of the Paleogene and Upper Cretaceous units are virtually free of strain, strain markers at lower levels (Fómeque and stratigraphically lower formations;

Figure 5) record axial ratios of strain ellipses (R_s) of $1.2 < R_s < 1.6$ within both cordilleran flanks. Muddy lithologies display an axial plane cleavage at strains as low as $R_s = 1.2$. An important transitional zone combines flexural slip folding with axial plane cleavage, suggesting a deformation mode that combines folding and homogeneous shortening (Kammer, 1997).

The structural style of the central region north of the High Plain of Bogotá is explored by means of section 4 (Figure 4), which again pertains to lithospheric transverse section 5 (Figure 2). Uplift is centered on the composite axial highs of the Arcabuco Anticline and the Floresta Massif, both of which are bounded by reactivated faults in their eastern flanks. These faults may be assigned to the extensional horsetail structure at the termination of a Late Triassic precursor of the Bucaramanga Fault, which accommodated dextral displacement within an overall NW–SE extensional regime (Figure 6). The NE–SW-trending splay faults accumulated normal displacement, as documented by Late Triassic graben fills that contain thick alluvial fan sequences near the fault traces (Figure 6). The Lower Jurassic intrusive suite (Santander Plutonic Group with Early Jurassic crystallization ages; van der Lelij et al., 2016) is represented by sheet-like bodies emplaced along formerly tilted basement blocks (Figure 6b), which document a close relationship between faulting, block tilting, and intrusive activity. The syntectonic emplacement of this Lower Jurassic intrusive suite is further demonstrated at a right-stepping relay between two overlapping fault strands, which converged through a fault linkage by curved terminations. The eastern hook-shaped fault of this relay is intruded by the Río Negro Batholith, which is also part of the Santander Plutonic Group (Figure 6b).

The Cenozoic reactivation of these faults dates back to the late Eocene – early Oligocene, as documented by a Paleogene sedimentary fill of a small foreland basin (Concentración Formation; Figure 5) and thermochronological data (Bayona et al., 2013; Mora et al., 2010a, 2015; Parra et al., 2009b; Saylor et al., 2012). Fault reactivation resulted in the formation of asymmetric, fault-related folds with a distinct east-directed vergence or emergent faults displaying rim synclines in their hanging wall (Kammer, 1996).

These basement-cored antiforms form first-order structures, whereas second-order folds of minor widths (<8 km) are located on gently dipping domains on the western (west of the Los Cobardes Anticline; section 4 in Figure 4) and eastern flanks (e.g., Kammer, 1997). The eastern foreland structures involve an imbricated stack of folded slices, the geometry of which was unraveled in detail by exploration campaigns of the oil industry (Jiménez et al., 2013; Martínez, 2006). Their gradual, foreland-directed decrease in fold amplitudes, and fold widths compares to analog experiments, where a decay in fold shape was produced by a push from the rear (Price, 1975). The juxtaposition between the intensely sliced deformation front and the undeformed Llanos Block highlights the contrasting



Eastern Cordillera of Colombia

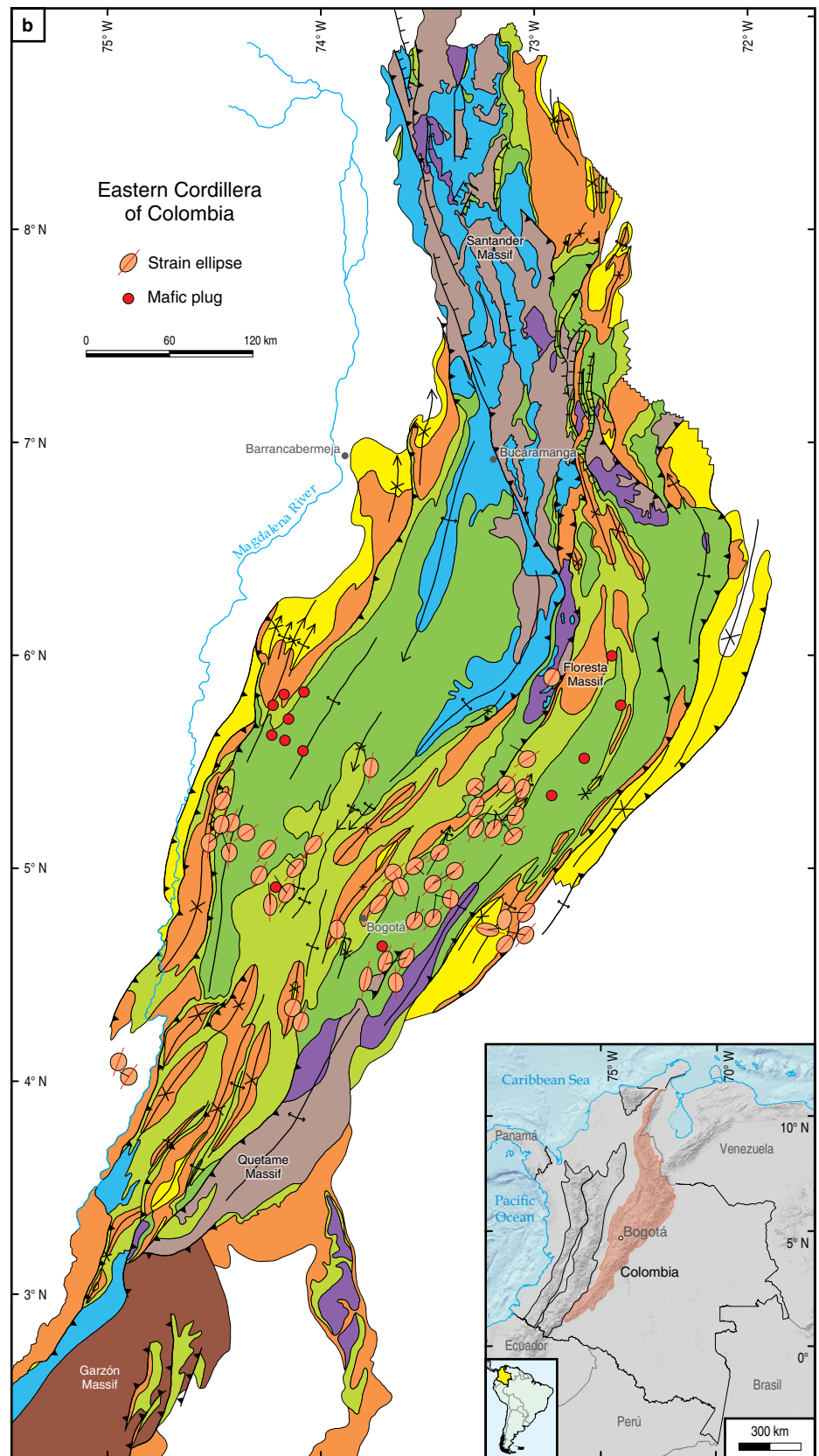
Faults

- FB: Bituima Fault
- FBa: Boyacá Fault
- FBu: Bucaramanga Fault
- FC: Cambao Fault
- FCh: Labateca Fault
- FG: Guaicáramo Fault
- FMa: Magdalena Fault
- FSa: La Salina Fault
- FSo: Soapaga Fault
- FY: Yopal Fault
- FBa: Baraya Fault
- FA: Algeciras Fault
- FAI: Altamira Fault

Folds

- AG: Arcabuco–Guantiva Anticline
- Ap: Carmen de Apicalá Syncline
- VI: Villeta Anticlinorium
- RE: Rio Ermitaño Syncline
- Co: Los Cobardes Anticline
- EP: El Peñon Anticline
- Ma: Montecristo Anticline
- Gd: Guaduas Syncline
- Gu: Guavio Anticline
- NM: Nuevo Mundo Syncline
- DA: De Armas Syncline
- Pr: Prado Syncline
- TN: Tierranegra Anticline
- Za: Zamaricote Syncline
- Nu: Nunchía Syncline

Figure 3. (a) Geological map of the Eastern Cordillera. Lines A–A' to E–E' indicate the locations of the partial and composite transverse sections shown in Figure 4. The dashed blue squares depict the location of the geological maps in Figures 6, 9, and 18. **(b)** Map of strain ellipses and mafic dikes and plugs. The ellipses are derived from deformed fossils and record bedding-parallel strains. Mafic plugs and dikes are restricted to Lower Cretaceous host units and occur in the western and eastern flanks of the EC, respectively.



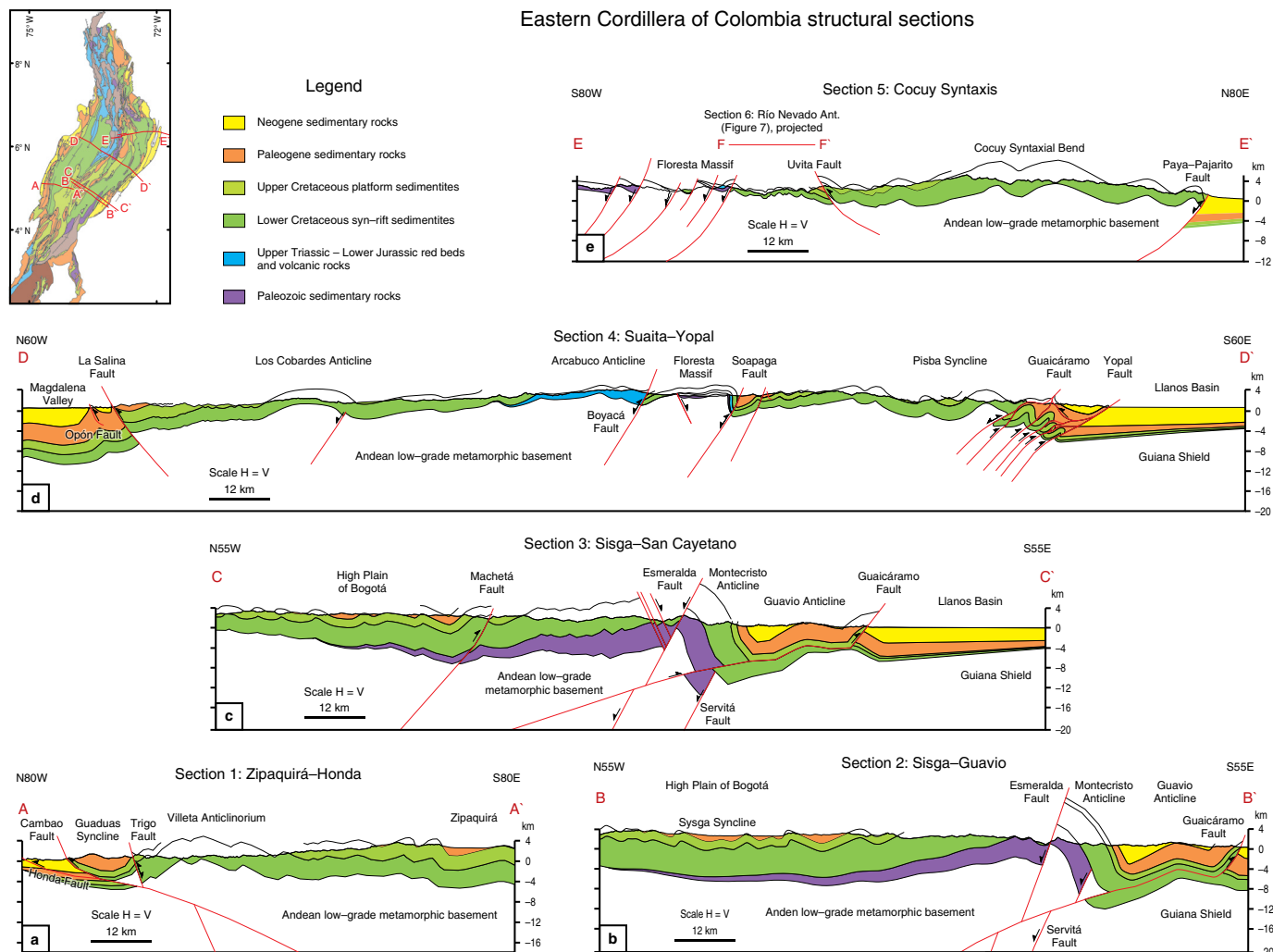


Figure 4. Composite and total transverse sections of the middle segment of the Eastern Cordillera. Locations are given in Figure 3a.

rheology between the cordilleran basement and the shield, which suggests that the latter behaved as a rigid backstop.

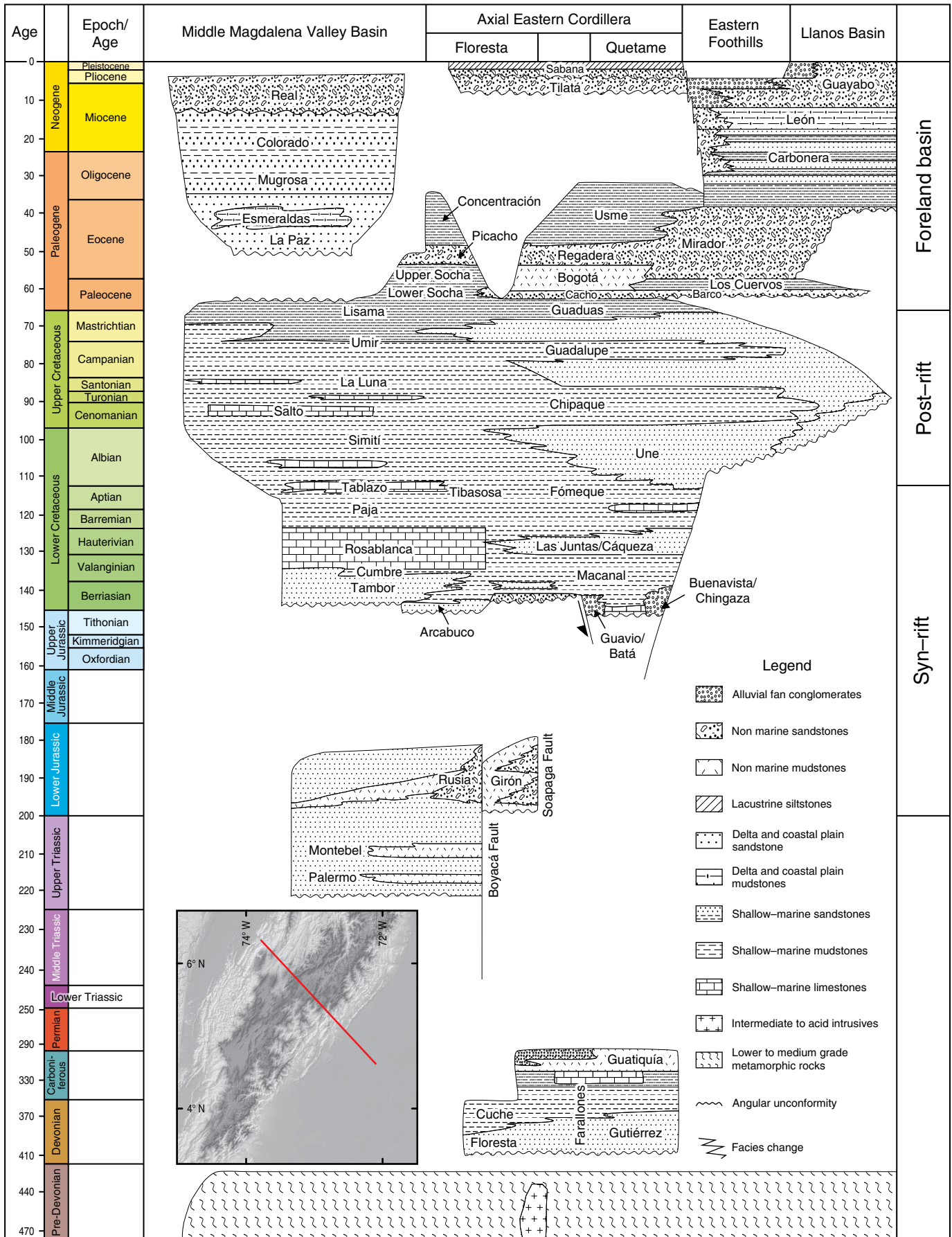
Internal rock deformations deduced from strain markers are mild along the anticlines, that form the backbone of the axial region ($R_s < 1.2$; Figure 3b). The domains affected by second-order folds on the western and eastern flanks display an axial-plane cleavage suggesting strain ratios of $R_s > 1.2$.

Several aspects of the structural style at the junction between the middle segment of the EC and the Santander Massif are shown in cross-section 5 (Figure 4). According to the exceptional topographic relief at the Cocuy Syntaxis, the outer bend of the subducting slab reaches its eastern-most position in this area, as documented by lithospheric transverse section 4 (Figure 2). This section is divided into three parts: a western part that exposes Jurassic batholiths and upper Paleozoic cover in the continuation of the Floresta Massif; an intermediate, intensely folded structural depression, that preserves a

condensed sequence of the Lower Cretaceous succession (Tibasosa to Une Formations, which are <1100 m thick; refer to the stratigraphic chart in Figure 5); and the eastern up-domed syntaxial bend, in which the thickness of this same Lower Cretaceous succession reaches 4700 m.

The salient structural features are closely related to the exhumation ages. The Floresta Massif and the northern Mogotes High expose pre-Cretaceous basement units at a structural level comparable to that of the Cocuy Syntaxis, though denudation reached a more advanced stage in the former areas. Accordingly, exhumation started in the western part in the late Eocene/early Oligocene and was followed by a second early Miocene pulse (Mora et al., 2015). The basement units are compartmentalized by extensional block tectonics with normal faults linked to the Late Triassic dextral precursor of the Bucaramanga Fault. These faults do not record Neogene reactivation, which implies an uplift mechanism by wholesale lithospheric buckling.

Figure 5. Stratigraphic chart of the southern and middle parts of the Eastern Cordillera, including the Llanos Foothills and the Middle Magdalena Valley. Modified from Mora et al. (2010b).



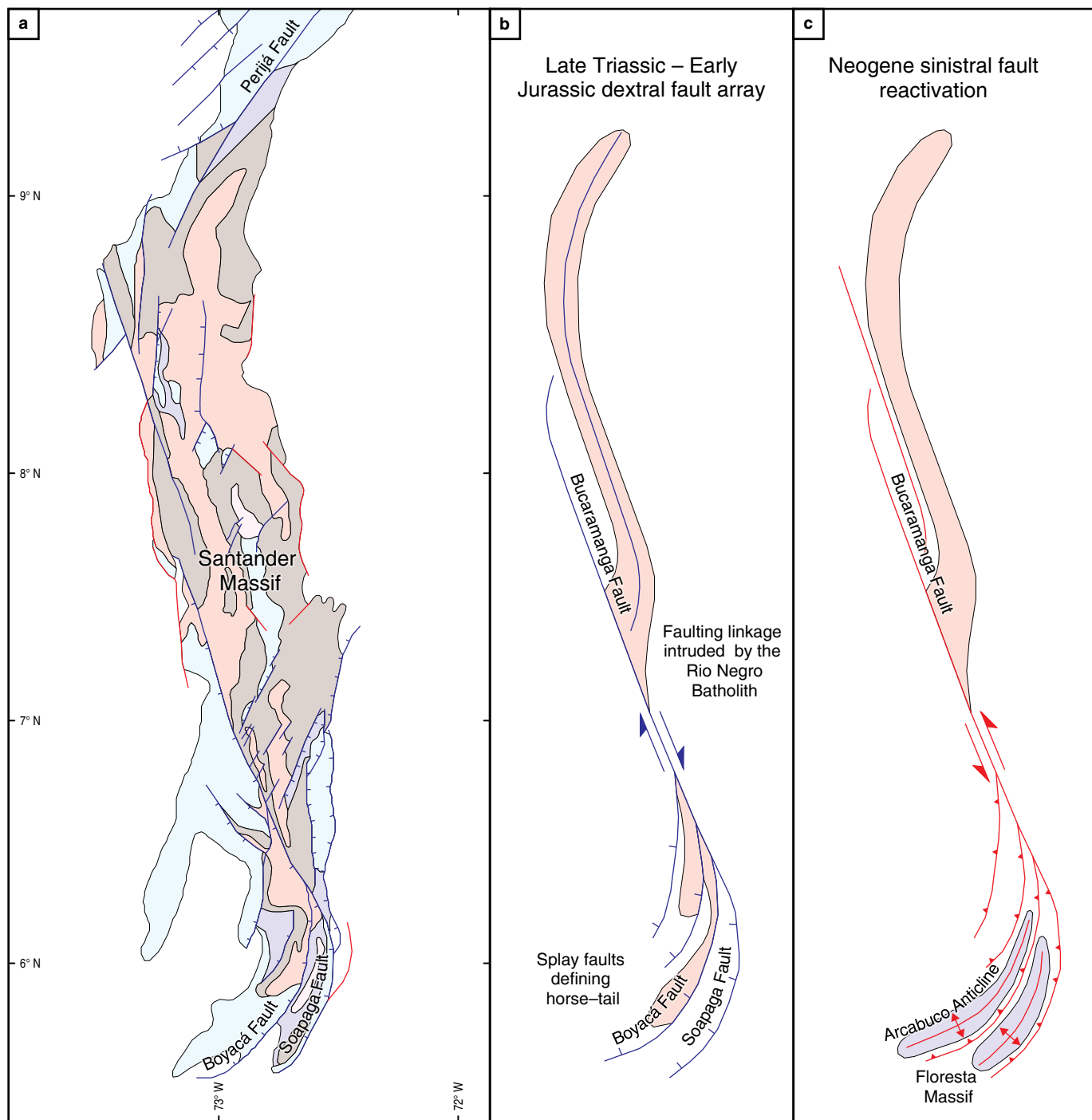


Figure 6. (a) Geological map of the Santander Massif and its southern connection to the middle segment of the Eastern Cordillera. Late Triassic – Early Jurassic faults are highlighted in blue and record a NW–SE extensional setting. The red faults are attributed to the Neogene uplift of this massif. Sketch (b) depicts some of the structural relations between the Santander Plutonic Group and the continental red beds with respect to a dextral ancestor Bucaramanga Fault and subsidiary splay faults. Sketch (c) illustrates the consequences of dextral fault reactivation under a Cenozoic NW–SE contractional deformation regime.

The Cocuy Syntaxis comprises slightly-deformed sequences, which is concluded from the absence of an axial plane cleavage in the Lower Cretaceous sequences. Its western monoclinial flank contains upright folds within the Lower Cretaceous units. Further up-section, their axial planes turn into a sub-horizontal attitude and folds show, inclusively, a down-dip vergence (the scale of section 5 does not allow for the documentation of these details), which suggests that the folding was partially driven by gravity. In the lower part of this flank, the sedimentary sequence is offset by backthrusts (shown in section 5 in Figure 4 by the Uvita Fault). Thermochronological data from the Lower Cretaceous units indicate a late Oligocene/early Miocene onset of exhumation (Mora et al., 2015).

The strongly folded, intermediate part records complex deformation patterns that are best unraveled with respect to a central, tightly folded syncline, which is referred to as Chicamocha Syncline in section 6 (Figure 7). Within the Lower Cretaceous succession, the fold vergence converges from both the Floresta Massif to the west and the monoclinial western flank of the Cocuy Syntaxis. The minor Chicamocha Anticlinorium of the latter flank is contains west-verging folds and displays an incipient, steeply inclined axial plane cleavage within the upper Paleozoic basement units with brachiopods affected by bed-parallel strains of $R_s = 1.2$. In the Upper Cretaceous units, the axial planes fan into a flat attitude, and the folds become increasingly angular. Chevron folds on the opposite (western) flank of the Chicamocha Syncline display a similar down-dip vergence (Figure 7). With regard to this composite fold pattern, the Chicamocha Syncline can be compared to a central syncline (analogous to a pinched “keel” of a Proterozoic structural setting) encased between two vertically rising anticlines, in which the vertical stretching of a core gradually flattens and merges with the axial planes of the enclosing cascading folds. Similar deformation styles typify fold patterns around diapirs, as experimentally shown by Dixon (1975).

The structural change from a plateau-like axial depression in the south to fault-controlled basement-involved and large antiformal lobes further north as well as the concomitant topographic increase may be compared with recently determined Moho depths, which have the greatest values approaching 60 km beneath the High Plain of Bogotá and smaller values of 45–55 km approaching the northern part of the study region (Poveda et al., 2015). By relating these depths to the degree of isostatic compensation, we conclude that isostatic compensation decreases as the topographic relief becomes more significant. This situation may indicate increased slab support in the northern sections.

Table 1 shows the shortening values for each section, which were deduced from a combination of line-length balancing and the de-straining of layers according to R_s values extrapolated from strain markers. Our strain analysis is still a preliminary

approximation and should be refined by textural 3D measurements. Even though, when the strain data are incorporated in the line-length balancing, our shortening estimate of approximately 65 km defines a lower bound with respect to other published shortening values of 70 to 80 km (Cortés et al., 2006; Mora et al., 2008; Teixell et al., 2015; Tesón et al., 2013). These disparities can be attributed to different assumed dips of the marginal faults and the preferred deformation style (shortening by thrusting vs. shortening by folding).

By considering a horizontal shortening of 65 km and averaging it over a time interval of 30 Ma, we obtain a mean shortening rate of 2.2 mm/y. This value is substantially lower than the present rate of 4 mm/y derived from GPS measurements (Mora-Páez et al., 2016). This discrepancy may be resolved by the assumption of an increased neotectonic displacement transfer to the hinterland.

4. Cretaceous Back-Arc Evolution

Knowledge of the geometry of the Cretaceous back-arc basin and its Neogene inversion is crucial for any attempt to restore the folded and faulted strata of the cordillera. The relative importance of rift basin inversion (equivalent to basement-involved shortening) and shortening by the stacking of decoupled supracrustal slices (Colletta et al., 1990; Cooper et al., 1995; Dengo & Covey, 1993; Roeder & Chamberlain, 1995) can only be evaluated by obtaining insight into the geodynamic significance of the inherited faults. For these reasons, we review the latest Jurassic to Early Cretaceous (Tithonian to Valanginian) rifting event.

Two scenarios provide possible tectonic frameworks for the inception of rifting: (1) Crustal stretching related to passive margin evolution that may have prevailed during the Early Cretaceous, before the initiation of a Cretaceous subduction cycle (Pindell & Kennan, 2009). Thinning would have been guided by tensional plate-parallel stresses, and regional breakaway faults would be expected to separate stretched crustal domains from undisturbed regions (Wernicke & Axen, 1988). (2) Rifting associated with an ascending thermal plume with the consequent thinning of the lithosphere mantle by upward displacement of its thermal boundary. This second alternative complies with an active margin setting (Faccenna et al., 2010; Hardebol et al., 2012).

To evaluate these hypotheses, we first re-examine the thermal subsidence curves developed by Sarmiento-Rojas (2001) and Sarmiento-Rojas et al. (2006). We consider a time interval from the Tithonian (i.e., the onset of a rift-related subsidence) to the Aptian (150 Ma to 115 Ma), epoch after which fairly uniform depositional conditions became established across the back-arc basin, as indicated by the near-shore depositional environments of the Une Formation, which prograded from the present Llanos Foothills toward the present axial part of the EC (Figure 5).

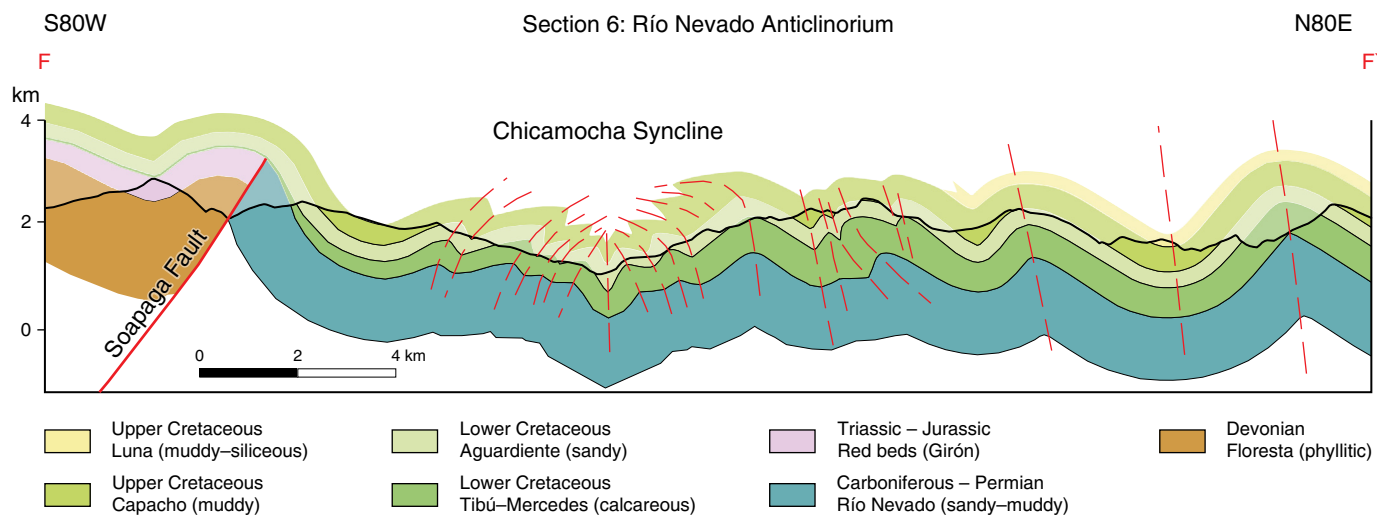


Figure 7. Folds of the Río Nevado section in the central part of the transverse section (Figure 4). The Chicamocha Syncline separates fold trains of different vergences. The axial plains deflect from a sub-vertical attitude at lower structural levels to a sub-horizontal attitude at higher structural levels on either side of the syncline. The Soapaga Fault acted as a graben-bounding fault for the Upper Triassic/Lower Jurassic red beds, and it was not reactivated during folding.

Table 1. Shortening values of the sections shown in Figure 4.

Section	Original length (km)*	Deformed length (km)	Shortening distance (km)	Extension (%)
1. Sisga-Guavio (section A-A')	160.728	128.575	32.153	-20.0
2. Zipaquirá-Honda (section B-B')	127.127	96.358	30.769	-24.2
3. Sisga-San Cayetano (section C-C')	170.406	135.504	34.902	-20.5
4. Suaita-Yopal (section D-D')	295.748	233.714	62.034	-21.0
5. Cocuy (section E-E')	123.143	97.305	25.838	-21.0

*The original lengths have been corrected by the strain values estimated from bed-parallel shortening assuming plain strain conditions.

An architectural framework for this back-arc basin is provided by two marginal troughs, which are referred to as the Magdalena-Tablazo and Cocuy Sub-basins (Fabre, 1983; Sarmiento-Rojas, 2001) and whose depocenters are located close to the Miocene mountain fronts of the present EC. An intervening depositional high coincides with the present Floresta Massif and its southern continuation (Figure 8). Typically, subsidence curves constructed for these sub-basins have a knickpoint between fast (>50 m/Ma) and slow (5 to 15 m/Ma) subsidence rates. These knickpoints lie within the Hauterivian and Barremian, as shown by shaded bars in Figure 8. The peak rates along the marginal troughs approach 100 m/Ma for the Neocomian and may indicate an active rift stage (Figure 5). For the southern Cocuy Sub-basin, however, we find evidence that fault activity was restricted to the Tithonian and Berriasian, as discussed below. In close agreement to elevated subsidence rates, marginal troughs record deeper depositional environments until the Barremian (Polanía & Rodríguez, 1978), suggesting some independence between fault activity and subsidence. The facies associations related to elevated subsidence rates comprise mass

flow and turbidite deposits with paleocurrent indicators oriented parallel to the marginal troughs (Dorado-Galindo, 1992; Pimpirev et al., 1992; Moreno-Murillo, 1991; Sarmiento-Rojas, 2001).

Important clues for the Cretaceous back-arc evolution are provided by mafic sills and minor stocks that were emplaced within Aptian to Albian successions on the western flank and Berriasian host units on the eastern flank, where they form a linear trend (Figure 3b; Fabre & Delaloye, 1983; Moreno-Murillo & Concha-Perdomo, 1993; Vásquez et al., 2010). $^{40}\text{Ar}/^{39}\text{Ar}$ plateau ages obtained from primary plagioclase and hornblende yielded a large range of ages from 136 to 74 Ma (Vásquez et al., 2010). This temporal range exceeds the previously defined periods of elevated subsidence (or “active” rift stage). The mafic intrusions are compositionally heterogeneous and define two different series: a trend similar to alkaline ocean island basalts and a tholeiitic trend with characteristics of mid-ocean ridge basalts. The trace-element patterns are enriched in light rare earth elements (LREE) and display high Ba/Nb and Sr/P ratios, which comply with a possible supra-subduction setting (Vásquez et al., 2010).

Subsidence curves for Eastern Cordillera

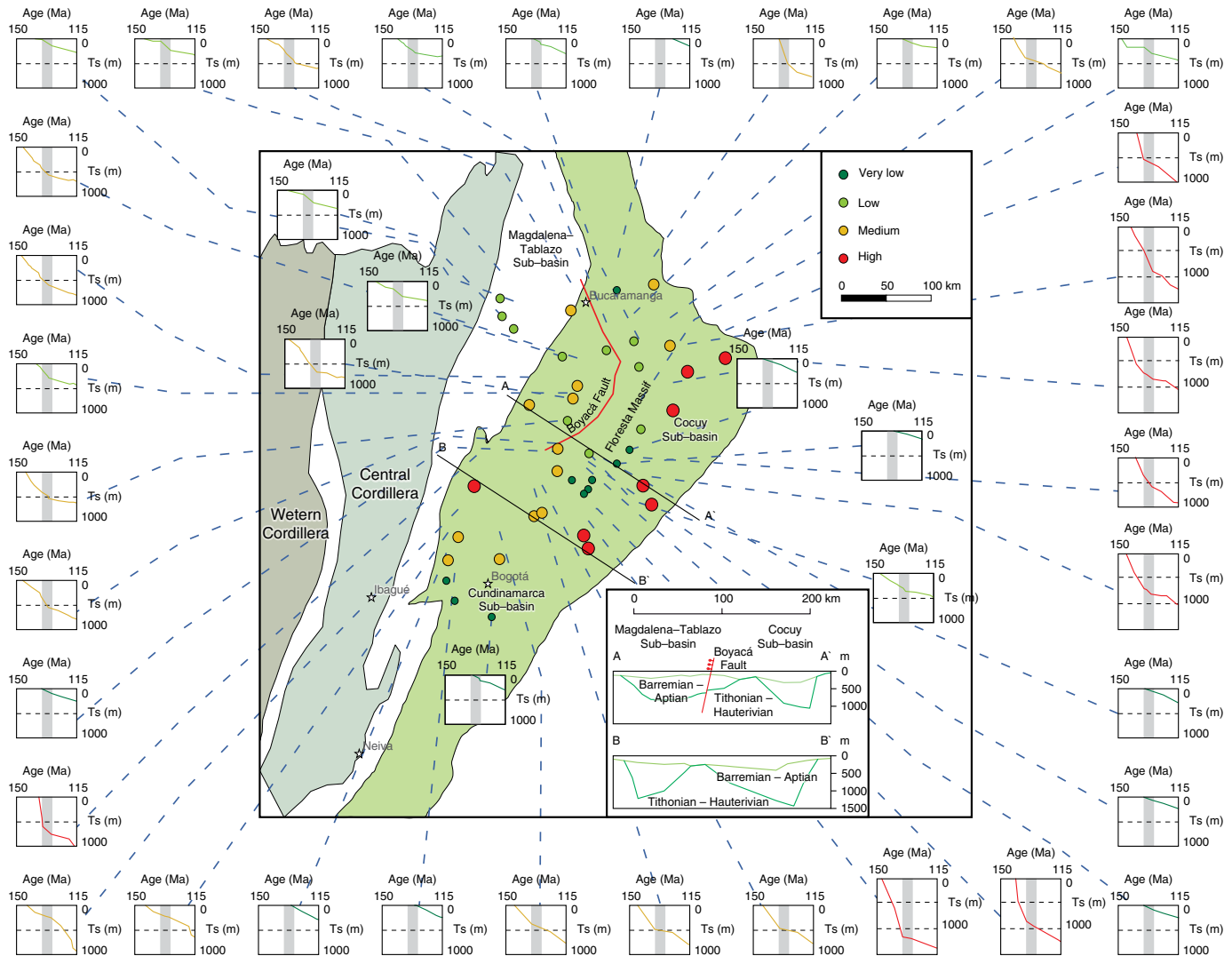


Figure 8. Site map of the Eastern Cordillera showing the locations of the stratigraphic columns for which tectonic subsidence curves were derived (modified from Sarmiento-Rojas, 2001). The tectonic subsidence (Ts) is plotted in small insets for representative stratigraphic profiles and covers an age range from 150 to 115 Ma (Tithonian to Aptian). Lines A-A' and B-B' indicate transverse sections of tectonic subsidence, as plotted in the large inset, in which we differentiate between a Tithonian–Hauterivian “syn-rift” and a Barremian–Aptian “post-rift” subsidence stage.

5. Structural and Sedimentological Evidence for Rift Events at the Eastern Mountain Front

The southern part of the eastern Miocene mountain front exposes upper Paleozoic sequences of an inverted marginal rift basin and the previously discussed Early Cretaceous basin fill of the Cocuy Sub-basin. We present arguments for a Neocomian fault-related subsidence cycle linked to a basal sequence of the Lower Cretaceous syn-rift successions.

5.1. The Late Paleozoic Servitá Fault

The Servitá Fault forms a rheological boundary between the folded Andean-type basement and the nearly undeformed Guiana basement. Its age and normal nature are readily deduced from a Late Devonian to an early Carboniferous rift fill, which is referred to as the Farallones Group (Figure 5; Bürgl, 1960; Stibane, 1967). With regard to its length (>150 km), this fault is comparable to the similarly NNE-trending Palestina Fault of the Central Cordillera (Feininger et al., 1972). Its graben fill

exceeds 3000 m in the proximal region near the fault trace but tapers significantly further west (see sections 2, 3 in Figure 4). The shield area only records an early Paleozoic rift event (Feo–Codecido et al., 1984), and the reported thicknesses of the upper Paleozoic sequences do not exceed 200 m (Dueñas & Césari, 2005). This late Paleozoic extensional setting might be linked to the Late Triassic extensional attenuation of the Andean margin (Riel et al., 2018; Spikings et al., 2015).

The fault plane is mostly concealed by the folded Cretaceous cover along the eastern flanks of the marginal highs (see sections 2, 3 in Figure 4). Evidence for the existence of an important crustal discontinuity is provided by the juxtaposition of cordilleran marginal highs that preserve the Farallones Group in their hinge areas and the more foreland-oriented basement-cored anticlines, where Paleozoic sedimentites are absent (as shown by anticlines immediately west of Villavicencio and further to the southwest; Figure 9).

5.2. Early Cretaceous Extensional Tectonics of the Guavio Region

Of the two marginal troughs of the Cretaceous forebulge, the eastern one deserves special attention because of its well-exposed graben structure in the Guavio area. To the east, this basin is bounded by two master faults, which currently displace the Toquiza and Montecristo Antiforms (Toquiza and Esmeralda Faults; Figure 9). These faults are discontinuous and define a left-stepping array (Figure 10b). Their western hanging-wall blocks are compartmentalized by secondary antithetic faults that curve into an N–S trend to the west of the relay zone (Figure 10b). Next, we re-examine the rift fills of these sub-basins and highlight their paleogeographic setting based on the work of Terraza et al. (2008), Mora et al. (2009), and proper observations.

Biostratigraphic determinations of ammonites indicate a Tithonian to Berriasian depositional interval for the graben fills (Haas, 1960; Terraza et al., 2008), which indicates a relatively short-lived transgressive–regressive cycle. This fault-related sequence is termed collectively as the Guavio Formation (Figure 10c; a more differentiated nomenclature is used by Terraza et al., 2008). The crests of the footwall blocks of the Toquiza and Esmeralda Faults separated this faulted sub-basin from a possibly unfaulted eastern sub-basin, where the coeval Batá Formation was deposited (Figure 10b, 10c). The sedimentites of these basal sequences are overlain by the Valanginian shaley Macanal Formation via inundation surface (Figure 10c). In the Guavio area, the basal strata of this latter unit comprise small-scale fining-upward depositional cycles with ripple laminations, which indicate a turbiditic depositional regime. The high subsidence rates of this marginal forebulge area thus outlasted the fault-related rift stage, according to our previous subsidence analysis.

The asymmetric nature of the composite rift fills west of the Toquiza–Esmeralda Faults is highlighted by a 50 m isochore

and a pinch-out line (Figure 10b). The block geometry of the minor sub-basins closely correlates with the thickness and facies variations of the measured columns (Figure 10a). A cursory inspection of the facies distribution (Figure 10c) reveals that (1) calcareous and evaporitic lithologies (facies associations G3 and G5; Table 2) increase in importance toward the western margin, and (2) evaporitic associations are ubiquitous in the basal transgressive layers and also predominate in the uppermost unit (facies association G3).

More specifically, facies association G1 (Table 2) comprises a basal mono- to polymict breccia composed of reworked dolostones of facies association G3 as well as quartz fragments and strongly altered sandstone blocks of the Farallones Group. Where it was deposited on faulted blocks along major faults, this basal breccia is several tens of meters thick. Association G2 contains pebble-cobble conglomerates, which are composed of sandstone and limestone fragments embedded in a sandy to muddy groundmass. The beds display trough and inclined stratification, in which conglomeratic sands alternate with sandy muds (“inclined heterolithic” stratification; Thomas et al., 1987). Facies association G3 comprises dolomitic mudstones and laminated dolostones with slightly contorted and variably brecciated laminae of microbial origin (algal mats). This sequence displays isolated to coalesced nodules that, where associated with a strongly contorted lamination, define enterolithic layering (Mora et al., 2009). G4 is a thinly layered, heterolithic mud-sand sequence with linsen and flaser structures that include layers of bivalve shells. G5 comprises mudstones and wackestones with bivalve shell fragments. Below the contact with the Macanal Formation, these sequences are overlain by dolostones of a recurrent G3 association.

The basal breccias and ensuing conglomerates (G1 and G2) are interpreted to represent a transgressive conglomerate above a Paleozoic ravinement surface on down-dropped fault blocks. Considering the remnants of reworked evaporates (G3), we may conclude about a restricted freshwater supply in this likely estuarine environment. This transgressive depositional cycle culminated with the deposition of tidally influenced mudstones (G4) but reverted to a regressive environment with the deposition of limestones and dolostones of salt marsh deposits (uppermost G3). Fault activity ceased at the onset of the ensuing transgressive cycle of the Macanal shales, which buried and sealed the faulted blocks and faults.

The Batá Formation forms a synchronous (Etayo–Serna et al., 2003) but compositionally independent lithic unit with respect to the Guavio Formation. It begins with a basal breccia made up of clast-supported cobble-sized sandstone and bright limestone fragments (<1%). Red sandstone fragments derive from variegated sandstone units and bright limestone pebbles derive from caliche concretions of the adjacent Farallones Group, which likely had undergone erosion at the crests of the fault blocks (Figure 10c).

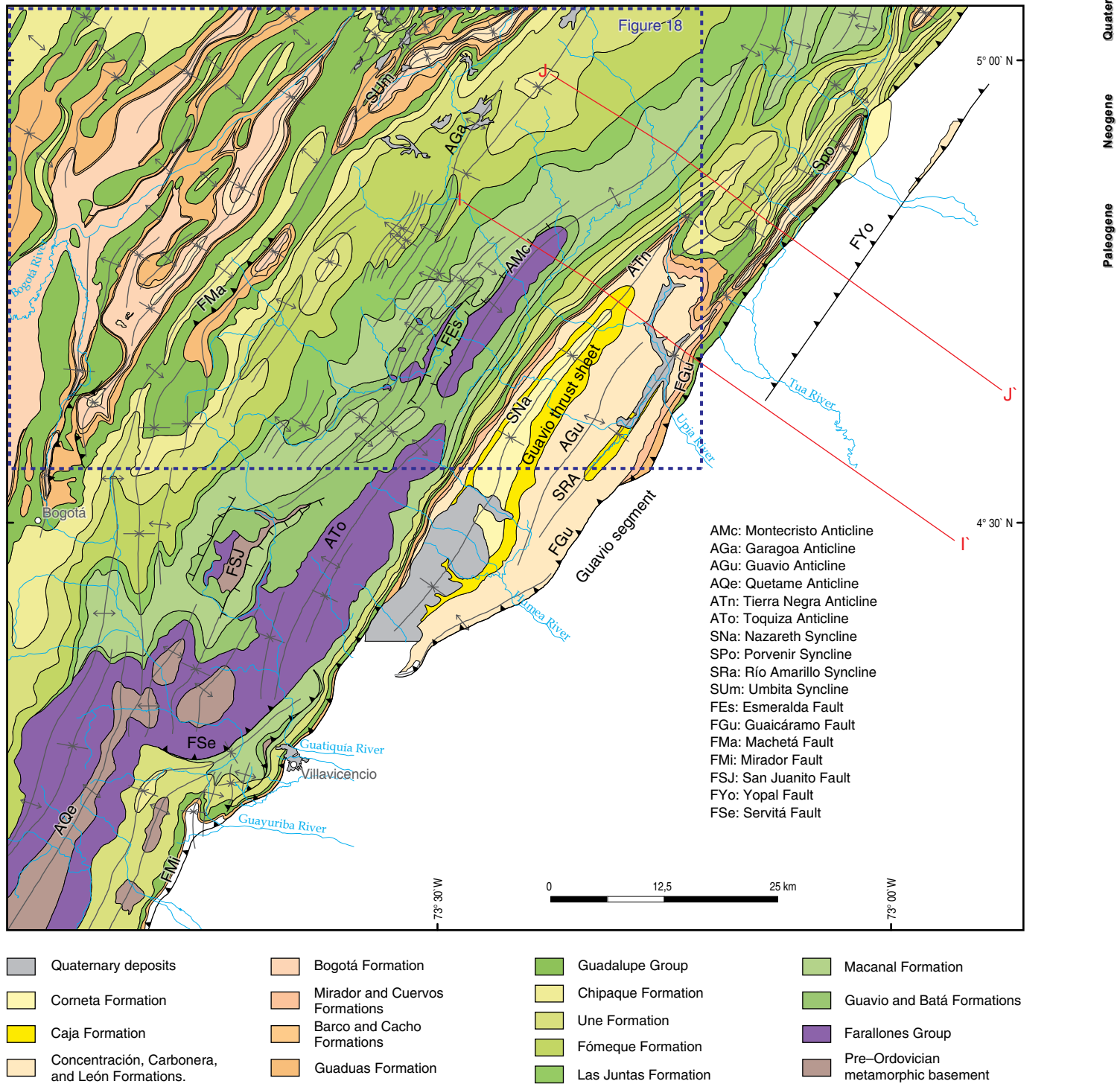


Figure 9. Geological map of the eastern flank and foothills of the EC. The red lines indicate the structural sections in Figure 13. For the map location, refer to Figure 3a. The blue rectangle depicts the outline of the map shown in Figure 18.

The succeeding conglomeratic sequence consists of amalgamated, medium-sized beds separated by thin muddy layers. The conglomeratic beds become thinner up-section and alternate with shaley intercalations. At the outcrop scale, the conglomeratic beds are planar or lenticular, lack sorting, and may have been affected by fluidization processes, to con-

clude from irregular contours and necking. The grain size variations of the conglomeratic beds reveal reverse grading or a combination of reverse and normal grading. We associate these beds with concentrated, non-cohesive flow units that may have settled in a delta complex (Haughton et al., 2009; Talling et al., 2012).

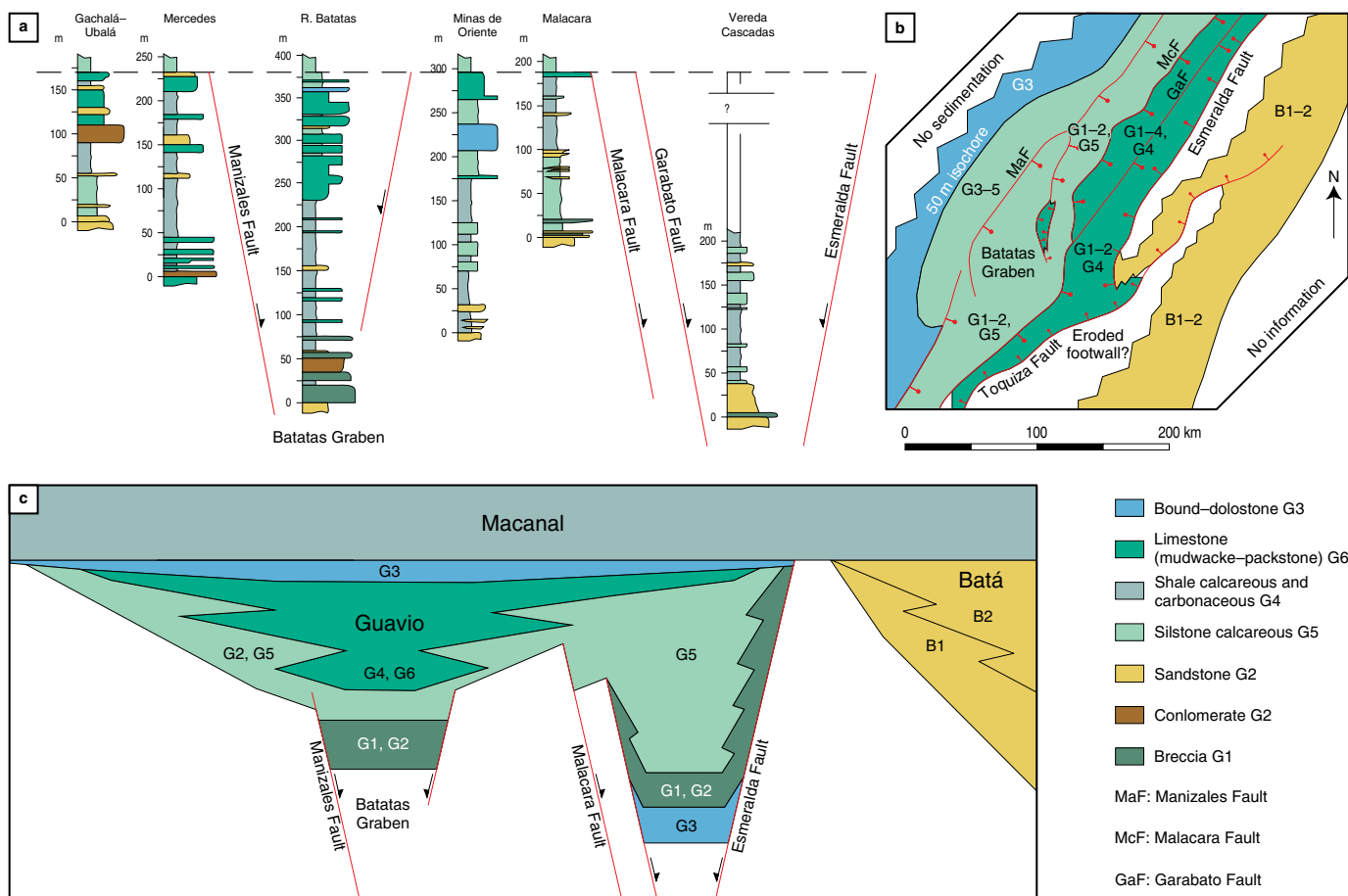


Figure 10. Palinspastic map of the Guavio area with stratigraphic columns in different structural settings. **(a)** Stratigraphic columns. **(b)** Palinspastic map. **(c)** Facial architecture projected into an E-W section.

Table 2. Facies associations and environmental interpretations of the Guavio Formation and the basal conglomeratic unit of the Batá Formation.

FA	Lithologies and principal structures	Interpretation
G1	Poorly sorted, clast-supported breccia with quartzose and lithic fragments.	Transgression lag on a Paleozoic ravinement surface.
G2	(1) Cobble-pebble conglomerate with sandy groundmass and sandstones; trough cross-stratified, scoured bases; or (2) inclined (heterolithic) stratification.	Fluvial to estuarine deposits of a drowned valley, variably influenced by tidal action.
G3	Calcareous or dolomitic shale, laminated or variably brecciated, with pseudomorphs of gypsum crystals and intercalated nodular layers (discrete and coalesced nodules), locally contorted into enterolithic folds; desiccation cracks.	Supratidal algal flats and salt marshes; inter- to supratidal dolostone/limestone beds with gypsum crystals.
G4	Carbonaceous shale with disseminated plant remains and bivalves, the latter including disarticulated shell layers; thinly bedded alternations of sandstone, siltstone, and mudstone layers with linsen-flaser laminations; bioturbation.	Upper and lower reaches of tidal flats and lagoonal deposits; intercalated tempestite beds.
G5	Wackestones and bivalve packstones with well-sorted shell fragments.	Shelf sediments above the base level of storm influence.
B1	Polymict breccia with clast-supported sandstone, quartz, limestone and pedogenetic fragments; variegated muddy groundmass.	Debris flows with few abraded components that derive from sub-aerial erosion of the Paleozoic substratum.
B2	Cobble-pebble conglomerate with a sandy groundmass in tabular to lenticular, medium-sized beds, alternating with sand- and sandy mudstones. The components of the conglomerates are unsorted and may display reverse or combined reverse-normal grading. The conglomeratic beds are affected by fluidization.	Gravity flows in slightly confined channels of a delta complex.

FA—Facies association.

In conclusion, the activity of the Toquiza–Esmeralda Fault System was relatively short-lived and did not exceed 10 my in time (accumulated period of the Tithonian and Berriasian). The composite footwall block separated an eastern marginal area from an intensely faulted western domain. In the western domain, a marine incursion was channeled into structural depressions, giving way to an estuarine depositional environment (Dalrymple & Choi, 2007). The abundance of supratidal evaporitic deposits (facies association G3) argues for a limited fluvial freshwater supply and temporarily suppressed connections to a major seaway, which led to significant brine concentration (Einsele, 1992). As the fault activity ceased, these marginal seaways retreated. Subsidence of the Valanginian successor basin was likewise high, although fault activity came to a standstill, and gave rise to the contrasting subsidence pattern between the marginal troughs and the forebulge high.

6. Time Frame of the Cenozoic Folding

Knowledge of the onset of the Neogene folding phases is closely related to the question of whether the cordillera was formed by migrating (or sequentially eastward-progressing) deformation phases, which implies a diachronous evolution of the mountain fronts and flexural foreland troughs, as envisioned by Villamil (1999), Gómez et al. (2005a) and Parra et al. (2009b), or whether it has acquired its bilateral architecture since the early Neogene. The latter scenario would be supported by concurrent or equally distributed deformation phases. Combining these scenarios, the first orogenic stage could have involved an eastward progression of deformation that was followed by wholesale shortening (Mora et al., 2015).

Thermochronological modeling provides evidence for an initial Paleogene cooling (comprising an interval of 50–30 Ma) within the Guaduas Syncline and the Floresta Massif (for locations see Figure 3a and sections 1 and 4 in Figure 4; Parra et al., 2009b). Clues for deciphering first Paleogene crustal perturbations are provided by the foredeep sediments of relatively narrow basins, as exemplified by the foreland basins straddling the eastern mountain front (Parra et al., 2009a), the Floresta Massif (Saylor et al., 2011) and some intrabasinal depocenters of the High Plain of Bogotá (Bayona et al., 2013).

Among the latter there is evidence for an Eocene folding, as reported from the western flank of the Usme Syncline to the south of the High Plain of Bogotá (Julivert, 1963; locality cited further by Gómez et al., 2005b and Teixell et al., 2015). Here, mid-Eocene estuarine strata of the Usme Formation (Figure 11; Bayona et al., 2010; Ochoa et al., 2012) cap an angular unconformity carved into vertical to overturned Upper Cretaceous strata and mid-Eocene sandstones of the Regadera Formation. The overturned mid-Eocene sandstones display growth unconformities, which indicate thickening toward a depocenter located further west, i.e., within the syncline's present axis. These

outcrop relations suggest a fold-related shortening aided by the diapiric rise of shales of the Chipaque Formation (>800 m thick; Figure 5) within the core of an adjacent, eastern anticline. In conclusion, the deformation appears to have initiated along pre-disposed positive areas that sub-divided the sub-basins of the present High Plain of Bogotá. Notably, the post-folding sediments overlying the overturned flank are paralic and exclude, therefore, a topographic relief that was significantly higher than sea level.

These widely dispersed back-arc basins (presently involved into an intra-cordilleran setting), are exceeded in both the thickness of the sedimentary fill (>2500 m) and the longitudinal dimension (>150 km) by a narrow depositional trough that prefigured the Neogene Guaduas Syncline (Figure 3a). This sedimentary fill is made up of the conglomeratic San Juan de Río Seco Formation (Figure 11), which originated from a stacked pattern of fluvial channel deposits, displaying intratrat growth unconformities and northward-directed paleocurrent directions (Gómez et al., 2003). This sedimentation pattern attests to a period of increased subsidence, during which the creation of accommodation space outpaced the accumulation rate. Toward higher stratigraphic levels monocrystalline quartz increases at the expense of polycrystalline quartz and metamorphic fragments (Gómez et al., 2003), suggesting a sourcing from a uniform rock unit, such as the igneous suite of the Jurassic Ibagué Batholith. This batholith constitutes the basement of the footwall block of the Cambao Fault (Figure 3a) and forms the base of an amply exposed pediment that constitutes the eastern flank of the Central Cordillera, some 10 km west of the Guaduas Syncline (refer also to section 1 in Figure 4).

More concise information about similar depositional settings is provided from eastern more sub-basins of the Magdalena Valley (Figure 3a), which have not been affected by the Cenozoic denudation of the Central Cordillera. These depositional systems typically consist of a deeply eroded antiformal high and two flanking synclines, which acted as depositional sinks during the denudational event, accumulating alluvial fan deposits and fluvial sediments during the middle to late Eocene (Figure 12). Their generally tripartite architecture (lower and upper coarse-grained units separated by a fine-grained unit) and conglomeratic nature of the coarse-grained successions compare to the sedimentary fill of the San Juan de Río Seco Formation (De Porta, 1974; van Houten & Travis, 1968).

The spatial association of eroded highs and adjacent marginal sinks suggests a clast supply produced by an unroofing of the antiforms. A gradual thickening of the conglomeratic units away from the antiformal crest has been documented for the Upper Magdalena Valley (see section 8 in Figure 12; Ramón & Rosero, 2006). Variations in clast composition may be explained by erosional windows which successively shifted toward the pre-Cretaceous basement (Anderson, 1972; van Houten & Travis, 1968). Similar relations may be deduced for the Middle Magdalena Valley to the north

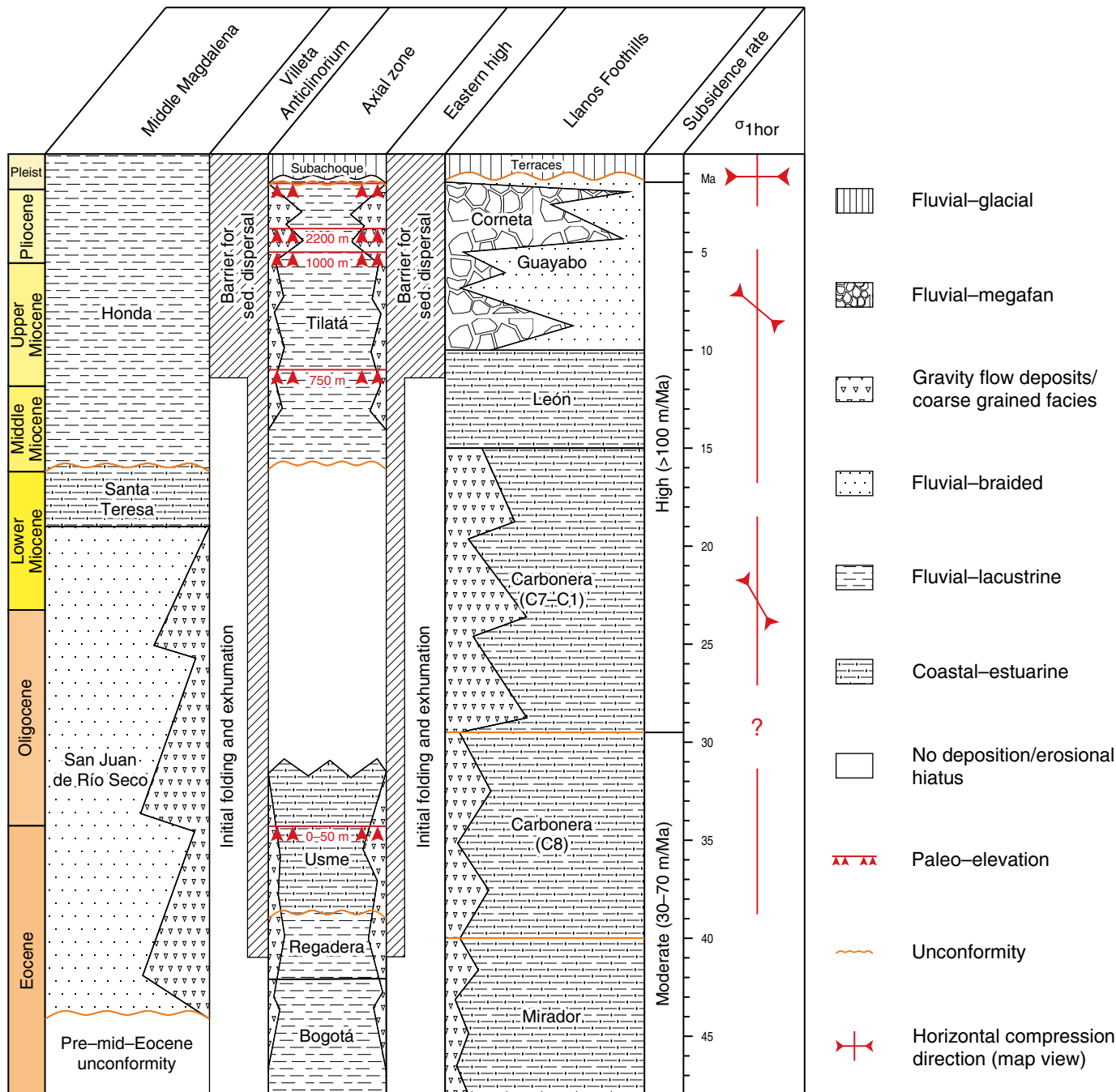


Figure 11. Stratigraphic event chart for the syntectonic basin fills and elevation estimates for the uplift of the axial zone (High Plain of Bogotá). Subsidence estimates for the Llanos Basin are shown on the right-hand side, as well as the regional horizontal stress directions derived from joint sets and sand dikes (horizontal σ_1 is projected in map view). The uplift estimates are taken from Hooghiemstra et al. (2006), and the subsidence estimates are taken from Parra et al. (2009a).

of the Guaduas Syncline, where the La Cira–Infantas Antiform (see section 7 in Figure 12) is bordered by fringing basins preserved within the Nuevo Mundo Syncline to the east (Figure 3a) and within the footwall block of the Cantagallo Fault to the west. Within the latter basin alluvial fan deposits have been identified (Suárez, 1996).

Subsequent to their unroofing, these central antiforms changed to depositional depressions, whose eroded hinge areas

may occupy a position below the Miocene to present drainage axis, as observed in the Upper Magdalena Valley (see section 8 in Figure 12) and as may be inferred for the basement high to the west of the Guaduas Syncline. Along the La Cira–Infantas Antiform, regional tilting of the foreland basin became a predominant factor in the basin evolution and obscured this subsidence pattern (see section 7 in Figure 12). This source-to-sink inversion of antiforms capped by the mid-Eocene unconformity

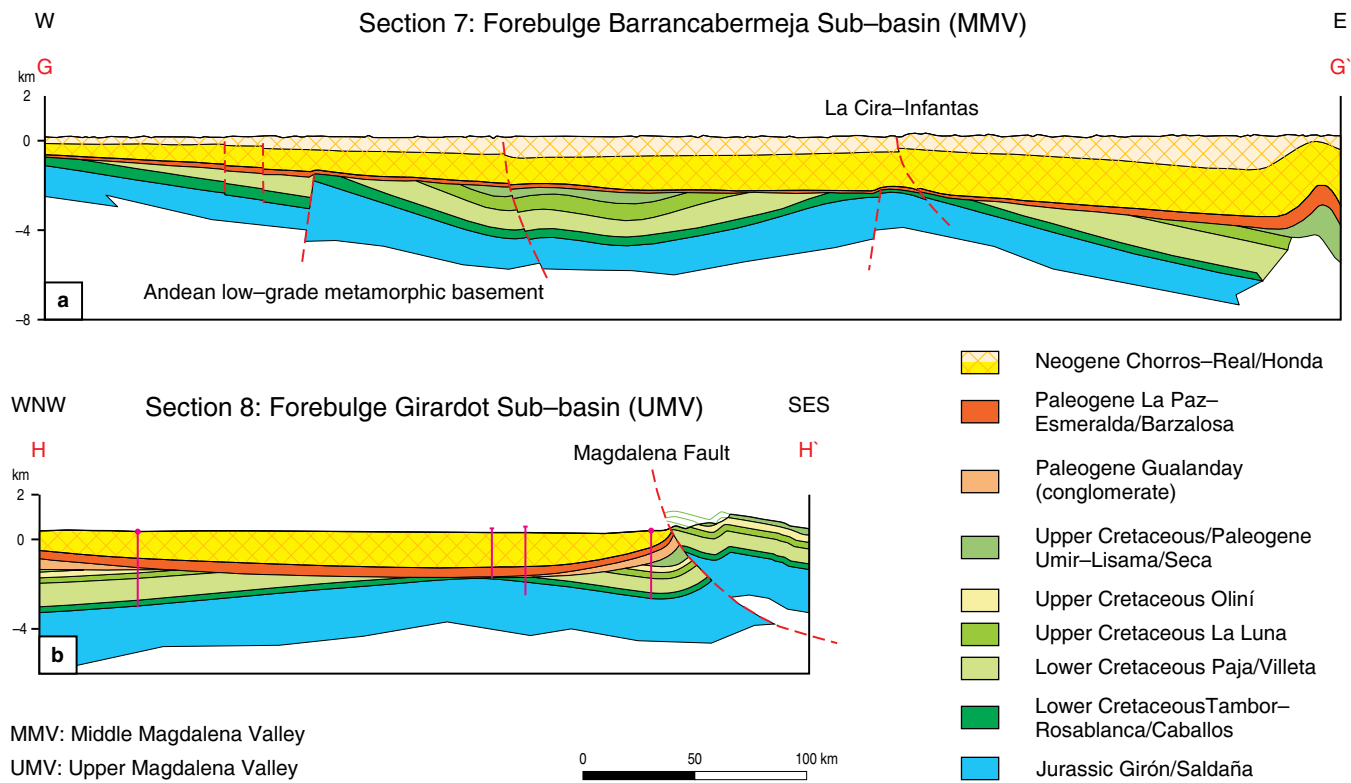


Figure 12. Two sections showing the Paleogene forebulge structures of the Magdalena Valley to the west of the Eastern Cordillera. Section 7 is from the Middle Magdalena Valley (redrawn from Morales, 1958), and section 8 is from the Upper Magdalena Valley (modified from Kammer & Piraquive-Bermúdez, 2013). For the locations, refer to Figure 3a. The forebulge structures of both sections are capped by a middle Eocene unconformity.

demonstrates a limited lifespan for the uplift of these highs, in accordance with the mid-Eocene to Oligocene sedimentary fills of their flanking synclines. Such a transient behavior is best explained by temporary vertical loads and may be compared to surface deflections driven by convective flows. The lateral dimensions (or wavelengths) of these depositional systems do not exceed some 10 km and preclude, by their short wavelengths, the existence of sub-lithospheric convective instabilities (Flament et al., 2013), though time spans of individual convective pulses (comprising 10 to 15 Ma) show a similar magnitude with respect to the denudational mid-Eocene event (Moucha et al., 2008). A crustal origin for these topographic instabilities may be inferred from the present structural setting of the North Andean Terrane, which shows a predominant seismic anisotropy according to the splitting of local shear waves, with fast directions being oriented preferentially parallel to the structural grain of the Andean back-arc realm (Idárraga-García et al., 2016). Accordingly, we may view this crustal corrugation as an expression of a lateral lithospheric flow, which may have been coupled to or largely independent of a lithospheric late Paleogene buckling. The transient nature and structural expression of this folding differs in two important aspects from a classical asymmetric foreland basin evolution associated to a mobile mountain front: (1) Antiformal highs and basins associated to flanking rim

synclines maintained a fixed position within the back-arc realm and (2) rim synclines cannot be related to flexural basins of a mountain front. In contrast to previous proposals (Gómez et al., 2005a; Parra et al., 2009b; Villamil, 1999), we disassociate this late Paleogene back-arc evolution from an early phase of mountain building at the western margin of the back-arc realm. Although not yet fully explainable, we believe that this event is crucial for an understanding as to why the back-arc realm became divided into two orogenic domains during the subsequent Oligocene to Neogene Andean evolution.

Within the region of the nascent EC thermochronological data indicate the onset of moderate exhumation (<1 mm/y) in the late Oligocene/early Miocene, which was followed by accelerated exhumation (>1 mm/y) since the Pliocene; these phases have been identified within both the eastern and western mountain fronts (Mora et al., 2008, 2010a, 2015; Parra et al., 2009b; Sánchez et al., 2012). Thermochronological data of this two-stage evolution support a synchronized tectonic activity at the two mountain fronts.

Information about the early Oligocene/Miocene contractional history of the cordillera may be extracted from its foreland basins. Within the Nuevo Mundo Syncline of the northern Middle Magdalena Valley (for location see Figure 3a), the Oligocene to Miocene Mugrosa and Colorado Formations (Figure

5) record higher sedimentation rates than the earlier Eocene deposits and are increasingly sourced from the EC (Caballero *et al.*, 2013). Their tilting has been associated to a flexural load of the nascent EC (tilted upper Eocene to Miocene sequences are shown in section 7 in Figure 12; Gómez *et al.*, 2005a). This evolution is matched by a coeval increase in the subsidence rate in the foreland basin evolution of the Llanos Foothills (Figure 11; Parra *et al.*, 2009a).

An accelerated mid- to late Miocene buildup of the eastern mountain front was preceded by a mid-Miocene flooding event that gave rise to estuarine deposits of the León Formation (Figure 11). The succeeding alluvial plane and fan deposits of the Guayabo Formation initiated molasse-type sedimentation that is >4000 m thick. Finally, tightly stacked flows of blocky conglomerates of an alluvial “mega-fan” (Corneta Formation; Figure 11) underscore the proximity of a mountain front. The mountain front itself maintained a stagnant position until the Pliocene/Pleistocene, when its foredeep became involved in the Guavio thrust sheet (as discussed in the next section).

The surface uplift of the High Plain of Bogotá has been tracked by pollen spectra (Figure 12; van der Hammen *et al.*, 1973; Hooghiemstra *et al.*, 2006). The vegetation belts evolved from middle Miocene tropical lowlands to pre-montane elevations, until reaching montane elevations in the Pliocene.

7. The Two-Phase Evolution of the Eastern Deformation Front

The major right-stepping thrust faults contributed to the conspicuous segmentation of the eastern foreland structures of the EC (Figure 3a). The southern Guavio segment exemplifies these foreland structures particularly well by the inception of the Guaicáramo Thrust within undeformed Cenozoic deposits to the south and their involvement within the Guavio thrust sheet further north (Figure 9). In its northern part, this segment exposes folded Cretaceous sequences. In this chapter, we return to the topic of the two-phase evolution of this deformation front and address two particular questions: (1) Is it possible to relate the Pliocene (or more recent) shortening absorbed by the southern thrust sheet to the folding of the northern Guavio segment?, and (2) is it kinematically feasible to relate the collapse of the Miocene mountain front with this late-stage thrusting?

7.1. Pliocene Fold-and-Thrust Tectonics

As previously disclosed, the Guavio segment comprises a southern detached domain of the Guavio thrust sheet and a tightly folded northern domain, which are separated by a relay zone (Figure 9). From its southern tip to the structural relay, the slip on the Guaicáramo Fault increases from a few 100 m to 6 km, which may be deduced from mapped and constructed cut-off lines between formation boundaries and the fault

plane (for different structural interpretations, refer to Rowan & Linares, 2000; Branquet *et al.*, 2002; Mora *et al.*, 2010b). As the slip increases, the fault soles into successively lower stratigraphic levels. In cross-section 9 (Figure 13), the Une Formation forms the basal competent sandstone unit of the thrust sheet, with its top marking a cut-off line on the up-ramping fault plane at the surface. This fault extends along its slightly folded flat into the eastern flank of the Montecristo Anticline, where it intersects the steeply inclined Servitá and Esmeralda Faults. From a purely kinematic point of view, the fault caused the translation of a triangular wedge, leaving a void behind it. This void was filled by the gradual collapse of the hanging wall, which may be inferred from the normal reactivation of minor faults that originated as antithetic satellite faults of the Early Cretaceous Esmeralda Fault. Normal faulting is also ubiquitous at a small scale within the Pliocene fluvial deposits of the High Plain of Bogotá (Tilatá Formation; Kammer, 2003) and attests to the distributed extension of the eastern cordilleran flank that might have contributed to the displacement of this out-of-sequence fault.

The relay zone marks a discontinuity between the folds affecting both the southern and northern domains. Exceptions are the marginal Nazareth and Río Amarillo Synclines, which border the Montecristo Anticline and the up-ramping thrust sheet of the Guaicáramo Fault (Figure 9). The folds in the northern domain display increasingly significant foreland-directed vergence toward the Guaicáramo Fault (see section 10 in Figure 13). Active fault planes have been imaged by the aftershocks of the 1995 Tauramena earthquake ($M_w = 6.5$), which occurred near the relay zone (Dimaté *et al.*, 2003). In section 10 (Figure 13; this section coincides with section K–K' of Dimaté *et al.*, 2003), the projected aftershocks cluster around linear arrays along the possible continuation of the Guaicáramo Fault and conjugate fracture planes. In the southern domain, the current slip on the Guaicáramo Fault is aseismic, as evidenced by a seismic gap in this part of the foothill region (Durán *et al.*, 2002).

The retrodeformation of sections 9 and 10 (Figure 13) yields shortening values of 4.5 km. These equivalent amounts of shortening within a similar structural setting are taken as an evidence for the Pliocene/Pleistocene folding of the northern domain. In the following considerations, we attempt to understand the deformation modes of the two domains and the interacting relay zone and sketch, for that purpose, two snapshots of a southward-propagating Guaicáramo Fault. The pre-faulting situation (Figure 14a) depicts the formation of the mountain front at the site of the future Guaicáramo Fault in the northern domain and, to the west, the Miocene mountain front pinned to the Servitá Fault in the southern domain. Assuming a common upper crustal detachment, the relay zone would have accommodated a dextral displacement transfer. In the second snapshot (Figure 14b), the Guaicáramo Fault propagates into the southern domain and may have transitioned to a flat attitude as it accumulated the

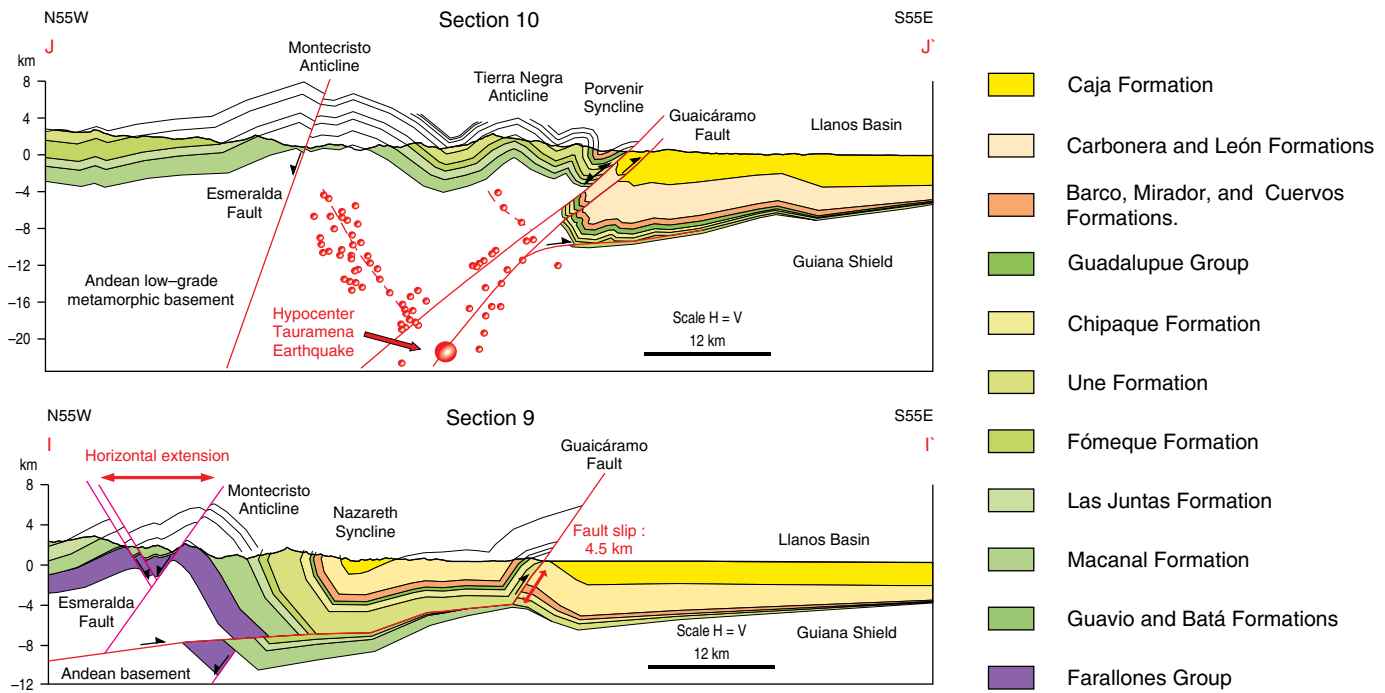


Figure 13. Two structural sections of the eastern deformation fronts, Guavio segment. For the locations, refer to Figure 9. In section 9, the frontal Guaicáramo Fault soles into the basal Cretaceous sequences and is assumed to break the Miocene mountain front of the Montecristo Anticline. In section 10, the same fault involves the pre-Cretaceous basement. Section 10 shows relocated aftershocks and the main shock (small and large red circles, respectively) of the Tauramena earthquake (19 January 1995) projected from a 5-km-wide corridor (Dimaté et al., 2003).

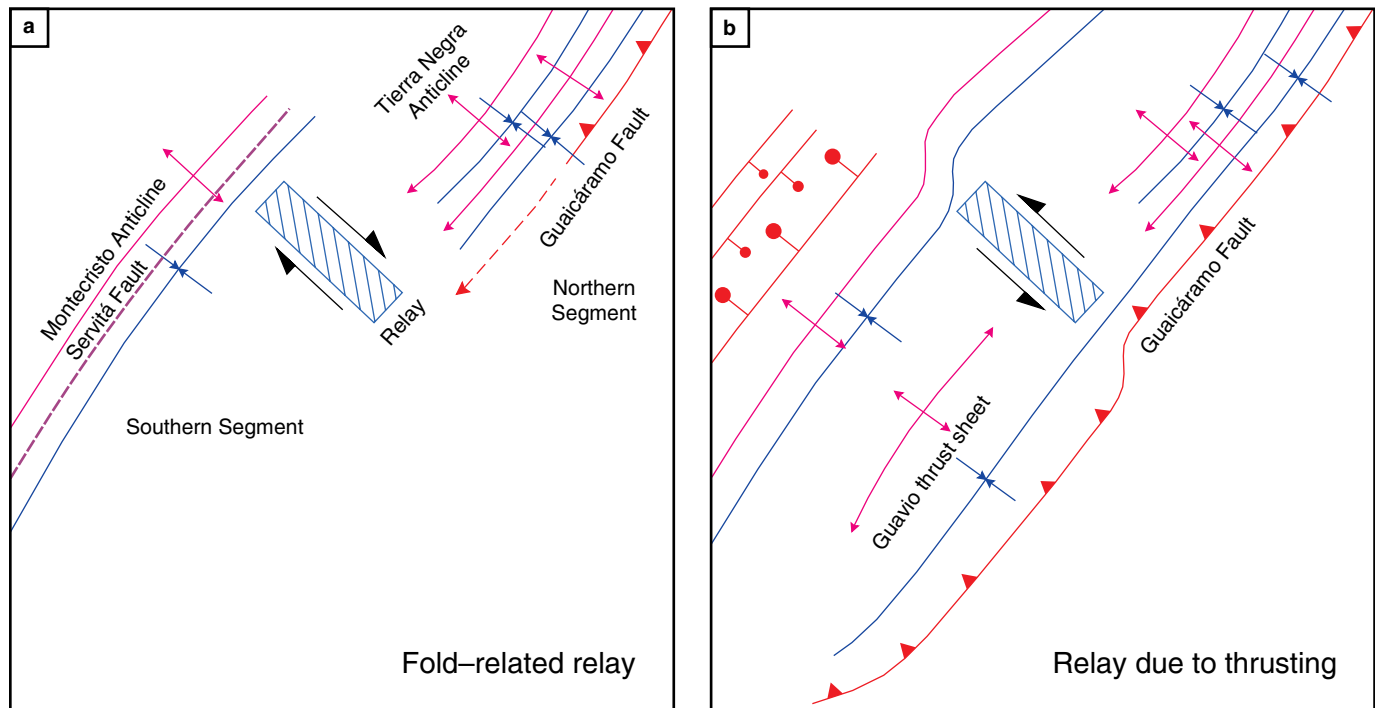


Figure 14. Snapshots of the kinematic evolution of a southward-propagating Guaicáramo Fault across a folded northern domain (a) and the breakdown of the Miocene mountain front in the southern domain (b) of the Guavio segment. (a) The right-stepping array between the Miocene mountain front pinned to the Servitá Fault in the southern domain and incipient folds in the northern domain implies dextral displacement transfer on the separating relay zone. (b) The activation of the Guavio thrust sheet implies sinistral displacement transfer on this same relay zone.

displacement of the extending Miocene mountain front. Collapse of this latter structure might have been triggered by a drop in lateral support during the initial fault propagation. At this stage, movement of the thrust sheet required the relay zone to accommodate a sinistral displacement transfer.

The juxtaposition between thin- and thick-skinned deformational styles requires further clarification. The relay zone did not behave as an impassable barrier during the southward propagating buckling stage. Limited transmission of the thick-skinned shortening from the northern domain to the southern domain is documented by the open folding of the Guavio Anticline, which affected also the overlying thrust sheet (see section 9 in Figure 13).

7.2. Miocene Mountain Front

The spatial link between the tip line of the Servitá Fault and the eastern flank of the Montecristo and Toquiza Antiforms suggests a fault–fold relationship. The tri–shear method, which was developed by Allmendinger (1998) and re–formulated by Zehnder & Allmendinger (2000), provides a kinematic approximation for testing such a structural framework. The model parameters are adjusted to obtain a satisfactory fold shape (Allmendinger *et al.*, 2004), while neglecting the effects of regional buckling. For the case of a blind fault, the approximate location of the fault tip can be estimated. A comparison between the strains required for the model fold to form and those observed in the field can provide valuable feedback. We base our analysis on the mountain front shown in section 3 (Figures 4, 15a). The restored late Miocene state was obtained by removing the displacements on the Guacáramo and Esmeralda Faults (Figure 15b). Two different solutions for the combined inverse/forward modeling of similar fold shapes are given in Figure 15c. They differ in the apex angles of the tri–shear zone and their internal velocity distributions. By applying a linear velocity gradient, we obtain a relatively open fold affected by moderate strains (though the axial ratios of the finite ellipses reach $R_s > 3$). However, the required fault tip propagation extends for a considerable distance, likely through the entire crust. An alternative case is based on a velocity distribution concentrated in the center of the tri–shear apex (in this case, applying a sine function for the velocity distribution). Under these conditions, the required trajectory of the fault tip is restricted to the upper crust, but the model requires higher strains ($R_s > 4$).

In our case, the strain compatibility between the simulated and the observed structures is a further criterion that helps to assess the relevance of the kinematic modeling. The Paleozoic basement is affected by a transverse cleavage that is concordant to a shape–preferred orientation of pebbles within conglomeratic layers. Measured strain values reflect axial ratios of $1.3 < R_s < 1.5$ (Figure 16). These values support the scenario of widely distributed deformation; however, this implies fault tip propagation over a considerable distance (as predicted by the model of a homogeneous velocity distribution in Figure 15c).

The discrepancy between the model strains and the observed deformations suggests that the tri–shear mechanism was not exclusive, but was combined with buckling.

In conclusion, the deformation style related to the eastern deformation front responded to both deep–seated processes guided by the crustal discontinuity of the Servitá Fault and to supracrustal dynamics. The long–lasting (>25 Ma) building of the Miocene mountain front ended its life cycle as its stability was surpassed. The ensuing supracrustal processes redistributed the crustal load of the eastern cordilleran flank, decreasing its structural relief and broadening the foreland belt, according to basic mechanical principles, which favor a reduction in the potential energy of a mountain chain (Lyon–Caen & Molnar, 1985). This two–phase evolution is well discernible by the juxtaposition of highly deformed tight internal folds and broad foreland structures, as evidenced in the southern part of the Guavio segment. Further north, this distinction is less clear and deformation may have affected progressively more foreland–oriented regions.

8. Folding and Faulting in the High Plain of Bogotá

As can be seen from the cross–sections, the first–order structure of the High Plain of Bogotá consists of a wide structural depression delimited by the Miocene structural highs on either side (composite sections 1 and 2 in Figure 4). In its axial area, folded strata are mostly composed of sandy Upper Cretaceous to Paleogene rock units, while in its gently inclined flanks Middle to Lower Cretaceous sequences of alternating shaley and sandy units, each from 500 m to 1200 m thick, become exposed. The Río Blanco Anticline is a prominent fold on the eastern margin of the high plain (see section 11 in Figure 17) and borders the central Sisga Syncline. Its eastern flank is segmented longitudinally by isolated faults with lengths of 3 to 10 km, which can be mapped based on the presence of hanging–wall synclines (see section 12 in Figure 17). Otherwise, these sections do not contain faults. All of the sequences are involved in secondary folds with wavelengths ranging between 5 to 10 km. Enveloping surfaces constructed on their trough points outline the regional dips of the cordilleran flanks, which are approximately 5° for the western flank and 12° for the eastern flank. The fold vergence generally points toward the marginal highs (see sections 11, 12 in Figure 17).

Within the eastern flank, the fold trains plunge slightly northeast, as shown by their map pattern (Figure 9) and measured planar and linear fabrics cluster around axes plunging 5° northeast. This regional plunge is not observed within the axial depression, where the fold plunges become highly variable (Figure 18). The fold pattern became established in the late Miocene, as shown by the architecture of the alluvial deposits of the Tilatá Formation (Figure 11). Within the major synclines, conglomeratic channel deposits define stacked patterns, which

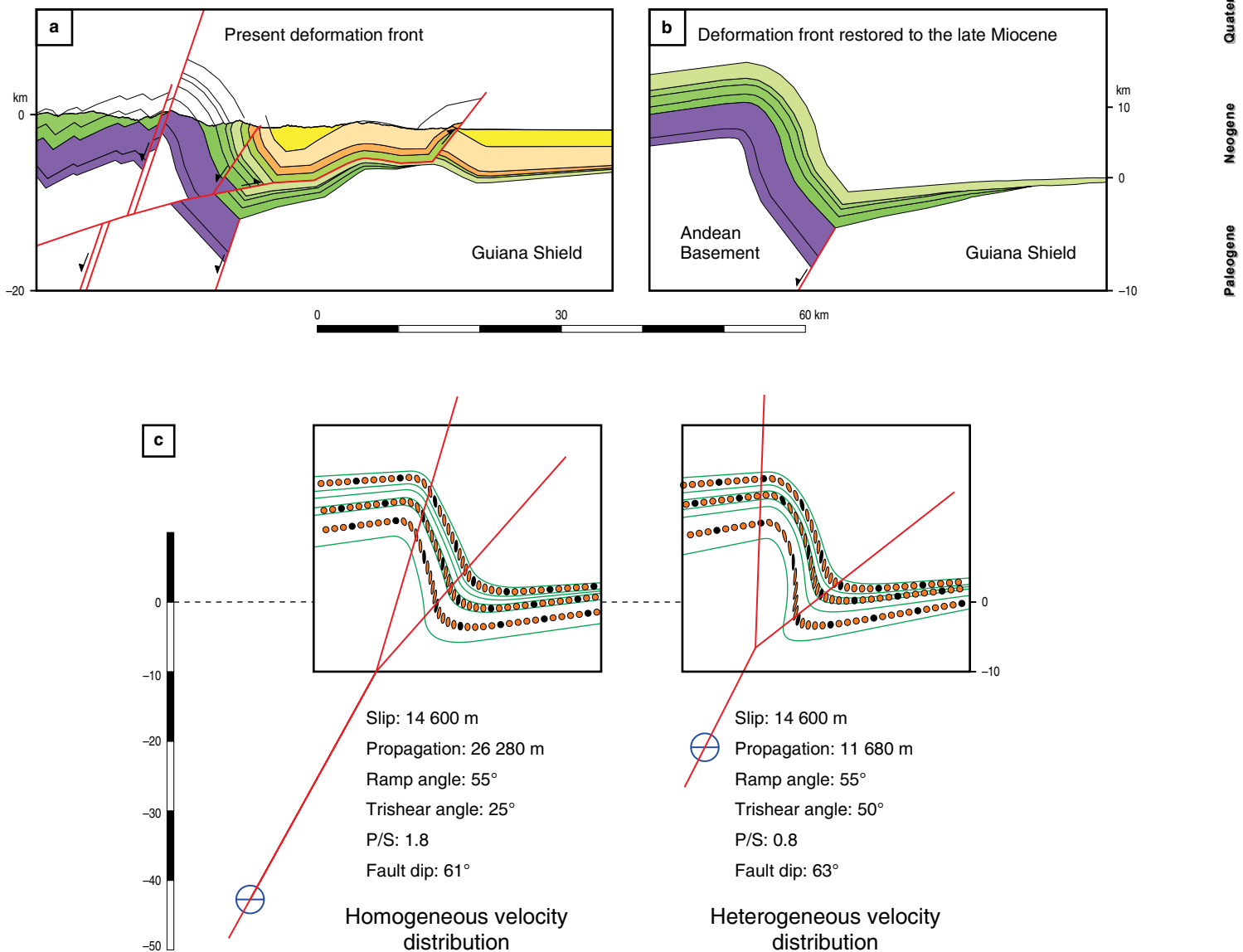


Figure 15. Kinematic model of the late Miocene deformation front of the Guavio segment. **(a)** Present structural section. **(b)** Restored late Miocene deformation front. **(c)** Tri-shear solutions for homogeneous and heterogeneous velocity fields. The model parameters are indicated. The nucleation point of the fault and the trajectory of its tip propagation (presently anchored at the apex point of the tri-shear zone) are plotted with reference to a vertical scale.

indicate that the fold axes have remained fixed since their syn-kinematic deposition during the Miocene (Kammer, 2003).

Adjacent to the Toquiza and Montecristo Antiforms, the fold trends are uniform and strike 45° NE. Toward the axial depression, the fold pattern is composite, as north-south oriented folds interfere with the folds of the regional cordilleran trend. Figure 18 highlights two particular patterns of this superposition: (1) the folds of the cordilleran trend sway into an N-S direction (sites F2(b) and (c); Figure 18), and (2) the gently dipping flanks of the synclines, that parallel the regional trend, are refolded by N-S or NNE-SSW-trending anticline-syncline pairs (sites F2(a) and F2(d); Figure 18). Based on these observations, we conclude that the deformational regime had a shortening

direction that rotated from strike-perpendicular to E-W. However, evidence for these changes in fold orientation are absent in the foothill area, which suggests that the cordilleran topographic load might have suppressed these regional changes in the shortening direction. Support for two different active stress regimes comes from the horizontal principal stress orientations (σ_{1-hor}) derived from borehole breakouts (Tesón et al., 2013; see their Figure 8). All available data define two domains separated by a boundary that coincides with the southern termination of the Guacáramo Fault. South of this boundary, σ_{1-hor} directions are E-W-oriented, whereas further north σ_{1-hor} directions are strike-perpendicular, illustrating the increased importance of the topographic load in the northern domain, where the eastern

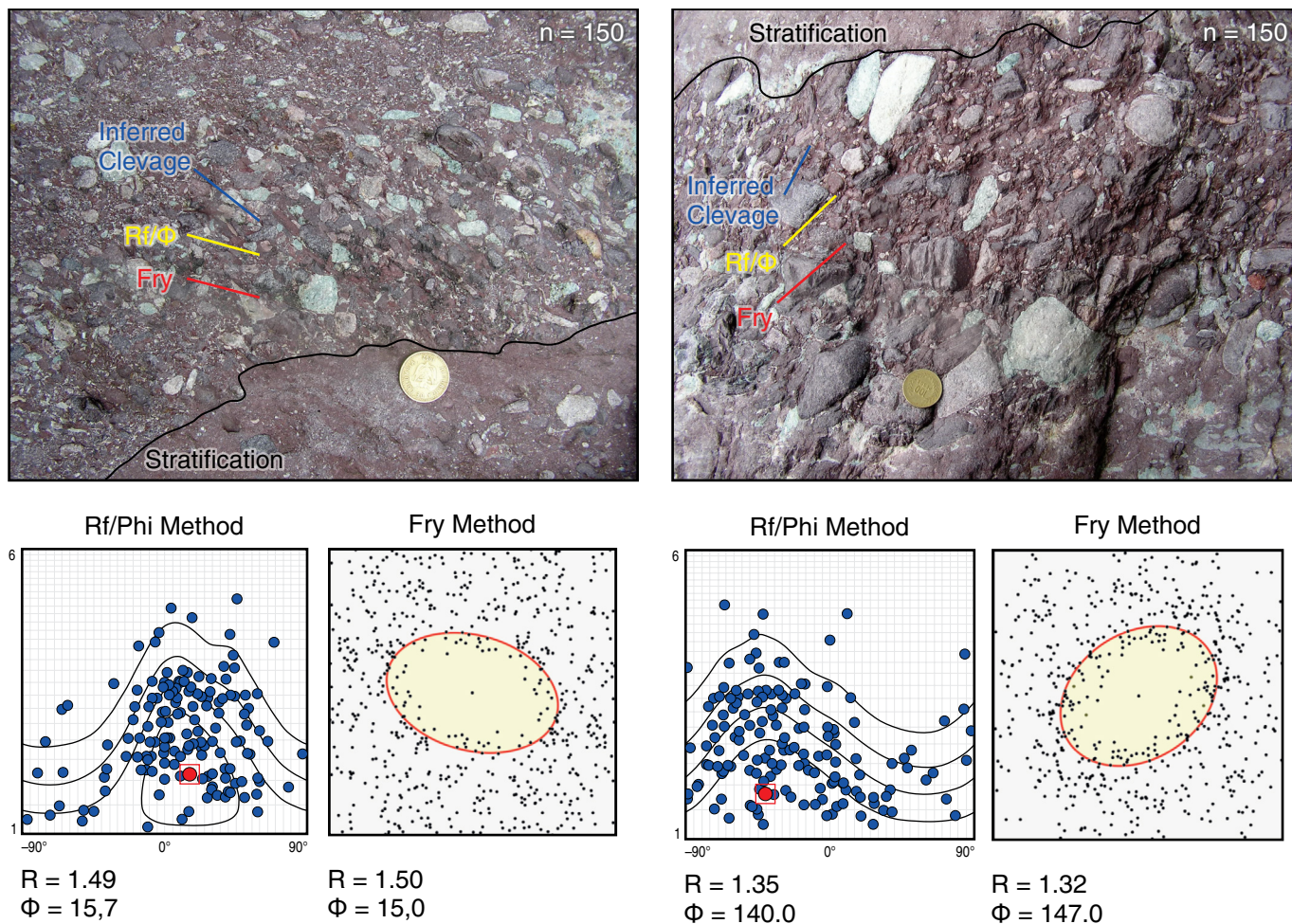


Figure 16. Deformed conglomeratic unit of the upper Paleozoic Farallones Group, eastern flank of the Montecristo Antiform, and strain diagrams. The outcrop faces contain the principal elongation and shortening directions of the pebbles. The strain values are determined by a shape and orientation analysis of the pebbles (Rf/Φ method) and visualized by the normalized distances between the central points of the pebbles (Fry method). For the strain evaluation, we used the program *EllipseFit*, which was written by Vollmer (2015). Textural inheritance of the sedimentary structures may account for the deviation between the calculated long elongation axis and the observed cleavage direction.

cordilleran flank attains its full width. A detailed fracture analysis is needed to demonstrate the existence of two competing recent stress directions and will be presented elsewhere.

The fold style in the western part of the axial depression is strongly influenced by transverse relay structures, which have been described in detail by Ujueta (1992). These relays may be identified by both sinistral and dextral local bends in the regional fold trend. For example, both right- and left-stepping bends of fold axes may be recognized along lineament R(d) (Figure 18). Left-stepping bends are most conspicuous where the western flank becomes more inclined, as evidenced by curved fold axes along the northwestern segments of lineaments R(b) and R(c) (Figure 18). They cannot be associated with post-fold wrenching because the panels bounded by these lineaments display independent folds. For example, the folds located between lineaments R(b) and R(c), as well as those between R(c) and R(d), differ in number and vergence.

In the eastern, more axial region, the fold axes are not bent but rather abut against these relays or form distinct necks. The particular fold style of each panel advocates for a pre-folding origin of the lineaments.

Linear arrays of minor salt stocks and thermal springs (Ujueta, 1992) provide clues about the origin of the lineaments. Lineament R(b) (Figure 18) hosts the Zipaquirá salt dome, which is a composite diapir with two lobes that are separated by a central saddle (McLaughlin, 1972). Internal structures, such as sheath folds and a foliation caused by intense mixing of recrystallized salt and broken shale fragments, attest to an intrusive emplacement (Warsitzka et al., 2013). The entrained shale fragments contain Berriasian fossils (López et al., 1991).

The salt occurrences are thus strictly limited to fold relays and their associated structures. Rather than associating these restricted occurrences to a regional basal detachment horizon,

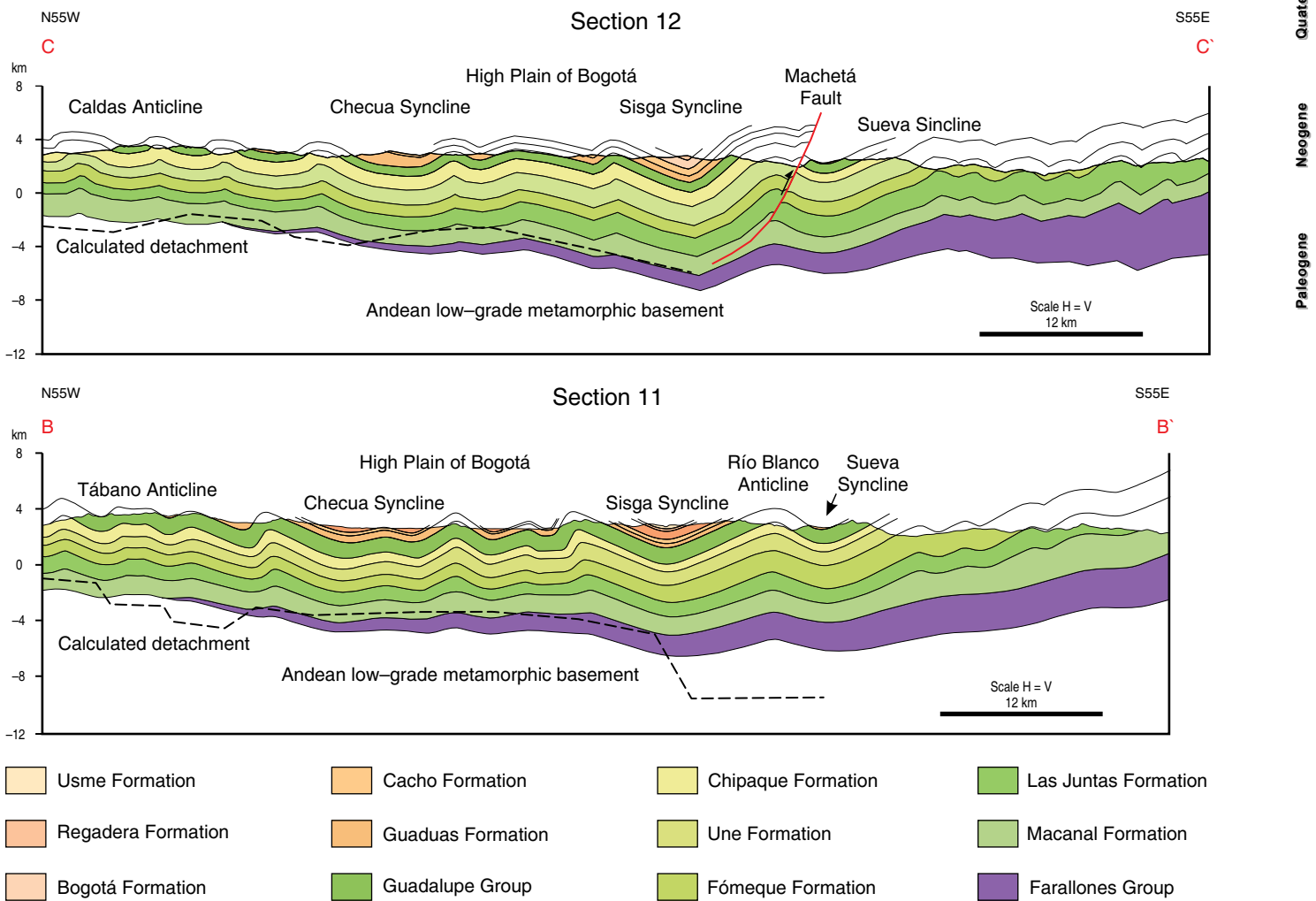


Figure 17. Detailed sections of the axial zone of the High Plain of Bogotá. These sections correspond to the enlarged central portions of sections 2 and 3 in Figure 4. The locations are shown in Figure 18.

as proposed by Cortés et al. (2006) and Teixell et al. (2015), we stress their importance in dividing the axial zone into structural domains. The presence of salt along transverse faults or relay zones might have contributed to their mobility, which is supported by the conspicuous left-lateral bends to the west of the axial zone (northeastern terminations of relay zones R(b) and R(c); Figure 18). This local wrenching may have occurred as a result of a “transpressional” E–W-oriented shortening, as set out above by means of the young folding phase detected in the eastern cordilleran flank. These relay zones are limited to the axial domain of the High Plain of Bogotá. On the western flank, they terminate against a continuous anticline in the Neusa area (northwestern corner of Figure 18); on the eastern flank, they are limited against the Río Blanco Anticline. Their restricted occurrence suggests a Berriasian paleogeographic framework, in which transverse faulting channeled local marine incursions with the subsequent formation of evaporitic deposits.

8.1. Fold Mechanisms

Dismissing the existence of a continuous salt layer that would have facilitated the detachment of the Cretaceous cover, we can investigate alternative fold mechanisms. Periodic wavelengths and systematic changes in the fold vergence across the central Sisga Syncline suggest buckling under uniform contraction. In contrast, the pre-Cretaceous basement underwent shortening by plane strain, as indicated by a ubiquitous axial plane cleavage at this structural level. A mixed deformation mode comprises a wide transitional zone encompassing the Fómeque to Macanal Formations (Figure 5) and combines flexural slip folding and homogeneous shortening by cleavage formation (Kammer, 1997). We address this structurally complex situation in a simple kinematic model that is used to construct cross-sections and a simple mechanical model that applies to buckle folds. Both approximations apply to the situation of detachment folds, in

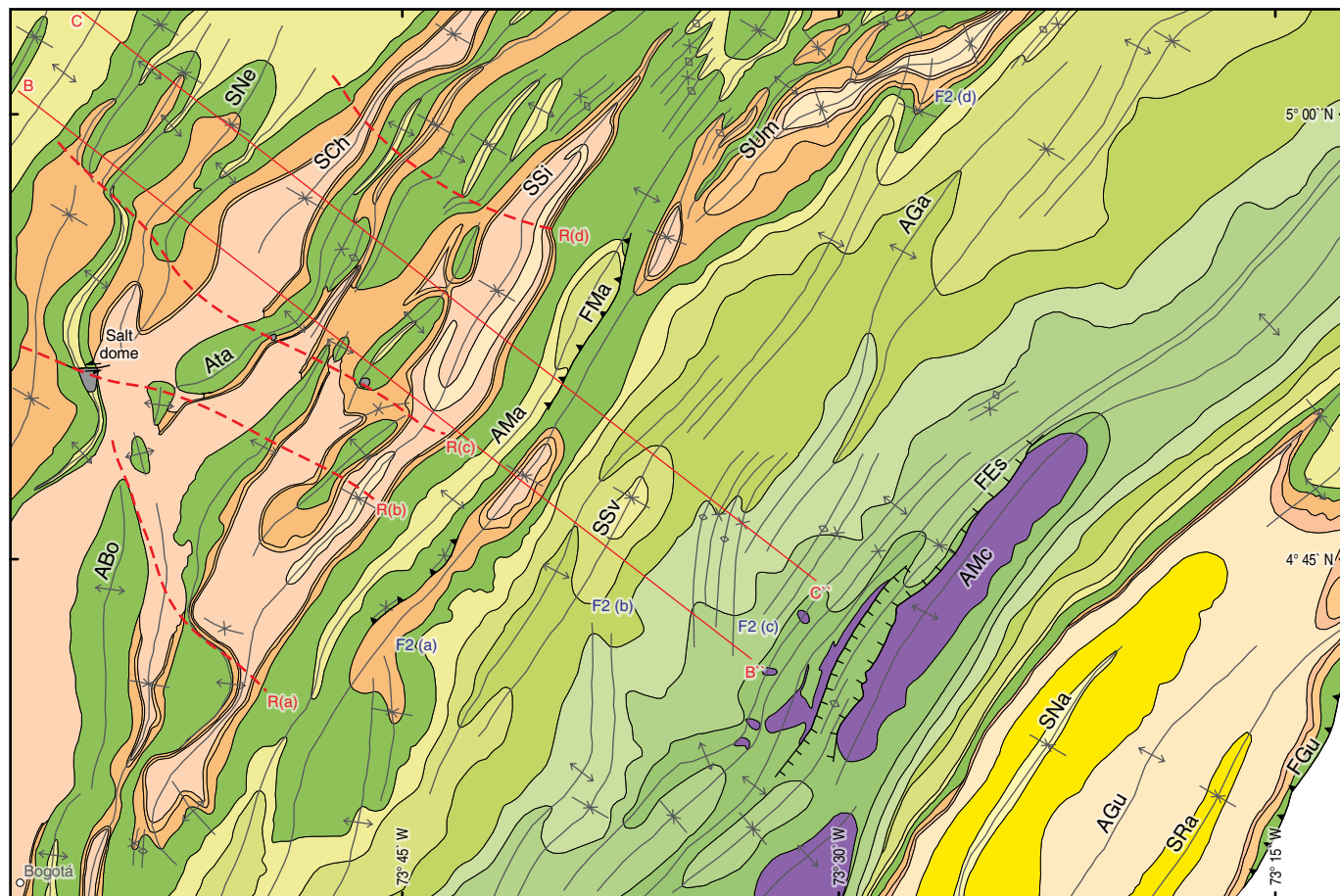


Figure 18. Geological map of the High Plain of Bogotá and its adjacent eastern flank. The Red lines indicate the structural sections in Figure 17. The Red stippled lines, labeled as R(a), R(b), R(c), and R(d), indicate structural relay zones, which are highlighted by fold bends, fold terminations, and aligned salt domes. Second-generation folds are recognized by N-S trending fold terminations, as observed at sites F2(b) and F2(c), and their superposition on folds of the SW-NE striking Cordilleran trend, as exemplified at sites F2(a) and F2(d). Location of relay zones: R(a) Zipaquirá-Río Teusaca, R(b) Zipaquirá-Guatavita, R(c) Neusa, R(d) Tausa-Choconta.

so far as we consider the folding of a layered sequence above an unfolded basement, whose depth is determined by the mitigation of fold amplitudes and whose interface mimics the regional dip of the cordilleran flanks and is, thus, comparable to a detachment.

Of the existing kinematic models, we chose that one developed by Epard & Groshong (1995), which assumes folding above a stratigraphically fixed horizon by a combination of

limb rotation and changes in bed length. We select the contact between the Lower Cretaceous shale unit of the Macanal Formation (Figure 5) and the underlying Paleozoic to Proterozoic sandstones and phyllites (Farallones and Quetame Groups) as the reference horizon for the mitigation of fold amplitudes. Where these pre-Cretaceous units consist of sandstones, they may have acted as a mechanical boundary. The deformation mode considered by Epard & Groshong (1995) allows for the

thickening of beds within anticlinal hinges but excludes material transfer through adjacent synclinal axial planes; stated differently, the fully developed fold shapes, that are observed at the surface, may be projected to the basement–cover interface, assuming a linear decrease in amplitude. This scenario clearly requires observational support. The argument in favor of thickened shaley units in the anticlinal hinges is based on the still poorly investigated diapiric phenomena, which caused the overlying sandstone units to break into overturned flanks or “flaps” (Harrison & Falcon, 1934), where erosion disrupted their continuity (Julivert, 1962, 1963).

The problem of locating the depth of the unfolded basement was overcome in three ways: (1) by extrapolation, we determined the depth of formational units within the cordilleran eastern flank; (2) based on the shortening values and excess areas determined at superficial folds, we estimated the “mitigation” depths for individual folds, according to the calculation of detachment depths (Chamberlin, 1910); this method assumes the beds to be undeformed at the surface, a requirement that is likely met within the Upper Cretaceous and Paleogene sandstone units of the High Plain of Bogotá; and (3) variation diagrams between excess areas and structural levels, as proposed by Epard & Groshong (1993), allow to determine the depth of the basement–cover interface by pinning it to the level where excess areas disappear. The latter method is based on the assumption of area conservation and does not depend on bed-length changes. It was used to check the internal consistency of the constructed sections.

The “mitigation” depths of folding calculated and checked by the two latter methods are plotted for individual anticlines in sections 11 and 12 (Figure 17). The results point to a uniformly east–dipping basement–cover interface within the axial depression and the cordilleran western flank and presume a gradual westward tapering of the Cretaceous units, which is confirmed by the mapped outcrop limits of equivalent units of the Une Formation in the western cordilleran flank. Given the large amplitude of the Río Blanco Anticline, its “mitigation depth” considerably exceeds these calculated depths below the High Plain of Bogotá; therefore, folding should involve the pre–Cretaceous basement units.

The regular spacing of folds within the High Plain of Bogotá suggests that the wavelength is related to the rheological properties of the folded rock units. We approximate this problem by considering the buckling of a competent Upper Cretaceous unit above a predominantly shaley lower sequence, as postulated for single–layer detachment folds (Poblet & McClay, 1996). Theoretical considerations postulate that for the initial buckling, a characteristic dominant wavelength λ_{dom} emerges from the preferential amplification of folds that form along randomly distributed perturbations. The dominant wavelength of detachment folds may be related to the viscosities and thicknesses of the layers involved, considering a viscous power law

rheology for the strong layer and a linear viscosity for the weak layer (Schmalholz et al., 2002):

$$\lambda_{\text{dom}} = 1.2\pi \left(\frac{\mu_{\text{eff}}}{3n\mu_m} \right)^{\frac{1}{6}} \sqrt{\frac{H_m}{H}} H$$

where H and H_m refer to the thicknesses of the strong layer and the weak substrate, respectively, the strong layer has an effective viscosity μ_{eff} and behaves according to a power law with an exponent n , and the viscous matrix has a linear viscosity μ_m .

This relationship ignores the multi–layered stratigraphy of the EC but emphasizes the importance of viscosity (or lithologic) contrasts and layer thicknesses. It predicts an increase in the dominant wavelength as the thickness of the strong layer and the viscosity contrasts increase. In our cross–sections, the matrix thickness decreases eastwards from 5800 m to 4100 m (resulting in a thickness reduction of 30%) and becomes weaker, as the distal facies of the Lower Cretaceous sandy units become muddier. The thickness of the folded Upper Cretaceous Guadalupe Group decreases eastwards to a lesser degree (10%) and keeps its lithological strength. Considering only the thickness variations, the dominant wavelength should decrease toward the east.

To identify regional variations in the wavelength of the High Plain of Bogotá and its adjacent flanks, we sampled fold trains in several sections and measured the fold widths between the mapped synclinal or anticlinal axes. We differentiate three domains (Figure 19). For the eastern cordilleran flank (or eastern domain), we exclude wavelengths that pertain to second–generation N–S oriented folds and folds located near marginal highs. The latter folds represent drape folds related to antithetic faults of the Esmeralda and Toquiza Faults and did not form by buckling. We sampled 4 transverse sections on the eastern flank and the high plain, including sections 2 and 3 (Figure 4). Within the western flank, we sampled section 1 (Figure 4) and 4 sections further north.

In the compilation (Figure 19) the longest wavelengths were recorded on the eastern flank (8 to 12 km) and slightly shorter wavelengths on the High Plain of Bogotá (5 to 10 km). The wavelengths measured on the western flank are bi–modal with a minor population attaining widths of the High Plain of Bogotá, in addition to very short wavelengths, which derive from the tightly folded Villeta Anticlinorium (see section 1 in Figure 4) and represent second–order folds of this marginal high. A comparison of the unimodal results points to a reduction of the wavelengths toward the east, according to the marked decrease in thickness of the Lower Cretaceous units. Further studies should be designed to examine the influence of lithological contrasts which, at present (and ignoring lateral lithological variations), may be approximated by a viscosity ratio of about 20. Assuming that the concept of a dominant wavelength may be applied to the scale of our cross–sections, these preliminary

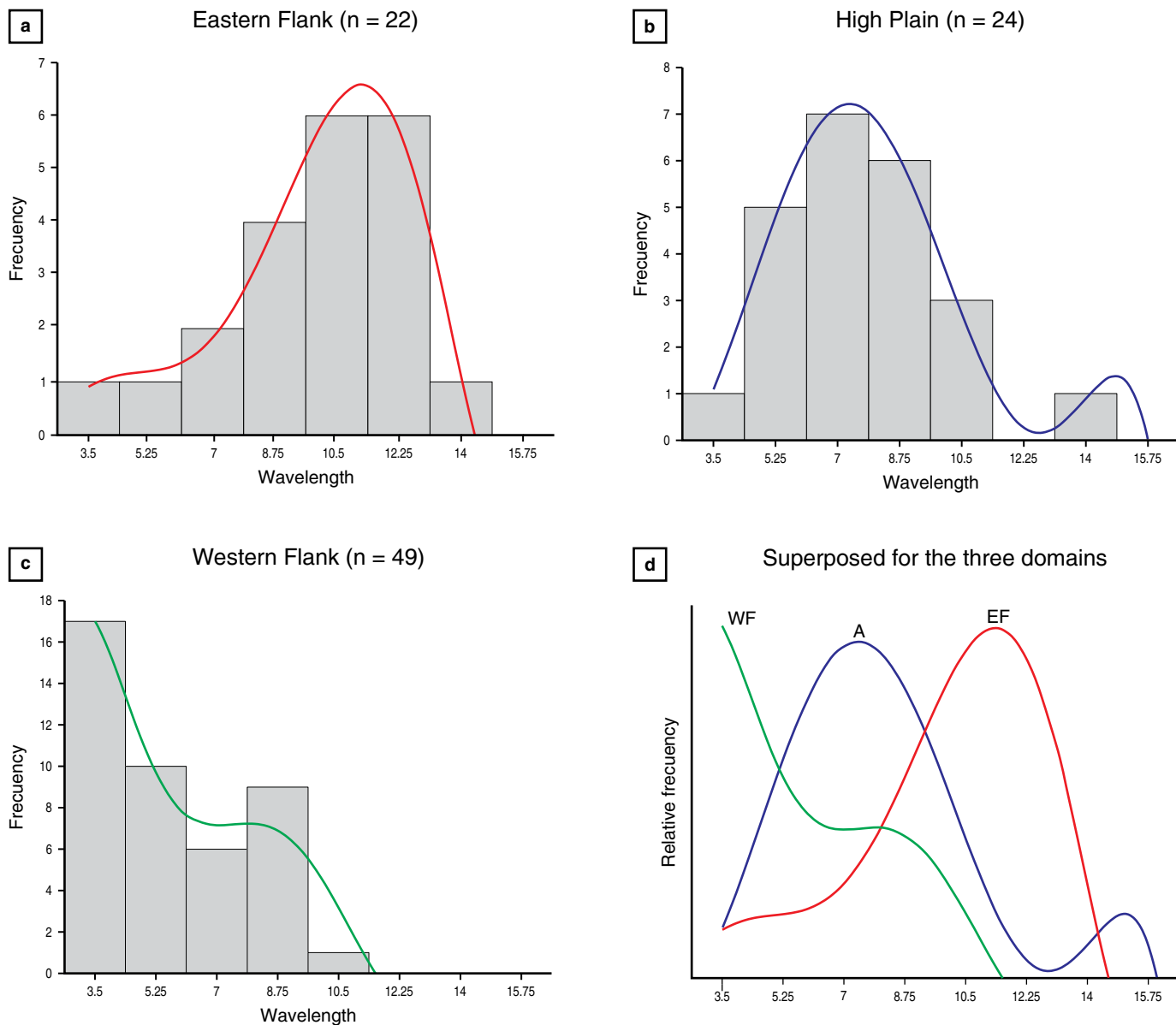


Figure 19. Distribution of fold widths in the structural domains of (a) the eastern flank, (b) the axial zone and (c), the western flank. Subfigure (d) displays the domains superposed. The fold widths of each anticline were determined as the distances between adjacent mapped synclinal axes.

results reinforce our hypothesis that buckling was the principal deformation mechanism at higher structural levels.

9. Discussion

The Cenozoic evolution of the EC is closely tied to the reactivation of inherited Late Triassic/Early Jurassic (splay faults at the southern termination of the Bucaramanga Fault) and Early Cretaceous faults (border faults of the Cretaceous back-arc basin). The reactivation modes include both inversion and further increase in normal displacement (Esmeralda and Toquiza Faults). Notably, some inherited faults lack any evidence of reactivation, even where associated with major folds or moun-

tain fronts. These relationships indicate a complex interplay of crustal rheology, dynamic equilibria, and kinematic conditions, which go beyond a simple mechanical analysis. Next, we discuss the salient features of the Early Cretaceous back-arc configuration and the Neogene folding.

9.1. Cretaceous Back-Arc Evolution

The scenario of a Cretaceous forebulge evolution provides explanations about the Lower Cretaceous paleogeographic division into an axial high and flanking marginal basins. The geodynamic framework should be based on the following considerations:

1. *Marginal basins may, but need not be, fault-bounded.* – Fault inheritance and reactivation has been surmised for many Neogene faults without clear evidence. The case of the Esmeralda Fault is unique because it allows for the identification of a Tithonian to Berriasian depositional cycle related to fault-bounded sag basins. However, elevated subsidence persisted beyond this syn-rift stage to the Hauterivian/Barremian and documents the poorly deciphered dynamics of increased forebulge activity. An enhanced Early Cretaceous subsidence has also been noted along the western margin of the EC (Moreno–Murillo, 1991; Sarmiento–Rojas, 2001), but the existence of conjugate border faults on this flank remains unconfirmed.
2. *Compared to intracontinental rift systems, the Cretaceous back-arc basin is exceptionally wide but is comparable to the dimensions of a cordilleran back-arc domain.* – Intracontinental rift arms, as exemplified by the East African graben systems, vary in width between 60 and 100 km (Corti et al., 2007; Ebinger, 1989). The Cretaceous back-arc realm of the EC, in contrast, displays a restored width of >250 km, which compares to the dimensions of a cordilleran back-arc region (Hyndman, 2010). These relations support the concept of a forebulge-related origin.
3. *Forebulge activity was conterminous with a Cretaceous subduction event.* – Chronologically, the forebulge evolution may be bracketed by the Tithonian rift initiation within the eastern marginal basin and the emplacement of the latest basic intrusive plug at 74 Ma (Vásquez et al., 2010). Within the back-arc realm, the creation of accommodation space along the marginal basins ceased during the Maastriichtian and Paleocene, as may be deduced from reduced subsidence rates and uniformly distributed shallow marine to subaerial depositional environments (Figure 5; Bayona et al., 2013; Cooper et al., 1995; Villamil, 1999). Looking for constraints of its inception, the Cretaceous subduction must have been active since the Aptian, as may be concluded from the supra-subduction signature of the basic effusive to sub-volcanic Quebradagrande suite that was emplaced along the continental margin (Nivia et al., 2006). Accordingly, $^{40}\text{Ar}/^{39}\text{Ar}$ plateau mica and hornblende ages of 120.7 ± 0.6 and 112.0 ± 3.7 Ma (Bustamante et al., 2012; Villagómez et al., 2011) obtained from high-pressure rocks in the suture zone record Aptian exhumation. The suture became locked by the Campanian, as demonstrated by siliciclastic sedimentary sequences that cap the Cretaceous subduction complex and a U–Pb age of 79.7 Ma obtained from a post-kinematic stock emplaced within a major fault zone (Stock of Córdoba; Villagómez et al., 2011). However, the precise onset of subduction (assuming that there was a pause in subduction since the Middle Jurassic) remains conjectural. Numerical modeling suggests that subduction-related plumes might date the initiation of slab foundering

and are most active during the first stage of slab descent (Faccenna et al., 2010).

This spatio-temporal framework for forebulge evolution may be reconciled with the formation of a small-scale upper mantle plume with long-term stability. An associated thermal anomaly could have thinned the lithospheric back-arc region, thereby contributing to a convectively sustained, positive dynamic topography (Flament et al., 2013). Numerical models suggest that the erosive effects of a collateral downwelling asthenospheric mantle flow can lead to highly unstable conditions (or “diffuse” limits; King & Anderson, 1998) unless a high viscosity is assigned to the cratonic lithosphere (Hardebol et al., 2012). Under these conditions, and excluding a thermal shield effect of the craton that could incite sub-lithospheric flow toward the back-arc region (King & Anderson, 1998), the back-arc plume may connect toward the craton side to a relatively narrow zone of a descending “edge-driven” flow at the leading edge of the craton (Figure 20; King & Ritsema, 2000). On the side of the active margin, a subduction-driven corner flow may form a complementary upper mantle circuit (Figure 20; Currie et al., 2004). Such combined convection cells have been postulated for the Canadian back-arc region (Hyndman, 2010) and, considering the similar scale, may be adapted to the Cretaceous back-arc basin of the EC (Figure 20). In these models, a sharp transition between the hot back-arc region and the adjacent cold craton may persist for tens of millions of years (Hardebol et al., 2012), providing thus an analogous setting for the lifetime of the proposed Cretaceous forebulge.

9.2. Cenozoic Faulting and Folding

With respect to the Cenozoic basin inversion, we ask if the proposed impingement of a Cretaceous back-arc plume and the consequent lithospheric thinning influenced the rheological properties of the Cenozoic back-arc region or if the lithospheric properties were restored subsequent to the end of plume activity. A weakened lithospheric block would explain a widely distributed “plain-strain” deformation mode since the onset of Cenozoic shortening. In this scenario of wholesale shortening, the EC is comparable to a “hot” orogenic belt, as conceived by the numerical vise model of Ellis et al. (1998) (see also Cruden et al., 2006). Such a crustal-scale stationary deformation mode stands in contrast to foreland tectonics resulting from migrating deformation fronts and the dynamics of orogenic wedges (as conceptualized, e.g., by DeCelles & DeCelles, 2001).

Support for a widely distributed deformation mode comes from the fold-related diapirism, which we associate with the mobilization of overpressured shales. The pre-late Eocene inversion of the western anticlinal flank at Usme reveals an early inversion of a fold flank, with a resulting structure comparable to the overturned flanks of the Neogene folds in the High Plain of Bogotá (Figure 11; Julivert, 1962, 1963). Evidence of widely

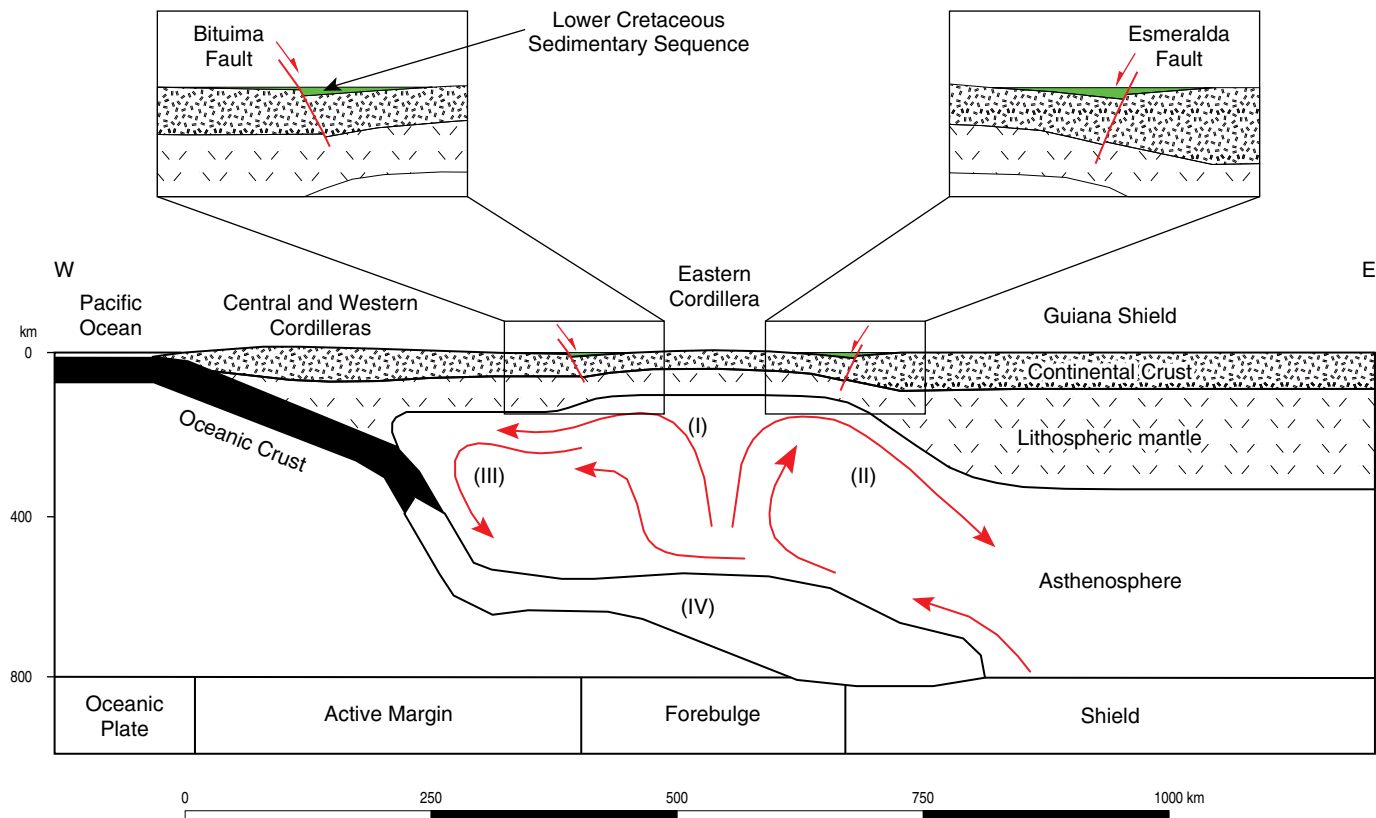


Figure 20. Scenario for the possible mantle dynamics of a cordilleran back-arc basin, as adapted from Hardebol et al. (2012). This model integrates the lithospheric structure, heat flow data, and seismic tomography of the Canadian Cordillera, the dimensions of which are comparable to those of the Cretaceous North Andean back-arc region. A mantle plume, possibly triggered by the initiation of subduction, accounts for lithospheric thinning below the back-arc region (I) and feeds two convection cells. The external western cell corresponds to a subduction-driven corner flow (III), whereas the internal eastern cell involves descending “edge-driven” mantle flow at the contact with the eastern shield area (II). The model depicts a major stage in the evolution of the subducting slab (IV) as it becomes docked at the 660 km discontinuity.

distributed shortening during Neogene folding may be deduced from the fold style in the High Plain of Bogotá, where the fold vergence systematically changes across the axial depression, with buckling involving shear toward the marginal highs. This shear acts up-slope (i.e., against gravity) and is viewed to be the result of incipient lateral escape toward the free cordilleran margins since the inception of folding. Fold-assisted diapirism is most pronounced in the axial depression of the High Plain of Bogotá, which attests to increased compression acting sideways from the elevated flanks.

The characteristic features of the formation of an axial depression (see sections 1–3 in Figure 4) have been simulated for both migrating and relatively stationary deformation fronts. A sandbox experiment of the formation of two deformation fronts was performed by Philip Prince of Virginia Tech, and its advanced stage is sketched in Figure 21a. In this experiment, a non-deforming ramp attached to a moving wall acts as a rigid foreland block. In the first deformation stage, the velocity discontinuity at its tip incites backthrusting of the sand layers toward the rear of the box and their thickening by secondary

forward-breaking thrusts. The wedge dynamics then become focused on a second deformation front by major forward-breaking thrusts and the consequent formation of a pop-up structure. Growth of this composite wedge occurs by a migrating deformation front from the backstop into the foreland (model setup) or from the foreland to the hinterland (EC) and results in the decoupling of the mobile sand layers from the base of the sandbox and the moving wedge. The geometric configuration of this scenario corresponds to that of a crustal flake detached above a ductilely deformed substratum of the lower crust or upper mantle. This scenario of mobile deformation fronts compares to crustal-scale setups of many published cross-sections (refer to the compilations of Cortés et al., 2006, and Tesón et al., 2013).

A contrasting analogue experiment involves a layered model lithosphere with scaled strength profiles that floats on a highly fluid asthenosphere (Figure 21b; Sokoutis & Willingshofer, 2011). During compression, a weak intermediate lithospheric block is squeezed between two rigid foreland blocks. A sand layer, which simulates a rigid upper crustal section, detaches from its base and overrides the converging foreland blocks.

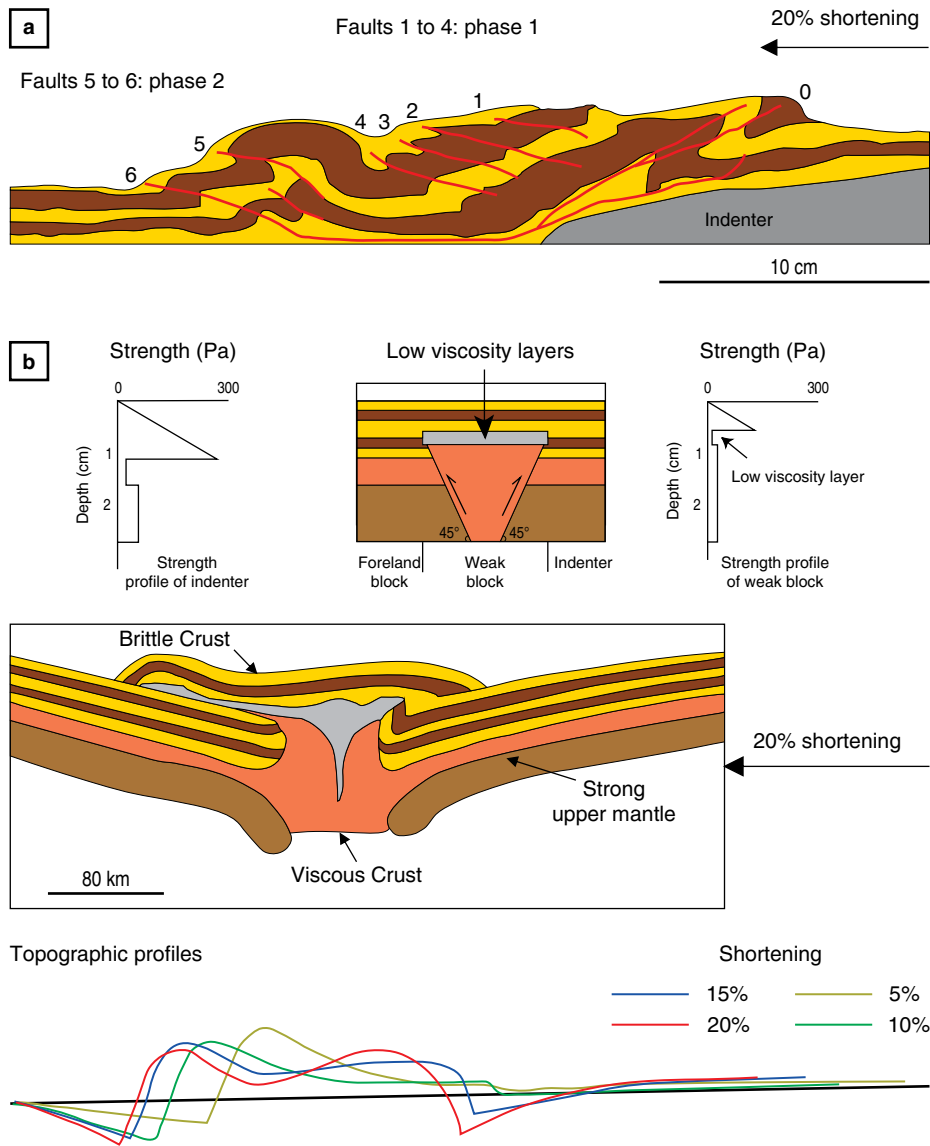


Figure 21. Contrasting experimental models that account for the formation of a plateau-shaped central depression. The sandbox experiment in (a) is a snapshot from a run performed by Prince (2015) and refers to the shortening of alternating sand and microbead layers. The layered nature of this granular material allows for some folding. A rigid wedge is attached to the moving wall (right-hand side). During the first stage, the advancing wedge causes the sand package to slip toward the rear (fault 0) and to thicken by the formation of faults 1 to 4. During the second stage, faults propagate from the leading edge of the moving wedge into the foreland block (faults 5 to 6), and associated backthrusts generate a distal pop-up. The resulting double wedge forms a central depression. The experiment in (b) is taken from Sokoutis & Willingshofer (2011) and involves the shortening of three layers representing the upper brittle crust (dry quartz sand) and the lower viscous crust (silicone mix I), which rest on a highly viscous upper mantle (silicone mix II). This package floats on a low-viscosity asthenosphere. During shortening, an intermediate downward-tapering weak block preferentially absorbs the convergence. A thin upper crustal layer detaches and overrides the adjacent indenting blocks, forming a central depression. This plateau becomes established in the early deformation stages, as shown by the topographic profiles.

This partial decoupling and lateral thrusting is aided by a low-viscosity layer, which represents a discontinuity between the upper and lower crust. The combination of a weak intermediate block and the partial detachment of an upper crustal lid overlying this same block produces a plateau-like axial depression.

The latter experiment fails to simulate a mountain front pinned to a rheological boundary, as occurred at the Servitá Fault

from the Oligocene to the Miocene. The decoupling of an upper crustal layer characterizes, however, the late Pliocene deformation phase in the Guavio area. In contrast to the continuously forward-breaking thrusts related to wedge dynamics in the first experiment, the setup involving a weak intermediate block allows for equally distributed deformation over the entire orogenic belt (Figure 21b). In this scenario of wholesale lithospheric shorten-

ing, the EC is comparable to a “hot” orogenic belt, as conceptualized by the numerical visé model of Ellis et al. (1998).

These considerations are valid for the High Plain of Bogotá (see sections 1–3 in Figure 4), where the conditions of isostatic equilibrium most likely prevailed, and slab tear may have contributed to an elevated thermal gradient. The long-lasting accumulation of shortening at the crustal discontinuity of the Servitá Fault may be explained by rheological contrasts between the orogenic and the foreland block, which were possibly inherited from the Cretaceous back–arc setting. The short wavelengths of the folds in the superficial Cretaceous units suggest buckling with a degree of decoupling with respect to the uniformly strained basement. Further north, inherited faults dictate the style of the basement–involved folding, but the faults became only partially reactivated (see section 4 in Figure 4). In the antiformal lobes of the Cocuy Syntaxis, the faults were not reactivated, and fault–controlled folding was limited to the weak zone associated with the Chicamocha Syncline (Figure 7). In this section, the concept of rheological contrasts between a weak orogenic block bracketed between rigid foreland blocks is not applicable.

10. Conclusions

We examined in detail the Cretaceous back–arc evolution and its constraints on Cenozoic basin inversion. We highlight the following points:

- The widely accepted scenario of an extensional back–arc province delimited by breakaway faults can be integrated into the evolutionary model of a forebulge flanked by marginal basins.
- Marginal basins need not be fault–bounded, even during their “syn–rift” stage of increased subsidence. In the Guavio area, a fault–related subsidence cycle is constrained to the initial break–up of the back–arc realm.
- The forebulge dynamics temporally coincide with a Cretaceous subduction cycle, and may have been driven by a minor plume within the then–established back–arc realm.

The Cenozoic deformation style of the middle segment of the EC closely relates to the tectonic framework of the North Andean flat–slab segment and the slab tear at its southern termination. We conclude the following:

- Of the three differentiated structural domains, the southern domain, which is typified by the High Plain of Bogotá in its axial depression, is affected by penetrative deformation and therefore behaved like a weak block. Shortening was consumed by small–scale buckling at high structural levels and homogeneous deformation within the pre–Cretaceous basement, with a wide transition zone that combines the two deformation modes.
- In the northern domain, buckling became wider, as it involved the basement and was controlled by inherited Early

Jurassic faults. Although these faults were only partially reactivated, they controlled the folding of their hanging wall blocks and represented, thus, rheological boundaries.

➤ Fault reactivation is absent within the antiformal lobes of the northernmost transverse section of the Cocuy Syntaxis. The exceptional topographic relief and a fold style that combines buckling and gravity–induced down–slope shear attest to increased surface uplift. The cordilleran eastern front extends to the outer hinge of the subducting slab, which suggests support from the shallowly dipping oceanic slab.

Acknowledgments

The senior authors thank the numerous graduate students and now colleagues who helped us explore the geology of the Llanos Foothills, when access to this area was still restricted. We are indebted to Carlos A. VARGAS, Pasquale DE GORI, and Claudio CHIARABBA for sharing their processed database of earthquake events. Camilo BETANCUR evaluated and compiled the deformation of the conglomerates presented in Figure 16. The tri–shear modeling was performed with the *FaultFold* program written by Rick ALLMENDINGER. We thank Rick for his generous contributions throughout the years. Data processing of earthquakes and cross–section restoration (not included in this chapter) was performed using Move™ (Midland Valley Exploration) through a software grant to the Universidad Nacional de Colombia. We thank Frederick VOLLMER for sharing his strain analysis software *ellipsefit* and Philip PRINCE for the divulgation of his ingenious sandbox experiments. We are indebted to the critical reviews and stimulating observations of Cees PASSCHIER and Eduardo ROSELLO. We especially thank the editorial team of *The Geology of Colombia* for their effort, generous support and patience.

References

- Acosta, J., Velandia, F., Osorio, J., Lonergan, L. & Mora, H. 2007. Strike–slip deformation within the Colombian Andes. In: Ries, A.C., Butler, R.W.H. & Graham, R.H. (editors), *Deformation of the continental crust: The legacy of Mike Coward*. Geological Society of London, Special Publication 272, p. 303–319. London. <https://doi.org/10.1144/GSL.SP.2007.272.01.16>
- Allmendinger, R.W. 1998. Inverse and forward numerical modeling of trishear fault–propagation folds. *Tectonics*, 17(4): 640–656. <https://doi.org/10.1029/98TC01907>
- Allmendinger, R.W., Zapata, T.R., Manceda, R. & Dzelalija, F. 2004. Trishear kinematic modeling of structures, with examples from the Neuquén Basin, Argentina. In: McClay, K.R. (editor), *Thrust tectonics and hydrocarbon systems*. American Association of Petroleum Geologists, Memoir 82, p. 356–371.
- Anderson, T.A. 1972. Paleogene nonmarine Gualanday Group, Neiva Basin, Colombia, and regional development of the Colombian

- Andes. *American Association of Petroleum Geologists Bulletin*, 83(8): 2423–2438. [https://doi.org/10.1130/0016-7606\(1972\)83\[2423:PNGGNB\]2.0.CO;2](https://doi.org/10.1130/0016-7606(1972)83[2423:PNGGNB]2.0.CO;2)
- Audemard, F.A., Ollarves, R., Bechtold, M., Diaz, G., Beck, C., Carrillo, E., Pantosti, D. & Diederix, H. 2008. Trench investigation on the main strand of the Boconó Fault in its central section, at Mesa del Caballo, Mérida Andes, Venezuela. *Tectonophysics*, 459(1–4): 38–53. <https://doi.org/10.1016/j.tecto.2007.08.020>
- Bayona, G., Montenegro, O.C., Cardona, A., Jaramillo, C., Lamus, F., Morón, S.E., Quiroz, L., Ruiz, M.C., Valencia, V., Parra, M. & Stockli, D.F. 2010. Estratigrafía, procedencia, subsidencia y exhumación de las unidades paleógenas en el Sinclinal de Usme, sur de la zona axial de la cordilla Oriental. *Geología Colombiana*, (35): 5–35.
- Bayona, G., Cardona, A., Jaramillo, C., Mora, A., Montes, C., Caballero, V., Mahecha, H., Lamus, F., Montenegro, O., Jiménez, G., Mesa, A. & Valencia, V. 2013. Onset of fault reactivation in the Eastern Cordillera of Colombia and proximal Llanos Basin: Response to Caribbean–South American convergence in early Paleogene time. In: Nemčok, M., Mora, A. & Cosgrove, J.W. (editors), *Thick-skin-dominated orogens: From initial inversion to full accretion*. Geological Society of London, Special Publication 377, p. 285–314. <https://doi.org/10.1144/SP377.5>
- Beck, M.E., Rojas, C. & Cembrano, J. 1993. On the nature of buttressing in margin-parallel strike-slip fault systems. *Geology*, 21(8): 755–758. [https://doi.org/10.1130/0091-7613\(1993\)021<0755:OTNOBI>2.3.CO;2](https://doi.org/10.1130/0091-7613(1993)021<0755:OTNOBI>2.3.CO;2)
- Branquet, Y., Cheilletz, A., Cobbold, P.R., Baby, P., Laumonier, B. & Giuliani, G. 2002. Andean deformation and rift inversion, eastern edge of Cordillera Oriental (Guateque–Medina area), Colombia. *Journal of South American Earth Sciences*, 15(4): 391–407. [https://doi.org/10.1016/S0895-9811\(02\)00063-9](https://doi.org/10.1016/S0895-9811(02)00063-9)
- Bürgl, H. 1960. El Jurásico e infracretáceo del río Batá, Boyacá. *Boletín Geológico*, 6(1–3): 169–211.
- Bürgl, H. 1967. The orogenesis in the Andean system of Colombia. *Tectonophysics*, 4(4–6): 429–443. [https://doi.org/10.1016/0040-1951\(67\)90009-1](https://doi.org/10.1016/0040-1951(67)90009-1)
- Bustamante, A., Juliani, C., Essene, E.J., Hall, C.M. & Hyppolito, T. 2012. Geochemical constraints on blueschist- and amphibolite facies rocks of the Central Cordillera of Colombia: The Andean Barragán region. *International Geology Review*, 54(9): 1013–1030. <https://doi.org/10.1080/00206814.2011.594226>
- Caballero, V., Mora, A., Quintero, I., Blanco, V., Parra, M., Rojas, L.E., Lopez, C., Sánchez, N., Horton, B.K., Stockli, D. & Duddy, I. 2013. Tectonic controls on sedimentation in an intermontane hinterland basin adjacent to inversion structures: The Nuevo Mundo Syncline, Middle Magdalena Valley, Colombia. In: Nemčok, M., Mora, A. & Cosgrove, J.W. (editors), *Thick-skin-dominated orogens: From initial inversion to full accretion*. Geological Society of London, Special Publication 377, p. 315–342. <https://doi.org/10.1144/SP377.12>
- Campbell, C.J. & Bürgl, H. 1965. Section through the Eastern Cordillera of Colombia, South America. *Geological Society of America Bulletin*, 76(5): 567–590. [https://doi.org/10.1130/0016-7606\(1965\)76\[567:STTECO\]2.0.CO;2](https://doi.org/10.1130/0016-7606(1965)76[567:STTECO]2.0.CO;2)
- Chamberlin, R.T. 1910. The Appalachian folds of central Pennsylvania. *The Journal of Geology*, 18(3): 228–251. <https://doi.org/10.1086/621722>
- Chiarabba, C., De Gori, P., Faccenna, C., Speranza, F., Seccia, D., Dionicio, V. & Prieto, G.A. 2015. Subduction system and flat slab beneath the Eastern Cordillera of Colombia. *Geochemistry, Geophysics, Geosystems*, 17(1): 16–27. <https://doi.org/10.1002/2015GC006048>
- Colletta, B., Hebrard, F., Letouzey, J., Werner, P. & Rudkiewicz, J.L. 1990. Tectonic style and crustal structure of the Eastern Cordillera, Colombia from a balanced cross section. In: Letouzey, J. (editor), *Petroleum and tectonics in mobile belts*. Editions Technip, p. 81–100. Paris.
- Cooper, M.A., Addison, F.T., Alvarez, R., Coral, M., Graham, R.H., Hayward, A.B., Howe, S., Martinez, J., Naar, J., Peñas, R., Pulham, A.J. & Taborda, A. 1995. Basin development and tectonic history of the Llanos Basin, Eastern Cordillera, and Middle Magdalena Valley, Colombia. *American Association of Petroleum Geologists Bulletin*, 79(10): 1421–1443.
- Cortés, M., Colletta, B. & Angelier, J. 2006. Structure and tectonics of the central segment of the Eastern Cordillera of Colombia. *Journal of South American Earth Sciences*, 21(4): 437–465. <https://doi.org/10.1016/j.jsames.2006.07.004>
- Corti, G., van Wijk, J., Cloetingh, S. & Morley, C.K. 2007. Tectonic inheritance and continental rift architecture: Numerical and analogue models of the East African Rift system. *Tectonics*, 26(6): 1–13. <https://doi.org/10.1029/2006TC002086>
- Cruden, A.R., Nasser, M.H.B. & Pysklywec, R. 2006. Surface topography and internal strain variation in wide hot orogens from three-dimensional analogue and two-dimensional numerical vice models. In: Buitert, S.J.H. & Schreurs, G. (editors), *Analogue and numerical modelling of crustal-scale processes*. Geological Society of London, Special Publication 253, p. 79–104. <http://dx.doi.org/10.1144/GSL.SP.2006.253.01.04>
- Currie, C.A., Wang, K., Hyndman, R.D. & He, J. 2004. The thermal effects of steady-state slab-driven mantle flow above a subducting plate: The Cascadia subduction zone and backarc. *Earth and Planetary Science Letters*, 223(1–2): 35–48. <https://doi.org/10.1016/j.epsl.2004.04.020>
- Dalrymple, R.W. & Choi, K. 2007. Morphologic and facies trends through the fluvial-marine transition in tide-dominated depositional systems: A schematic framework for environmental and sequence-stratigraphic interpretation. *Earth Science Reviews*, 81(3–4): 135–174. <https://doi.org/10.1016/j.earsci-rev.2006.10.002>
- DeCelles, P.G. & DeCelles, P.C. 2001. Rates of shortening, propagation, underthrusting, and flexural wave migration in continen-

- tal orogenic systems. *Geology*, 29(2): 135–138. [https://doi.org/10.1130/0091-7613\(2001\)029<0135:ROSPUA>2.0.CO;2](https://doi.org/10.1130/0091-7613(2001)029<0135:ROSPUA>2.0.CO;2)
- Dengo, C.A. & Covey, M.C. 1993. Structure of the Eastern Cordillera of Colombia: Implications for trap styles and regional tectonics. *American Association of Petroleum Geologists Bulletin*, 77(8): 1315–1337. <https://doi.org/10.1306/BDF8E7A-1718-11D7-8645000102C1865D>
- De Porta, J. 1974. *Léxique Stratigraphique International. Amérique Latine, Colombie: (deuxième partie) Tertiaire et Quaternaire.* Centre National de la Recherche Scientifique 5, fascicule 4 b, 626 p. Paris.
- Dimaté, C., Rivera, L.A., Taboada, A., Delouis, B., Osorio, A., Jiménez, E., Fuenzalida, A., Cisternas, A. & Gómez, I. 2003. The 19 January 1995 Tauramena (Colombia) earthquake: Geometry and stress regime. *Tectonophysics*, 363(3–4): 159–180. [https://doi.org/10.1016/S0040-1951\(02\)00670-4](https://doi.org/10.1016/S0040-1951(02)00670-4)
- Dixon, J.M., 1975. Finite strain and progressive deformation in models of diapiric structures. *Tectonophysics*, 28 (1–2): 89–124. [https://doi.org/10.1016/0040-1951\(75\)90060-8](https://doi.org/10.1016/0040-1951(75)90060-8)
- Dorado-Galindo, J. 1992. Contribución al conocimiento de la estratigrafía de la Formación Brechas de Buenavista (límite Jurásico-Cretácico). Región noroeste de Villavicencio, Meta. *Geología Colombiana*, (17): 7–39.
- Dueñas, H. & Césari, S.N. 2005. Systematic study of Early Carboniferous palynological assemblages from the Llanos Orientales Basin, Colombia. *Revista del Museo Argentino de Ciencias Naturales*, 7(2): 139–152. <https://doi.org/10.22179/REVMACN.7.331>
- Durán, J.P., Vargas, C.A. & Briceño, L.A. 2002. Análisis espacial y temporal de Q-Coda en el piedemonte llanero (Colombia). *Earth Sciences Research Journal*, (6): 33–39.
- Ebinger, C.J. 1989. Tectonic development of the western branch of the East African Rift system. *Geological Society of America Bulletin*, 101(7): 885–903. [https://doi.org/10.1130/0016-7606\(1989\)101<0885:TDOTWB>2.3.CO;2](https://doi.org/10.1130/0016-7606(1989)101<0885:TDOTWB>2.3.CO;2)
- Egbue, O. & Kellogg, J. 2010. Pleistocene to present north Andean “escape”. *Tectonophysics*, 489(1–4): 248–257. <https://doi.org/10.1016/j.tecto.2010.04.021>
- Einsele, G. 1992. *Sedimentary basins: Evolution, facies and sediment budget.* Springer-Verlag, 628 p. Berlin. <https://doi.org/10.1007/978-3-662-04029-4>
- Ellis, S., Beaumont, C., Jamieson, R.A. & Quinlan, G. 1998. Continental collision including a weak zone: The vise model and its application to the Newfoundland Appalachians. *Canadian Journal of Earth Sciences*, 35(11): 1323–1346. <https://doi.org/10.1139/e97-100>
- Epard, J.L. & Groshong, R.H. 1993. Excess area and depth to detachment. *American Association of Petroleum Geologists Bulletin*, 77(8): 1291–1302.
- Epard, J.L. & Groshong Jr., R.H. 1995. Kinematic model of detachment folding including limb rotation, fixed hinges and layer-parallel strain. *Tectonophysics*, 247(1–4): 85–103. [https://doi.org/10.1016/0040-1951\(94\)00266-C](https://doi.org/10.1016/0040-1951(94)00266-C)
- Etayo-Serna, F., De Porta, N.S., De Porta, J. & Gaona, T. 2003. The Batá Formation of Colombia is truly Cretaceous, not Jurassic. *Journal of South American Earth Sciences*, 16(3): 113–117. [https://doi.org/10.1016/S0895-9811\(03\)00048-8](https://doi.org/10.1016/S0895-9811(03)00048-8)
- Fabre, A. 1983. La subsidencia de la cuenca del Cocuy (cordillera Oriental de Colombia) durante el Cretáceo y el terciario. Primera parte: Estudio cuantitativo de la subsidencia. *Geología Norandina*, (8): 22–27.
- Fabre, A. & Delaloye, M. 1983. Intrusiones básicas cretácicas en las sedimentitas de la parte central de la cordillera Oriental. *Geología Norandina*, (6): 19–28.
- Faccenna, C., Becker, T.W., Lallemand, S., Lagabrielle, Y., Funicello, F. & Piromallo, C. 2010. Subduction-triggered magmatic pulses: A new class of plumes? *Earth and Planetary Science Letters*, 299(1–2): 54–68. <https://doi.org/10.1016/j.epsl.2010.08.012>
- Flament, N., Gurnis, M. & Müller, R.D., 2013. A review of observations and models of dynamic topography. *Lithosphere* 5(2): 189–210. <https://dx.doi.org/10.1130/L245.1>
- Feininger, T., Barrero, D. & Castro, N. 1972. Geología de parte de los departamentos de Antioquia y Caldas-subzona II-B. *Boletín Geológico*, 20(2): 1–173.
- Feo-Codécido, G., Smith, F.D., Aboud, N. & de Di Giacomo, E. 1984. Basement and Paleozoic rocks of the Venezuelan Llanos basins. In: Bonini, W.E., Hargraves, R.B. & Shagam, R. (editors), *The Caribbean-South American Plate boundary and regional tectonics.* Geological Society of America, Memoir 162, p. 175–187. <https://doi.org/10.1130/MEM162-p175>
- Gephart, J.W. 1994. Topography and subduction geometry in the central Andes: Clues to the mechanics of a noncollisional orogeny. *Journal of Geophysical Research: Solid Earth*, 99(B6): 12279–12288. <https://doi.org/10.1029/94JB00129>
- Gómez, E., Jordan, T., Allmendinger, R.W., Hegarty, K., Kelly, S. & Heizler, M. 2003. Controls on architecture of the Late Cretaceous to Cenozoic southern Middle Magdalena Valley Basin, Colombia. *Geological Society of America Bulletin*, 115(2): 131–147. [https://doi.org/10.1130/0016-7606\(2003\)115<0131:COAOTL>2.0.CO;2](https://doi.org/10.1130/0016-7606(2003)115<0131:COAOTL>2.0.CO;2)
- Gómez, E., Jordan, T.E., Allmendinger, R.W., Hegarty, K. & Kelley, S. 2005a. Syntectonic Cenozoic sedimentation in the northern Middle Magdalena Valley Basin of Colombia and implications for exhumation of the northern Andes. *Geological Society of America Bulletin*, 117(5–6): 547–569. <https://doi.org/10.1130/B25454.1>
- Gómez, E., Jordan, T.E., Allmendinger, R.W. & Cardozo, N. 2005b. Development of the Colombian Foreland-Basin system as a consequence of diachronous exhumation of the northern Andes. *Geological Society of America Bulletin*, 117(9–10): 1272–1292. <https://doi.org/10.1130/B25456.1>

- Guerrero, J. 2002. A proposal on the classification of systems tracts: Application to the allostratigraphy and sequence stratigraphy of the Cretaceous Colombian Basin. Part 2: Barremian to Maastrichtian. *Geología Colombiana*, (27): 27–49.
- Haas, O. 1960. Lower Cretaceous ammonites from Colombia, South America. *American Museum Novitates*, (2005), 62 p. New York.
- Hardebol, N.J., Pysklywec, R.N. & Stephenson, R. 2012. Small-scale convection at a continental back-arc to craton transition: Application to the southern Canadian Cordillera. *Journal of Geophysical Research: Solid Earth*, 117(B1): 1–18. <https://doi.org/10.1029/2011JB008431>
- Harrison, J.V. & Falcon, N.L. 1934. Collapse structures. *Geological Magazine*, 71(12): 529–539. <https://doi.org/10.1017/S0016756800095005>
- Haughton, P., Davis, C., McCaffrey, W. & Barker, S. 2009. Hybrid sediment gravity flow deposits—classification, origin and significance. *Marine and Petroleum Geology*, 26(10): 1900–1918. <https://doi.org/10.1016/j.marpetgeo.2009.02.012>
- Hooghiemstra, H., Wijninga, V.M. & Cleef, A.M. 2006. The paleobotanical record of Colombia: Implications for biogeography and biodiversity. *Annals of the Missouri Botanical Garden*, 93(2): 297–325. [https://doi.org/10.3417/0026-6493\(2006\)93\[297:T-PROCI\]2.0.CO;2](https://doi.org/10.3417/0026-6493(2006)93[297:T-PROCI]2.0.CO;2)
- Hyndman, R.D. 2010. The consequences of Canadian Cordillera thermal regime in recent tectonics and elevation: A review. *Canadian Journal of Earth Sciences*, 47(5): 621–632. <https://doi.org/10.1139/E10-016>
- Hyndman, R.D. & Currie, C.A. 2011. Why is the North America Cordillera high? Hot backarcs, thermal isostasy, and mountain belts. *Geology*, 39(8): 783–786. <https://doi.org/10.1130/G31998.1>
- Idárraga-García, J., Kendall, J.M. & Vargas, C.A. 2016. Shear wave anisotropy in northwestern South America and its link to the Caribbean and Nazca subduction geodynamics. *Geochemistry, Geophysics, Geosystems*, 17(9): 3655–3673. <https://doi.org/10.1002/2016GC006323>
- Jiménez, L., Mora, A., Casallas, W., Silva, A., Tesón, E., Támara, J., Namson, J., Higuera-Díaz, I.C., Lasso, A. & Stockli, D. 2013. Segmentation and growth of foothill thrust-belts adjacent to inverted grabens: The case of the Colombian Llanos Foothills. In: Nemčok, M., Mora, A.R. & Cosgrove, J.W. (editors), *Thick-skin-dominated orogens: From initial inversion to full accretion*. Geological Society of London, Special Publication 377, p. 189–220. <https://doi.org/10.1144/SP377.11>
- Julivert, M. 1962. La estratigrafía de la Formación Guadalupe y las estructuras por gravedad en la serranía de Chía (Sabana de Bogotá). *Boletín de Geología*, (11): 5–21.
- Julivert, M. 1963. Los rasgos tectónicos de la región de la Sabana de Bogotá y los mecanismos de formación de las estructuras. *Boletín de Geología*, (13–14): 5–104.
- Julivert, M. 1970. Cover and basement tectonics in the cordillera Oriental of Colombia, South America, and a comparison with some other folded chains. *Geological Society of America Bulletin*, 81(12): 3623–3646. [https://doi.org/10.1130/0016-7606\(1970\)81\[3623:CABTIT\]2.0.CO;2](https://doi.org/10.1130/0016-7606(1970)81[3623:CABTIT]2.0.CO;2)
- Kammer, A. 1996. Estructuras y deformaciones del borde oriental del Macizo de Floresta. *Geología Colombiana*, (21): 65–80.
- Kammer, A. 1997. Los pliegues del Sinclinal de Tunja: Análisis estructural y modelamiento geométrico. *Geología Colombiana*, (22): 3–25.
- Kammer, A. 2003. La Formación Tilatá en los alrededores de Chocotá: Marco tectónico y ambientes deposicionales. In: van der Hammen, T. (editor), *Neógeno y Cuaternario del altiplano de Bogotá y alrededores II, zona norte y aspectos generales*. Instituto Geográfico Agustín Codazzi, Análisis Geográficos 26, p. 69–100. Bogotá.
- Kammer, A. & Mora, A. 1999. Structural style and amount of shortening of the folded Bogota segment, Eastern Cordillera of Colombia. *Zentralblatt für Geologie und Paläontologie, Teil I*(7–8), p. 823–838. Bayreuth, Germany.
- Kammer, A. & Piraquive-Bermúdez, A. 2013. Evidencias sedimentológicas y estructurales para un origen paleógeno de la Falla de Chusma, Valle Superior del Magdalena, borde occidental de la sub-cuenca de Neiva. *Geología Colombiana*, (38): 43–64.
- Kammer, A. & Sánchez, J. 2006. Early Jurassic rift structures associated with the Soapaga and Boyacá Faults of the Eastern Cordillera, Colombia: Sedimentological inferences and regional implications. *Journal of South American Earth Sciences*, 21(4): 412–422. <https://doi.org/10.1016/j.jsames.2006.07.006>
- Kammer, A., Tamara, J., Beltrán, A. & Robles, W. 2007. Pliegues sobrepuestos en el Anticlinal de Buenavista, piedemonte llanero. *Boletín de Geología*, 29(2): 85–93.
- King, S.D. & Anderson, D.L. 1998. Edge-driven convection. *Earth and Planetary Science Letters*, 160(3–4): 289–296. [https://doi.org/10.1016/S0012-821X\(98\)00089-2](https://doi.org/10.1016/S0012-821X(98)00089-2)
- King, S.D. & Ritsema, J. 2000. African hot spot volcanism: Small-scale convection in the upper mantle beneath cratons. *Science*, 290(5494): 1137–1140. <https://doi.org/10.1126/science.290.5494.1137>
- López, C., Briceño, A. & Buitrago, J. 1991. Edad y origen de los diapiros de sal de la Sabana de Bogotá. IV Simposio Bolivariano Exploración Petrolera en las Cuencas Subandinas. Trabajo 19, 40 p. Bogotá.
- Lyon-Caen, H. & Molnar, P. 1985. Gravity anomalies, flexure of the Indian Plate, and the structure, support and evolution of the Himalaya and Ganga Basin. *Tectonics*, 4(6): 513–538. <https://doi.org/10.1029/TC004i006p00513>
- Martínez, J.A. 2006. Structural evolution of the Llanos Foothills, Eastern Cordillera, Colombia. *Journal of South American*

- Earth Sciences, 21(4): 510–520. <https://doi.org/10.1016/j.jsames.2006.07.010>
- McLaughlin Jr., D.H. 1972. Evaporite deposits of Bogotá area, Cordillera Oriental, Colombia. *American Association of Petroleum Geologists Bulletin*, 56(11): 2240–2259.
- Mora, A., Parra, M., Strecker, M.R., Kammer, A., Dimaté, C. & Rodríguez, F. 2006. Cenozoic contractional reactivation of Mesozoic extensional structures in the Eastern Cordillera of Colombia. *Tectonics*, 25(2): 1–19. <https://doi.org/10.1029/2005TC001854>
- Mora, A., Parra, M., Strecker, M.R., Sobel, E.R., Hooghiemstra, H., Torres, V. & Vallejo–Jaramillo, J. 2008. Climatic forcing of asymmetric orogenic evolution in the Eastern Cordillera of Colombia. *Geological Society of America Bulletin*, 120(7–8): 930–949. <https://doi.org/10.1130/B26186.1>
- Mora, A., Gaona, T., Kley, J., Montoya, D., Parra, M., Quiroz, L.I., Reyes, G. & Strecker, M. 2009. The role of inherited extensional fault segmentation and linkage in contractional orogenesis: A reconstruction of Lower Cretaceous inverted rift basins in the Eastern Cordillera of Colombia. *Basin Research*, 21(1): 111–137. <https://doi.org/10.1111/j.1365-2117.2008.00367.x>
- Mora, A., Horton, B.K., Mesa, A., Rubiano, J., Ketcham, R.A., Parra, M., Blanco, V., Garcia, D. & Stockli, D.F. 2010a. Migration of Cenozoic deformation in the Eastern Cordillera of Colombia interpreted from fission track results and structural relationships: Implications for petroleum systems. *American Association of Petroleum Geologists Bulletin*, 94(10): 1543–1580. <https://doi.org/10.1306/01051009111>
- Mora, A., Parra, M., Strecker, M.R., Sobel, E.R., Zeilinger, G., Jaramillo, C., Ferreira Da Silva, S. & Blanco, M. 2010b. The eastern foothills of the Eastern Cordillera of Colombia: An example of multiple factors controlling structural styles and active tectonics. *Geological Society of America Bulletin*, 112(11–12): 1846–1864. <https://doi.org/10.1130/B30033.1>
- Mora, A., Reyes–Harker, A., Rodríguez, G., Tesón, E., Ramírez–Arias, J.C., Parra, M., Caballero, V., Mora, J.P., Quintero, I., Valencia, V., Ibañez–Mejía, M., Horton, B.K. & Stockli, D.F. 2013. Inversion tectonics under increasing rates of shortening and sedimentation: Cenozoic example from the Eastern Cordillera of Colombia. In: Nemčok, M., Mora, A. & Cosgrove, J.W. (editors), *Thick–skin–dominated orogens: From initial inversion to full accretion*. Geological Society of London, Special Publication 377, p. 411–442. <https://doi.org/10.1144/SP377.6>
- Mora, A., Parra, M., Rodríguez–Forero, G., Blanco, V., Moreno, N., Caballero, V., Stockli, D.F., Duddy, I. & Ghorbal, B. 2015. What drives orogenic asymmetry in the northern Andes? A case study from the apex of the northern Andean orocline. In: Bartolini, C. & Mann, P. (editors), *Petroleum geology and potential of the Colombian Caribbean margin*. American Association of Petroleum Geologists, Memoir 108, p. 547–586. <https://doi.org/10.1306/13531949M1083652>
- Morales, L.G. 1958. General geology and oil occurrences of Middle Magdalena Valley, Colombia, South America. In: Weeks, L.G. (editor), *Habitat of oil*. American Association of Petroleum Geologists, Special Publications SP18, p. 641–695. Tulsa, USA.
- Mora–Páez, H., Mencin, D.J., Molnar, P., Diederix, H., Cardona–Piedrahita, L., Peláez–Gaviria, J.R. & Corchuelo–Cuervo, Y. 2016. GPS velocities and the construction of the Eastern Cordillera of the Colombian Andes. *Geophysical Research Letters*, 43(16): 8407–8416. <https://doi.org/10.1002/2016GL069795>
- Moreno–Murillo, J.M. 1991. Provenance of the Lower Cretaceous sedimentary sequences, central part, Eastern Cordillera, Colombia. *Revista de la Academia Colombiana de Ciencias Exactas, Físicas y Naturales*, 18(69): 159–173.
- Moreno–Murillo, J.M. & Concha–Perdomo, A.E. 1993. Nuevas manifestaciones ígneas básicas en el flanco occidental de la cordillera Oriental, Colombia. *Geología Colombiana*, (18): 143–150.
- Moucha, R., Forte, A.M., Mitrovica, J.X., Rowley, D.B., Quéré, S., Simmons, N.A. & Grand, S.P. 2008. Dynamic topography and long–term sea–level variations: There is no such thing as a stable continental platform. *Earth and Planetary Science Letters*, 271(1–4): 101–108. <https://doi.org/10.1016/j.epsl.2008.03.056>
- Nivia, Á., Marriner, G.F., Kerr, A.C. & Tarney, J. 2006. The Quebradagrande Complex: A Lower Cretaceous ensialic marginal basin in the Central Cordillera of the Colombian Andes. *Journal of South American Earth Sciences*, 21(4): 423–436. <https://doi.org/10.1016/j.jsames.2006.07.002>
- Ochoa, D., Hoorn, C., Jaramillo, C., Bayona, G., Parra, M. & De la Parra, F. 2012. The final phase of tropical lowland conditions in the axial zone of the Eastern Cordillera of Colombia: Evidence from three palynological records. *Journal of South American Earth Sciences*, 39: 157–169. <https://doi.org/10.1016/j.jsames.2012.04.010>
- Parra, M., Mora, A., Jaramillo, C., Strecker, M.R., Sobel, E.R., Quiroz, L., Rueda, M. & Torres, V. 2009a. Orogenic wedge advance in the northern Andes: Evidence from the Oligocene – Miocene sedimentary record of the Medina Basin, Eastern Cordillera, Colombia. *Geological Society of America Bulletin*, 121(5–6): 780–800. <https://doi.org/10.1130/B26257.1>
- Parra, M., Mora, A., Sobel, E.R., Strecker, M.R. & González, R. 2009b. Episodic orogenic–front migration in the northern Andes: Constraints from low–temperature thermochronology in the Eastern Cordillera, Colombia. *Tectonics*, 28(4): 27 p. <https://doi.org/10.1029/2008TC002423>
- Pennington, W.D. 1981. Subduction of the eastern Panama Basin and seismotectonics of northwestern South America. *Journal of Geophysical Research: Solid Earth*, 86(B11): 10753–10770. <https://doi.org/10.1029/JB086iB11p10753>
- Pimpirev, C.T., Patarroyo, P. & Sarmiento, G. 1992. Stratigraphy and facies analysis of the Caqueza Group: A sequence of Lower Cretaceous turbidites in the cordillera Oriental of the Colombian Andes. *Journal of South American Earth Sciences*, 5(3–4): 297–308. [https://doi.org/10.1016/0895-9811\(92\)90027-V](https://doi.org/10.1016/0895-9811(92)90027-V)
- Pindell, J.L. & Kennan, L. 2009. Tectonic evolution of the Gulf of Mexico, Caribbean and northern South America in the mantle

- reference frame: An update. In: James, K.H., Lorente, M.A. & Pindell, J.L. (editors), *The origin and evolution of the Caribbean Plate*. Geological Society of London, Special Publication 328, p. 1–55. <https://doi.org/10.1144/SP328.1>
- Poblet, J. & McClay, K. 1996. Geometry and kinematics of single-layer detachment folds. *American Association of Petroleum Geologists Bulletin*, 80(7): 1085–1109. <https://doi.org/10.1306/64ED8CA0-1724-11D7-8645000102C1865D>
- Polanía, H. & Rodríguez, G. 1978. Posibles turbiditas del Cretáceo Inferior (Miembro Socotá) en el área de Anapoima (Cundinamarca). *Geología Colombiana*, (10): 87–113.
- Poveda, E., Monsalve, G. & Vargas, C.A. 2015. Receiver functions and crustal structure of the northwestern Andean region, Colombia. *Journal of Geophysical Research: Solid Earth*, 120(4): 2408–2425. <https://doi.org/10.1002/2014JB011304>
- Price, N.J. 1975. Rates of deformation. *Journal of the Geological Society*, 131(6): 553–575. <https://doi.org/10.1144/gsjgs.131.6.0553>
- Prince, P. 2015. Eastern Cordillera, Colombia, northern Andes. TheGeoModels. Active tectonics and geomorphology lab, department of geosciences, Virginia Tech. Virginia, USA. <https://www.youtube.com/watch?v=ruaej-br2c> (consulted in September 2015).
- Ramón, J. C., & Rosero, A. 2006. Multiphase structural evolution of the western margin of the Girardot subbasin, Upper Magdalena Valley, Colombia. *Journal of South American Earth Sciences*, 21(4): 493–509. <https://doi.org/10.1016/j.jsames.2006.07.012>
- Rey, P., Vanderhaeghe, O. & Teyssier, C. 2001. Gravitational collapse of the continental crust: Definition, regimes and modes. *Tectonophysics*, 342(3–4): 435–449. [https://doi.org/10.1016/S0040-1951\(01\)00174-3](https://doi.org/10.1016/S0040-1951(01)00174-3)
- Riel, N., Jaillard, E., Martelat, J.E., Guillot, S. & Braun, J. 2018. Permian – Triassic Tethyan realm reorganization: Implications for the outward Pangea margin. *Journal of South American Earth Sciences*, 81: 78–86. <https://doi.org/10.1016/j.jsames.2017.11.007>
- Roeder, D. & Chamberlain, R.L. 1995. Eastern Cordillera of Colombia: Jurassic–Neogene crustal evolution. In: Tankard, A.J., Suárez–Soruco, R. & Welsink, H.J. (editors), *Petroleum basins of South America*. American Association of Petroleum Geologists, Memoir 62, p. 633–645. Tulsa, USA.
- Rowan, M.G. & Linares, R. 2000. Fold–evolution matrices and axial–surface analysis of fault–bend folds: Application to the Medina Anticline, Eastern Cordillera, Colombia. *American Association of Petroleum Geologists Bulletin*, 84(6): 741–764. <https://doi.org/10.1306/A96733E2-1738-11D7-8645000102C1865D>
- Russo, R.M. & Silver, P.G. 1994. Trench–parallel flow beneath the Nazca Plate from seismic anisotropy. *Science*, 263(5150): 1105–1111. <https://doi.org/10.1126/science.263.5150.1105>
- Sánchez, J., Horton, B.K., Tesón, E., Mora, A., Ketcham, R.A. & Stockli, D.F. 2012. Kinematic evolution of Andean fold–thrust structures along the boundary between the Eastern Cordillera and Middle Magdalena Valley Basin, Colombia. *Tectonics*, 31(3): 1–24. <https://doi.org/10.1029/2011TC003089>
- Sarmiento–Rojas, L.F. 2001. Mesozoic rifting and Cenozoic basin inversion history of the Eastern Cordillera, Colombian Andes: Inferences from tectonic models. Doctoral thesis, Vrije Universiteit, 295 p. Amsterdam, the Netherlands.
- Sarmiento–Rojas, L.F., van Wess, J.D. & Cloetingh, S. 2006. Mesozoic transtensional basin history of the Eastern Cordillera, Colombian Andes: Inferences from tectonic models. *Journal of South American Earth Sciences*, 21(4): 383–411. <https://doi.org/10.1016/j.jsames.2006.07.003>
- Saylor, J.E., Horton, B.K., Nie, J., Corredor, J. & Mora, A. 2011. Evaluating foreland basin partitioning in the northern Andes using Cenozoic fill of the Floresta Basin, Eastern Cordillera, Colombia. *Basin Research*, 23(4): 377–402. <https://doi.org/10.1111/j.1365-2117.2010.00493.x>
- Saylor, J.E., Horton, B., Stockli, D.F., Mora, A. & Corredor, J. 2012. Structural and thermochronological evidence for Paleogene basement–involved shortening in the axial Eastern Cordillera, Colombia. *Journal of South American Earth Sciences*, 39: 202–215. <https://doi.org/10.1016/j.jsames.2012.04.009>
- Schmalholz, S.M., Podladchikov, Y.Y. & Burg, J.P. 2002. Control of folding by gravity and matrix thickness: Implications for large–scale folding. *Journal of Geophysical Research: Solid Earth*, 107(B1): ETG 1–1–ETG 1–16. <https://doi.org/10.1029/2001JB000355>
- Sokoutis, D. & Willingshofer, E. 2011. Decoupling during continental collision and intra–plate deformation. *Earth and Planetary Science Letters*, 305(3–4): 435–444. <https://doi.org/10.1016/j.epsl.2011.03.028>
- Spikings, R., Cochrane, R., Villagómez, D., van der Lelij, R., Vallejo, C., Winkler, W. & Beate, B. 2015. The geological history of northwestern South America: From Pangaea to the early collision of the Caribbean Large Igneous Province (290–75 Ma). *Gondwana Research*, 27(1): 95–139. <https://doi.org/10.1016/j.gr.2014.06.004>
- Stibane, F.R. 1967. Paläogeographie und Tektogenese der kolumbianischen Anden. *Geologische Rundschau*, 56(1): 629–642. <https://doi.org/10.1007/BF01848746>
- Suárez, M. A., 1996. Facies analysis of the Upper Eocene La Paz Formation, and regional evaluation of post–middle Eocene stratigraphy, northern Middle Magdalena Valley Basin, Colombia. Master thesis, University of Colorado, 88 p. Boulder, USA.
- Taboada, A., Rivera, L.A., Fuenzalida, A., Cisternas, A., Philip, H., Bijwaard, H., Olaya, J. & Rivera, C. 2000. Geodynamics of the northern Andes: Subductions and intracontinental deformation (Colombia). *Tectonics*, 19(5): 787–813. <https://doi.org/10.1029/2000TC900004>
- Talling, P.J., Masson, D.G., Sumner, E.J. & Malgesini, G. 2012. Subaqueous sediment density flows: Depositional processes and

- deposit types. *Sedimentology*, 59(7): 1937–2003. <https://doi.org/10.1111/j.1365-3091.2012.01353.x>
- Teixell, A., Ruiz, J.C., Teson, E. & Mora, A. 2015. The structure of an inverted back–arc rift: Insights from a transect across the Eastern Cordillera of Colombia near Bogota. In: Bartolini, C. & Mann, P. (editors), *Petroleum geology and potential of the Colombian Caribbean margin*. American Association of Petroleum Geologists, Memoir 108, p. 499–515. <https://doi.org/10.1306/13531947M1083650>
- Terraza, R., Montoya, D., Reyes, G., Moreno, G. & Fúquen, J. 2008. Geología del cinturón esmeraldífero oriental, planchas 210, 228 y 229. Ingeominas, Internal report 2877, 129 p. Bogotá.
- Teson, E., Mora, A., Silva, A., Namson, J., Teixell, A., Castellanos, J., Casallas, W., Julivert, M., Taylor, M., Ibañez–Mejia, M. & Valencia, V. 2013. Relationship of Mesozoic graben development, stress, shortening magnitude, and structural style in the Eastern Cordillera of the Colombian Andes. In: Nemčok, M., Mora, A. & Cosgrove, J.W. (editors), *Thick–skin–dominated orogens: From initial inversion to full accretion*. Geological Society of London, Special Publication 377, p. 257–283. London. <https://doi.org/10.1144/SP377.10>
- Thomas, R.G., Smith, D.G., Wood, J.M., Visser, J., Calverley–Range, E.A. & Koster, E.H. 1987. Inclined heterolithic stratification–terminology, description, interpretation and significance. *Sedimentary Geology*, 53(1–2): 123–179. [https://doi.org/10.1016/S0037-0738\(87\)80006-4](https://doi.org/10.1016/S0037-0738(87)80006-4)
- Torres, V., Vandenberghe, J. & Hooghiemstra, H. 2005. An environmental reconstruction of the sediment infill of the Bogotá Basin (Colombia) during the last 3 million years from abiotic and biotic proxies. *Palaeogeography, Palaeoclimatology, Palaeoecology*, 226(1–2): 127–148. <https://doi.org/10.1016/j.palaeo.2005.05.005>
- Trenkamp, R., Kellogg, J.N., Freymueller, J.T. & Mora, H. 2002. Wide plate margin deformation, southern Central America and northwestern South America, CASA GPS observations. *Journal of South American Earth Sciences*, 15(2): 157–171. [https://doi.org/10.1016/S0895-9811\(02\)00018-4](https://doi.org/10.1016/S0895-9811(02)00018-4)
- Ujueta, G. 1992. Lineamientos río Ariari, Bogotá y Gachalá en los departamentos de Cundinamarca y Meta, Colombia. *Revista Academia Colombiana de Ciencias Exactas, Físicas y Naturales*, 18(70): 345–358.
- van der Hammen, T., Werner, J.H. & van Dommelen, H. 1973. Palynological record of the upheaval of the northern Andes: A study of the Pliocene and lower Quaternary of the Colombian Eastern Cordillera and the early evolution of its high–Andean biota. *Review of Palaeobotany and Palynology*, 16(1–2): 1–122. [https://doi.org/10.1016/0034-6667\(73\)90031-6](https://doi.org/10.1016/0034-6667(73)90031-6)
- van der Lelij, R., Spikings, R., Ulianov, A., Chiaradia, M. & Mora, A. 2016. Palaeozoic to Early Jurassic history of the northwestern corner of Gondwana, and implications for the evolution of the Iapetus, Rheic and Pacific Oceans. *Gondwana Research*, 31: 271–294. <https://doi.org/10.1016/j.gr.2015.01.011>
- van Houten, F.B. & Travis, R.B. 1968. Cenozoic deposits, Upper Magdalena Valley, Colombia. *American Association of Petroleum Geologists Bulletin*, 52(4): 675–702.
- Vargas, C.A. & Mann, P. 2013. Tearing and breaking off of subducted slabs as the result of collision of the Panama arc–indenter with northwestern South America. *Bulletin of the Seismological Society of America*, 103(3): 2025–2046. <https://doi.org/10.1785/0120120328>
- Vásquez, M., Altenberger, U., Romer, R.L., Sudo, M. & Moreno–Murillo, J.M. 2010. Magmatic evolution of the Andean Eastern Cordillera of Colombia during the Cretaceous: Influence of previous tectonic processes. *Journal of South American Earth Sciences*, 29(2): 171–186. <https://doi.org/10.1016/j.jsames.2009.02.003>
- Velandia, F. & Bermúdez, M.A. 2018. The transpressive southern termination of the Bucaramanga Fault (Colombia): Insights from geological mapping, stress tensors, and fractal analysis. *Journal of Structural Geology*, 115: 190–207. <https://doi.org/10.1016/j.jsg.2018.07.020>
- Villagómez, D., Spikings, R., Magna, T., Kammer, A., Winkler, W. & Beltrán, A. 2011. Geochronology, geochemistry and tectonic evolution of the Western and Central cordilleras of Colombia. *Lithos*, 125(3–4): 875–896. <https://doi.org/10.1016/j.lithos.2011.05.003>
- Villamil, T. 1999. Campanian – Miocene tectonostratigraphy, depocenter evolution and basin development of Colombia and western Venezuela. *Palaeogeography, Palaeoclimatology, Palaeoecology*, 153(1–4): 239–275. [https://doi.org/10.1016/S0031-0182\(99\)00075-9](https://doi.org/10.1016/S0031-0182(99)00075-9)
- Vollmer, F.W. 2015. EllipseFit 3.2.1. Strain Analysis Software. <http://www.frederickvollmer.com/ellipsefit/> (consulted in December 2017).
- Warsitzka, M., Kley, J. & Kukowski, N. 2013. Salt diapirism driven by differential loading–Some insights from analogue modeling. *Tectonophysics*, 591: 83–97. <https://doi.org/10.1016/j.tecto.2011.11.018>
- Wernicke, B. & Axen, G.J. 1988. On the role of isostasy in the evolution of normal fault systems. *Geology*, 16(9): 848–851. [https://doi.org/10.1130/0091-7613\(1988\)016<0848:OTROII>2.3.CO;2](https://doi.org/10.1130/0091-7613(1988)016<0848:OTROII>2.3.CO;2)
- Zehnder, A.T. & Allmendinger, R.W. 2000. Velocity field for the trishear model. *Journal of Structural Geology*, 22(8): 1009–1014. [https://doi.org/10.1016/S0191-8141\(00\)00037-7](https://doi.org/10.1016/S0191-8141(00)00037-7)

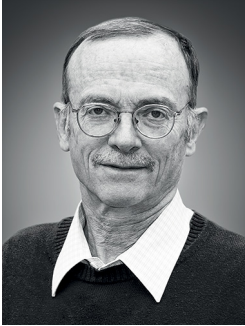
Explanation of Acronyms, Abbreviations, and Symbols:

EC Eastern Cordillera

LREE

Light rare earth element

Authors' Biographical Notes



Andreas KAMMER has been a structural geology professor at the Universidad Nacional de Colombia since 1991. He completed his PhD in 1985 at Neuchâtel, working on the tectonic evolution of the Aar Massif, Central Alps. His work has been focused on the structure, tectonics, and sedimentary evolution of the Colombian Andes since 1985. Together with the senior authors of this

paper, he has initiated research projects on the Eastern foothills of the Eastern Cordillera since 1991.



Alejandro PIRAQUIVE received his Bachelor of Science and Master of Science degrees in geology from the Universidad Nacional de Colombia working on the Eastern foothills of the Eastern Cordillera. For his PhD thesis, he unraveled the tectonic evolution of the Sierra Nevada de Santa Marta, applying geo- and thermochronological methods sponsored by a cotutelle program between the

Université Grenoble—Alpes and the Universidad Nacional de Colombia. He presently holds a research position at the Servicio Geológico Colombiano, which is funded by the postdoc program of Colciencias.



Cristhian GÓMEZ received his Bachelor of Science and Master of Science degrees in geology from the Universidad Nacional de Colombia working on the Triassic rift tectonics of the southern flank of the Sierra Nevada de Santa Marta. His research interests include tectonic sedimentology and thermochronology.



Andrés MORA is the technical leader of onshore Colombia and foothills exploration at Ecopetrol. He received his BS in geology from the Universidad Nacional de Colombia and PhD from the Institut für Geowissenschaften, Universität Potsdam. His research interests include structural geology, petroleum exploration, and petroleum geology.



Antonio VELÁSQUEZ received his Bachelor of Science and Master of Science degrees in geology from the Universidad Nacional de Colombia, evaluating the structural evolution of the Llanos foothills and modeling their gravitational expression by means of crustal-scale anomalies.

